Routing and Resource Allocation in Space Division Multiplexing Elastic Optical Networks

March 2023

ZHENG WEICHANG

Routing and Resource Allocation in Space Division Multiplexing Elastic Optical Networks

Graduate School of Science and Technology
Degree Programs in Systems and Information Engineering
University of Tsukuba

March 2023

ZHENG WEICHANG

Contents

List of Figures

List of Tables

List of Acronyms

AABN	American ATT Backbone Network
ADC	Analog to Digital Conversation
AI	Artificial Intelligence
ATM	Asynchronous Transfer Mode
ATU	Average Transceiver Utilization
BP	Blocking Probability
BPF	Bundle Packing Fraction
BV-WSS	Bandwidth Variable Wavelength Selective Switch
B&S	Broadcast-and-Select
CAGR	Compound Annual Growth Rate
CAPEX	Capital Expenditure
CO-OFDM	Coherent Optical Orthogonal Frequency Division Multiplexing
DAC	Digital to Analog Conversation
DMUX	Demultiplexer
DPP	Dedicated Path Protection
DRV	Optical Modulator Driver Amplifier
DSP	Digital Signal Processing
DT	Deterministic Traffic
EDFA	Erbium Doped Fiber Amplifier
EOBN	European Optical Backbone Network
EON	Elastic Optical Networking
FFSA	First Fit Spectrum Assignment
FIFO	Fan-In Fan-Out

FJoS	Fractional Joint Switching
FMF	Few Mode Fiber
FM-MCF	Few Mode Multi Core Fiber
FRA	Fiber Raman Amplifier
FS	Frequency Slot
GB	Guard Band
HOXC	Hierarchical Optical Cross Connect
InS	Independent Switching
IP	Internet Protocol
ITU-T	International Telecommunication Union Telecommunication Standardization Sector
I/Q MZM	In-phase/Quadrature Mach-Zehnder Modulator
JoS	Joint Switching
KSP	K Shortest Path
LAN	Local Area Network
LCoS	Liquid Crystal on Silicon
LCSA	Low-Cost Single-stage Amplifier
LO	Local Oscillator
LPF	Low-Pass Filter
LS	Laser Source
MAT	Maximum Average Throughput
MCF	Multi-Core Fiber
MCS	Multicast Switch
MC-EDFA	Multicore Erbium-Doped Fiber Amplifiers
MDM	Mode Division Multiplexing
MEMS	Micro Electro-Mechanical System
MILP	Mixed Integer Linear Programming
ML	Machine Learning
MMF	Multi Mode Fiber
MUX	Multiplexer

NP	Nondeterministic Polynomial
N-WDM	Nyquist Wavelength Division Multiplexing
OADM	Optical Add/Drop Multiplexer
OC	Optical Carrier
OCh	Optical Channel
ODU-XC	Optical Channel Data Unit Cross Connect
OFA	Optical Fiber Amplifier
OLA	Optical Line Amplifier
OTM	Optical Terminal Multiplexer
OTN	Optical Transport Network
OXC	Optical Cross Connect
PBC	Polarization Beam Combiner
PBS	Polarization Beam Splitter
PD	Photo Diode
PDH	Plesiochronous Digital Hierarchy
QAM	Quadrature Amplitude Modulation
QoS	Quality of Service
QPSK	Quadrature Phase Shift Keying
REG	Regeneration Station
ROADM	Reconfigurable Optical Add/Drop Multiplexer
RSA	Routing and Spectrum Assignment
RSCA	Routing, Spectrum, and Core Assignment
RSCSA	Routing, Spatial Channel, and Spectrum Assignment
RSSA	Routing, Spectrum and Space Assignment
RWA	Routing and Wavelength Assignment
Rx	Receiver
R&S	Route-and-Select
SBPP	Shared Backup Path Protection
SCh	Spatial Channel

SCN	Spatial Channel Network
SDH	Synchronous Digital Hierarchy
SDM	Space Division Multiplexing
SDN	Software Defined Networking
SE	Spectral Efficiency
SL	Spatial Lane
SLC	Spatial Lane Change
SLICE	Spectrum Sliced Elastic
SMFB	Single-Mode Fiber Bundle
SNR	Signal to Noise Ratio
SOA	Semiconductor Optical Amplifier
SONET	Synchronous Optical Network
Spa & Spe SpCh	Spatial and Spectral Superchannel
SRLG	Shared Risk Link Group
SRS	Stimulated Raman Scattering
SXC	Spatial Cross Connect
TDM	Time Division Multiplexing
TMC	Tapered Multi-core Connector
TxRx	Transceiver
Tx	Transmitter
VGDA	Variable-Gain Dual-stage Amplifier
VNI	Visual Networking Index
WDM	Wavelength Division Multiplexing
WSS	Wavelength Selective Switch
WXC	Wavelength Cross Connect
XC	Cross Connect
XT	Crosstalk

Acknowledgments

First and foremost I am deeply grateful to my advisor, professor Yongbing Zhang, for his insightful advice, continuous support, and patience during my Ph.D. carrier. His immense knowledge, open-minded personality, and plentiful experience have encouraged me in all the time of my academic study and daily life.

I would also like to thank my AG professors Maiko Shigeno, Ying Miao, Tuan Phung-Duc, and Shigetomo Kimura the professors for their treasured support and valuable comments, which was really influential in shaping my experiment methods and critiquing my results.

My heartiest thanks flow to my lab mates and friends - Mingcong Yang, Chenxiao Zhang, and Yu Zheng for their help in the cherished time spent together in the lab.

My appreciation also goes out to the *JST-SPRING* for their financial support by means of a full scholarship.

Finally, my deep gratefulness to my parents and my girlfriend Keyi Xu, for their love and support throughout my Ph.D. degree.

Publications in Journals

1. **Zheng W***, Yang M, Zhang C, et al., "Application-aware QoS routing in SDNs using machine learning techniques", *Peer-to-Peer Networking and Applications*, vol. 15, no. 1, pp. 529–548, Nov. 2021.

2. **Zheng W***, Yang M, Zhang C, et al., "Evaluation of Optical Transport Unit Line-Card Integration in Spatially and Spectrally Flexible Optical Networks in Terms of Device Cost and Network Performance", *Journal of Lightwave Technology*, vol. 40, no. 19, pp. 6319–6330, Oct. 2022.

3. Zhang C, Yang M, **Zheng W***, et al., "Analysis of wavelength deployment schemes in terms of optical network unit cost and upstream transmission performance in NG-EPONs", *Journal of Optical Communications and Networking*, vol. 13, no. 9, pp. 214–223, Jul. 2021.

Publications accepted

1. "Robust Design against Network Failures of Shared Backup Path Protected SDM-EONs", accepted by *Journal of Lightwave Technology* on 21st Jan. 2023.

Publications in Conferences

1. **Zheng W***, Q. Wu, K. Guo, Y. Zhang, "Time-Aware Machine Learning-based Traffic QoS Classification", in *IPSJ SIG IOT*, Mar. 2022.

Abstract

With the sustainable development of the Internet, network traffic has grown explosively in recent years. According to the Cisco visual networking index (VNI) global IP traffic forecast report, the increasing trend of the Internet is mainly reflected in the global population of Internet users, the average data transmission, and the type of Internet services. The coronavirus disease (COVID-19) pandemic has greatly increased the frequency and highlighted the necessity of communication through the Internet. Therefore, the continuous and rapid increase in network traffic has magnified the problems of transmission capacity limitation, network reliability, and traffic uncertainty in current optical networks.

Facing those above problems, the optical network architectures have experienced several periods of development from the early wavelength division multiplexing (WDM)-based optical networks. To overcome the capacity upper limit, two crucial techniques called elastic optical networking (EON) and space division multiplexing (SDM) have been proposed as viable solutions. EON yields a more flexible and efficient optical transmission system by dividing spectrum resources for transmission into finer frequency slots (FSs) compared with WDM. Moreover, the expansion of spatial domains from the current one dimension in WDM to multiple dimensions by SDM increases the network capacity. To guarantee network reliability, the software defined networking (SDN)-based optical networks provide the functionalities of controlling and data forwarding by the separate control and data plane for network transmission. The central controllers in SDN-based optical networks grasp the overall information of traffic data and devices, achieving effective management and fast reconfiguration. In addition, as part of the trend toward more automation and intelligence in future networks, artificial intelligence (AI) and machine learning (ML) are increasingly in-demand for network management due to their powerful ability of programmatically identifying network problems and providing instant diagnosis. Furthermore, to face future massive SDM era and demand uncertainty, the newly designed optical transport networks (OTNs) called spatial channel networks (SCNs) are proposed to serve the connection request with different traffic demands in the corresponding specific types of spatial channels (SChs). Otherwise, some robust optimization techniques such as Γ-robust optimization have been applied in network design with nondeterministic traffic.

As two main topics of optical network planning and management, routing and resource al-

location problems have been updated to accommodate the new characteristics introduced by the architecture evolution of optical networks. For example, with the spatial dimension added by SDM, the routing and spectrum assignment (RWA) problem in conventional WDM-based optical networks has been changed into the routing, spectrum, and space assignment (RSSA) problem in SDM-based optical networks. Generally, the routing and resource allocation problems in optical networks can be divided into static problems and dynamic problems. In the static case, the traffic request matrix with certain demands is given, and the main objective is to minimize the utilization of network resources such as the spectrum resources allocated in the network. In the dynamic case, the traffic request matrix is unknown and each request arrives at the network one after another. To solve the problems in the dynamic case, the overall network resources supported are given and the main objective is to find the best blocking probability or network throughput.

In summary, the development of optical network architectures introduces not only opportunities but also additional challenges to be addressed. The ML techniques and the SDN paradigm make it easier and more efficient for users and operators to control and manage the optical networks. However, it is difficult to achieve widespread deployment of programmable switches and fast reconfiguration of SDN control plane. Furthermore, a high capacity, high spectral efficiency, and flexible optical transmission can be realized in next generation SDM-EONs, but the implementation of SDM and EON brings some challenges such as the SDM fiber deployment issue, the intercore crosstalk (XT) avoidance issue and the survivability of such a complex SDM network. These findings demonstrate the critical importance and necessity of methods specifically designed to solve the routing and resource allocation problem. In this dissertation, we will introduce our research works on routing and resource allocation problems in optical networks detailed and summarize our contributions.

The organization of this dissertation is as follows. In Chapter 1, we give an overall introduction to the topics mentioned in this dissertation and give a brief illustration of our research works and contributions. In Chapter 2, we introduce the background of optical networks evolution and relevant communication technologies including five periods: 1) early fiber optics networks; 2) wavelength division multiplexing-based optical networks; 3) elastic optical networks; 4) space division multiplexing-based optical networks; 5) spatial channel networks. In Chapter 3, we introduce the research work of the device cost and network performance analysis for the SDM network deployment issues under different spatial and spectral granularity combinations. In Chapter 4, we introduce the research work of robust design for the SDM network with shared backup path protection considering network reliability against various network failures and uncertainty in traffic volume. In Chapter 5, we draw conclusions and future works of this dissertation.

Chapter 1

Introduction

With the development of communication technology and the increasing popularity of network services, multiple opportunities along with challenges have been brought to network communication. The communication system is composed of two categories according to the mode of signal transmission-wired communication system and wireless communication system. The main difference between wired communication and wireless communication lies in the transmission medium. In wireless communication systems, the antenna is an essential part and data is transmitted through non-physical media. In wired communication, data transmission is based on physical mediums such as cables and wires using electrical or optical signals. Optical communication, the topic that this dissertation focuses on, is one type of wired communication.

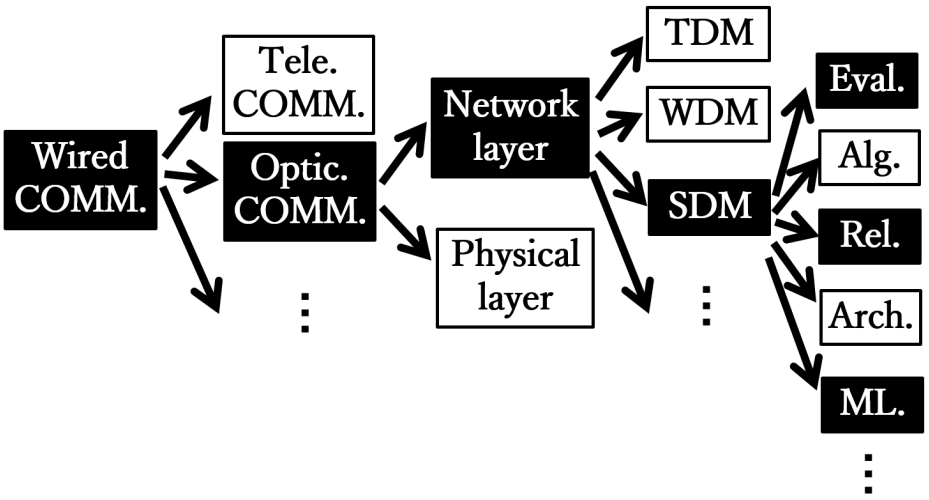

Figure 1.1: The main topics mentioned in this dissertation.

The tree view of the research topics mentioned in this dissertation is shown in Figure 1.1. There are two main topics of research works including the research on the physical layer and the research

on the network layer in optical communication. On the one hand, the increasing popularity of Internet services and users promotes the requirements for high communication levels of optical networks supported by emerging and promising optical technologies and physical components. On the other hand, the improvement of optical technologies and physical components introduces opportunities and challenges to problems of the network layer such as routing, resource allocation, and network protection.

According to different optical communication technologies, the research topics of the network layer are based on different architectures of optical networks. From the earliest TDM-based optical networks to WDM-based optical networks, further to flexible EONs and high-capacity SDM-EONs, and finally to future SCN-based optical networks facing massive SDM era. The research works in this dissertation mainly focus on solving the problems in SDM-based optical networks. The topics that this dissertation focus on including network planning considering routing and spectrum assignment problems, performance evaluation considering different architectures of SDM-based optical networks, design of heuristic routing and spectrum assignment algorithm, network reliability based on network protection techniques.

The research work "Evaluation of Optical Transport Unit Line-Card Integration in Spatially and Spectrally Flexible Optical Networks in terms of Device Cost and Network Performance" focuses on the network design and evaluation in SDM-EONs. We do the performance analysis with the metrics of device cost, maximum average throughput, average transceiver utilization and spectral efficiency for the N-core multi-core fiber (MCF)-based network deployment issues under different spatial and spectral granularity combinations. The results are obtained by solving a dynamic routing and resource allocation problem within an acceptable blocking probability.

The research work "Robust Design against Network Failures of Shared Backup Path Protected SDM-EONs" focused on the robust design of a N-single-mode-fiber-bundle (N-SMFB)-based SDM-EON with shared backup path protection (SBPP). Considering the network reliability in the face of different types of network failures and the uncertainty in traffic volume, we formulate the static RSSA problems for working and backup paths determination as two mixed integer linear programming (MILP) models with the objective of minimizing the maximal FS index used and the total number of backup FSs. In this scenario, we propose heuristic algorithms for routing decision and spectrum assignment, and we compare the spectrum efficiency and execution time among MILP models, our proposed algorithms, and the existing algorithm.

Chapter 2

Background

A network has the basic functionality of enabling data communication over a point-to-point or point-to-multipoint channel by means of different transmission approaches, including electronic signals along conductors, optical signals along optical fibers and so on. Therefore, the underlying properties have a significant impact on the network in terms of capacity, cost, and reliability.

Fiber optics was first introduced into telecommunication networks as a transmission medium in the 1980s when the first generation of fiber optics called graded-index fibers was implemented [1]. Fiber optics refers to a low loss and high efficiency technology that the data information is transmitted as light pulses through strands of fiber made of plastic or glass. It offers a selection of new features to the communication field, most notably a tremendous increase in transmission capacity. Such a promising technology not only opens a sweeping vista for data transmission but also promotes the development of optical networks.

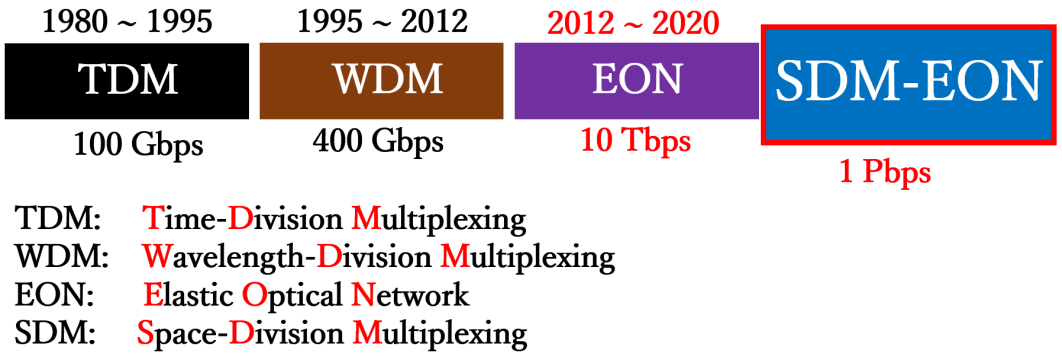

Figure 2.1: The evolution of the optical transmission system in the past few decades.

Optical networking is a communication system composed of fiber optic cables carrying data encoded in light and the optical components deployed processing light. The capabilities of optical networks are closely related to optical components and optical transmission technologies. Therefore, optical networks have undergone a remarkable change with the emergence and development

of exciting breakthrough technologies [2]. Although the evolution of optical networks shown in Figure 2.1 meets the high demand for transmission capacity, it also brings challenges in routing, resource allocation, and network management. In this chapter, we introduce the overview of the evolution of optical networks beginning with the earliest time division multiplexing (TDM)-based optical network using synchronous digital hierarchy (SDH), as well as the routing and resource allocation problem corresponding to each generation of optical networks.

2.1 Early Fiber Optics Transmission System

In response to the demand for increased bandwidth, high-quality service, and reliability, fiber optics transmission system was introduced to telecommunication networks in the 1980s. Compared to the older multiplex hierarchy known as plesiochronous digital hierarchy (PDH), SDH technology, which is the International Telecommunication Union Telecommunication Standardization Sector (ITU-T) version of the synchronous optical network (SONET) standard, provides faster and cheaper network interconnections. Due to the characteristic of global standardization, it is possible for SDH to be used in the optical layer as the interface, where the tributary signals of services such as PDH, asynchronous transfer mode (ATM), and Internet protocol (IP) are packed into SDH transport modules [3]. As shown in Figure 2.2, the TDM frames are multiplexed into high order ones by using SDH and SDH cross connect (XC) can flexibly and effectively manage the fiber optics transmission networks through electrical switching.

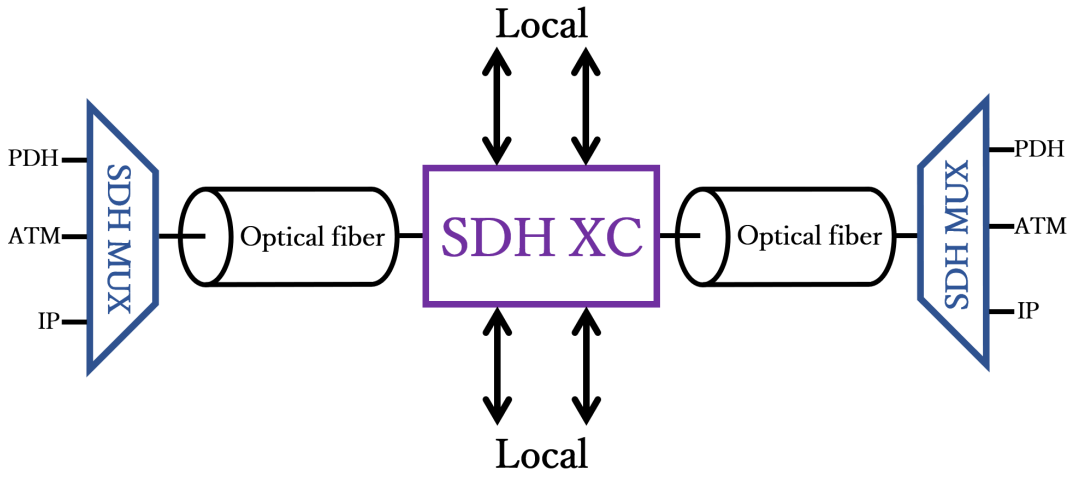

Figure 2.2: TDM-based optical transmission system using SDH.

2.2 Wavelength Division Multiplexing-based Optical Networks

Wavelength division multiplexing (WDM) became a better choice for large data transmission compared with electrical TDM after it was realized in the laboratory by 1980 [4]. WDM expands transmission bandwidth substantially by multiplexing numbers of optical signals onto an optical fiber through different wavelengths (frequencies). In this way, it allows different data streams to be sent simultaneously and maximizes fiber utilization.

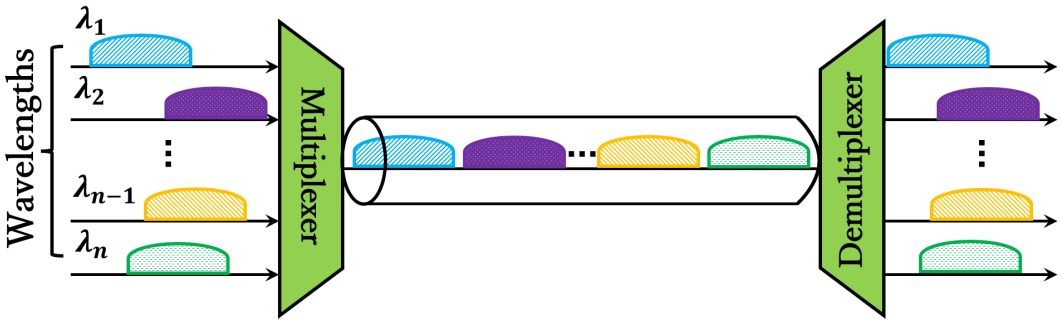

Figure 2.3: WDM operating principle.

As shown in Figure 2.3, a multiplexer (MUX) in the WDM system is used to join different wavelengths denoted by $\lambda_1, ..., \lambda_n$ together at the transmitter and a demultiplexer (DMUX) is used to separate them. WDM is based on the ability to carry different types of service by the light over an optical fiber. Instead of using multiple optical fibers for each service, it is possible to share a single optical fiber for several services.

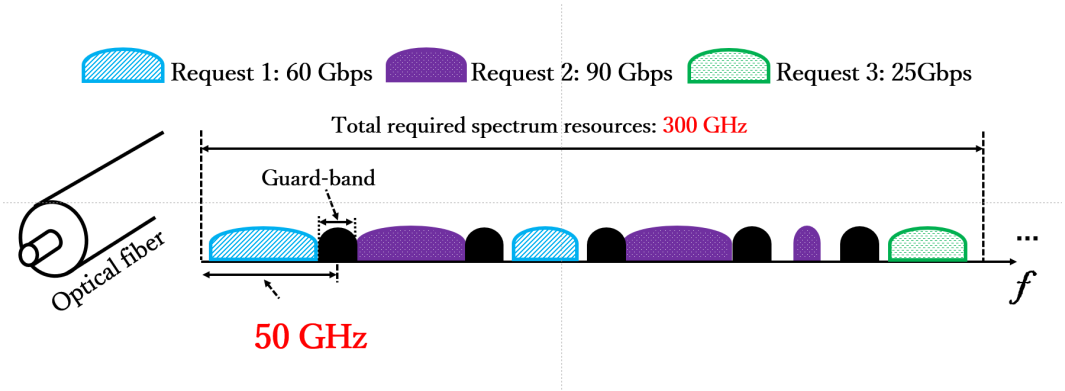

Figure 2.4: A fixed grid with 50 GHz channel spacing in WDM-based optical networks.

ITU-T G.694.1 standard WDM region is from 1528.77 nm to 1563.86 nm which resides mainly within the C-band. In a typical WDM system, 40 channels or 80 channels would be generalized at 100GHz (0.8nm) or 50 GHz (0.4nm) spacing, respectively [5]. As shown in Figure 2.4, a fixed grid

with 50 GHz channel spacing is used as an optical carrier in WDM-based optical networks to support three connection requests with different traffic demands. An optical carrier is the standard unit of measurement for the bandwidth rate of data transmitted, and the spectrum used for an optical carrier in Figure 2.4 should be less than 50 GHz due to the additional spectrum required for the switching guard band between two adjacent optical carriers. For example, with the 40 Gbps supportable bit rate, the total required spectrum resources are 300 GHz to support transmission for three requests with 25Gbps, 60 Gbps, and 90 Gbps.

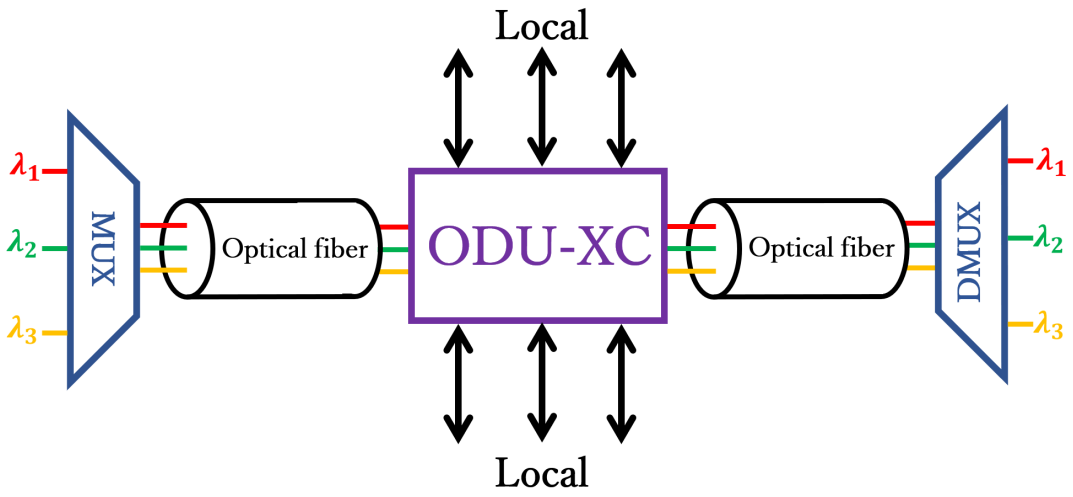

(a) WDM-based optical transmission system using ODU-XC

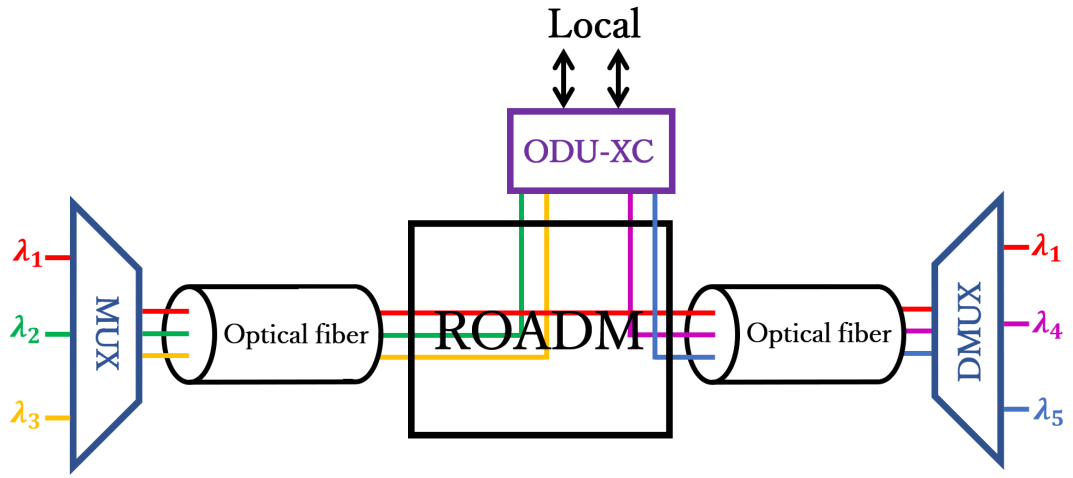

(b) WDM-based optical transmission system using ROADM

Figure 2.5: WDM-based optical transmission system using different technologies.

The first commercial WDM system was deployed in the early 2000s [6]. The explosive increase of capacity in WDM systems has emphasized the necessity of deploying a large number of electrical

terminals and switching devices, such as optical transceivers (transceivers and receivers) and optical channel data unit cross connects (ODU-XCs)/routers [50]. As shown in Figure 2.5(a), the processing of the data entering the node is implemented in the electrical domain, which causes problems of equipment costs and energy consumption. However, it is unnecessary to deal with all the data passing through a node electronically, but only part of the traffic serving this node as the source node or the destination node. To deal with a tremendous burden on ODU-XCs or routers, the fixed grid reconfigurable optical add/drop multiplexer (ROADM) is introduced to WDM systems. It allows wavelengths that are added or dropped at the node to be processed electronically and the remaining wavelengths to bypass the node electronics optically. Such a WDM-based optical transmission system with optical bypass technology, which is shown in Figure 2.5(b), can reduce overall electronic processing.

2.3 Elastic Optical Networks

Network traffic is increasingly demanding in terms of transmission capacity and distance due to the continuous development of the Internet. Traditional WDM-based optical networks are rigid and homogeneous, in which a fixed spectrum grid composed of multiple wavelengths is supported under a single modulation format [8]. Such a low spectral efficiency network can no longer meet the increasing traffic demands in transport networks.

The main requirements for next generation optical networks include: 1) Higher fiber capacity due to the increasing Internet traffic. 2) Higher optical channel capacity due to the increasing speed of the client interface. 3) Lower resource and cost consumption due to the goals of economization and ecologization. To achieve those goals mentioned above, an emerging and improved technology called elastic optical networking (EON) has been put forward to increase spectral efficiency as a solution for next generation optical networks.

EON, which was first proposed as the spectrum sliced elastic (SLICE) optical network in 2008, enables the technologies of spectrum resource slicing and elastic allocation [9–11]. The key feature of EON is to provide more efficient traffic grooming by increasing spectral efficiency. On the one hand, due to the implementation of coherent optical detection by digital signal processing (DSP), and it makes it possible to use the in-phase and quadrature-phase components and the optical filed polarization [12]. Through the usage of DSP in the optical transceiver, some multicarrier modulation technologies such as coherent optical orthogonal frequency division multiplexing (CO-OFDM) and nyquist wavelength division multiplexing (N-WDM) are realized to make the optical transmission more spectrally efficient. On the other hand, the spectral efficiency in bits per second per hertz (bit/s/Hz) can be computed by the product of the modulation level in bits per symbol (bit/symbol) and the baud rate in symbols per second per hertz (symbol/s/Hz). Therefore, increasing the mod-

ulation level and baud rate can also improve spectral efficiency. However, due to the nonlinear Shannon limit and the boundedness of current conversion technology (analog to digital/digital to analog conversion (ADC/DAC)), increasing the number of bits per symbol and symbol rate becomes increasingly difficult and challenging.

Multiple promising technologies in EON enable the optical networks to be more flexible and heterogeneous, leading to a more flexible and efficient optical transmission. Those enabling technologies for EON are introduced in detail as follows.

2.3.1 Spectral Superchannel

A superchannel in elastic optical networks (EONs) refers to a group of modulated and multiplexed optical signals that are transmitted together. CO-OFDM and N-WDM are the two most effective multiplexing techniques that encode data on multiple carrier frequencies. As mentioned in Section 2.3, two methods are commonly used to increase spectral efficiency. One method uses high-level modulation formats such as quadrature phase shift keying (QPSK), 8-quadrature amplitude modulation (QAM), and 16-QAM [13]. However, the modulation level can not increase indefinitely because higher-order modulation formats will cause a worse signal to noise ratio (SNR). Another method uses modulating technologies with high spectral efficiency such as CO–OFDM and N-WDM. By aggregating multiple OFDM subcarriers or N-WDM subbands together, high spectral efficiency and high speed superchannels in EON can be obtained.

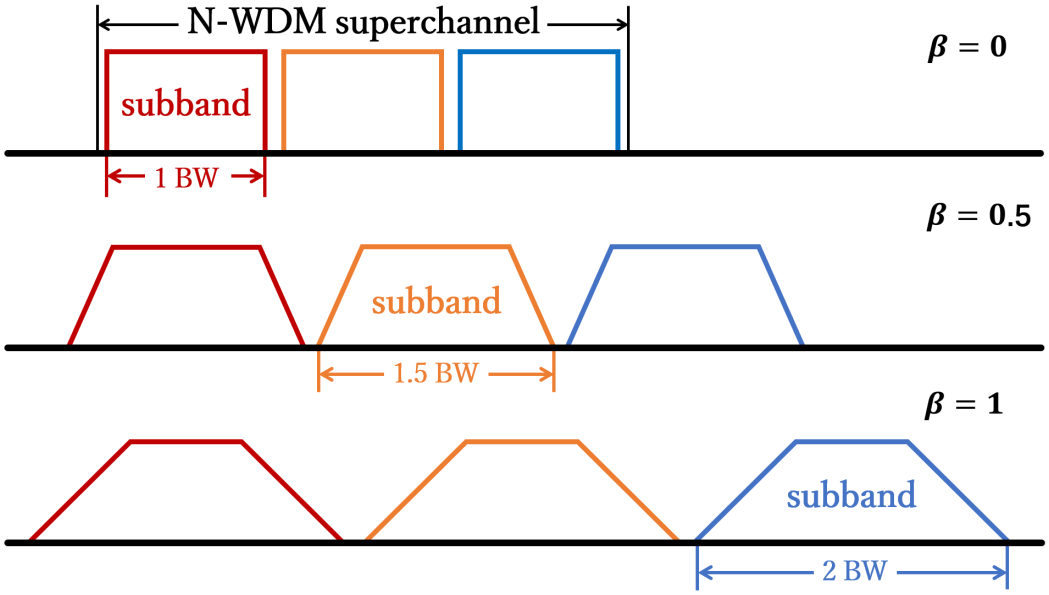

Figure 2.6: Nyquist-WDM superchannel.

As shown in Figure 2.6, an N-WDM superchannel is obtained by the aggregation of multiple subbands in a WDM way. The occupied spectrum of an N-WDM subband is identical to the symbol

rate of the data BW in the ideal case, which is indicated at the top of Figure 2.6. However, due to the spectral penalty caused by the Nyquist-shaping filter with a certain resolution, the actual spectrum occupation denoted by $(1+\beta)BW$ is related to the filter roll-off factor β. The N-WDM superchannels with different values of β are shown at the bottom of Figure 2.6.

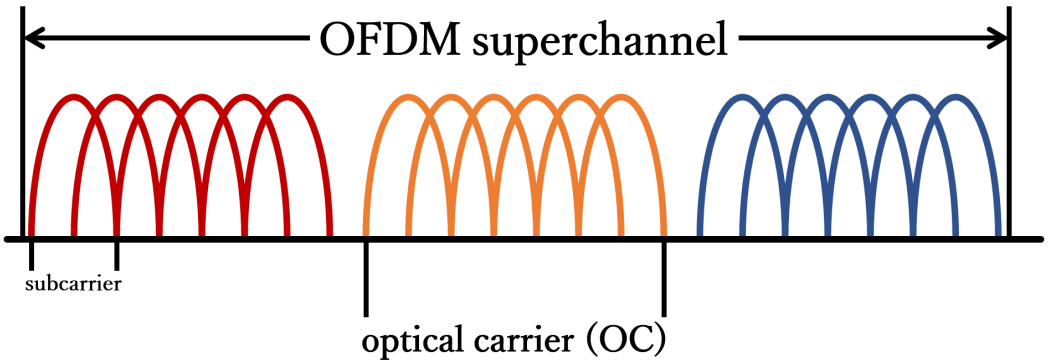

Figure 2.7: OFDM superchannel.

On the other hand, an OFDM superchannel is composed of multiple subcarriers, each of which uses a rectangular pulse and its frequency spectrum has a sinusoidal shape [14]. As shown in Figure 2.7, OFDM subcarriers are separated at baud rate intervals so that there is no interference between subcarriers. Using spectral superchannel technology, the transmission system becomes flexible and high-capacity. Breaking through the bottleneck of electrical bandwidth makes it possible to improve the line rate. Furthermore, the line rate can be flexibly adjusted with varying numbers of subchannels according to traffic demands.

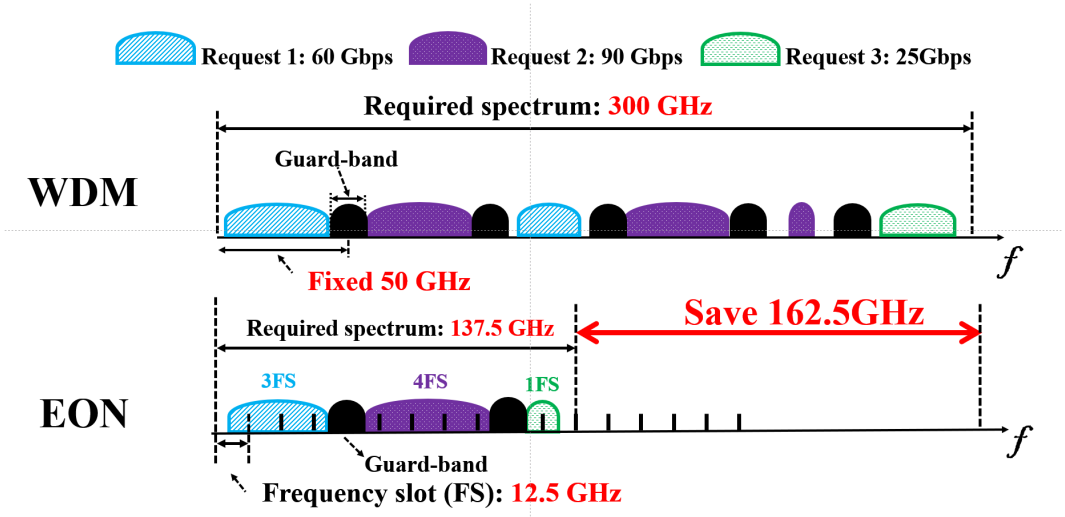

Figure 2.8: WDM-based optical transmission vs. EON-based optical transmission.

According to ITU-T G.694.1, a new concept called frequency slot (FS) is defined as the overall occupied frequency range in an optical channel. The width of an FS can be computed by an integral multiple of 12.5 GHz and the central frequency of FSs is defined by 193.1 THz plus or minus an integral multiple of 6.25 GHz. A simple example of comparison with WDM-based optical networks mentioned in Section 2.2, to support three requests with different traffic demands of 25 Gbps, 60 Gbps, and 90 Gbps, respectively, the total spectrum resource requirement in EON-based optical networks is 137.5 GHz, which achieves significant 162.5 GHz spectrum savings as shown in Figure 2.8.

2.3.2 Wavelength Selective Switch

Another technology that enables elastic optical networking is the bandwidth variable wavelength selective switch (BV-WSS). In traditional WDM-based networks, wavelength cross connects (WXCs) and ROADMs are essential components for optical transmission. However, with the rapid development of internet traffic, the challenges of increased structural complexity, footprint, and cost faced by the WXCs emphasized the necessity of its improvement. Therefore, the WSS is proposed as an emerging optical component to increase the switching flexibility and reduce the complexity of architecture [15].

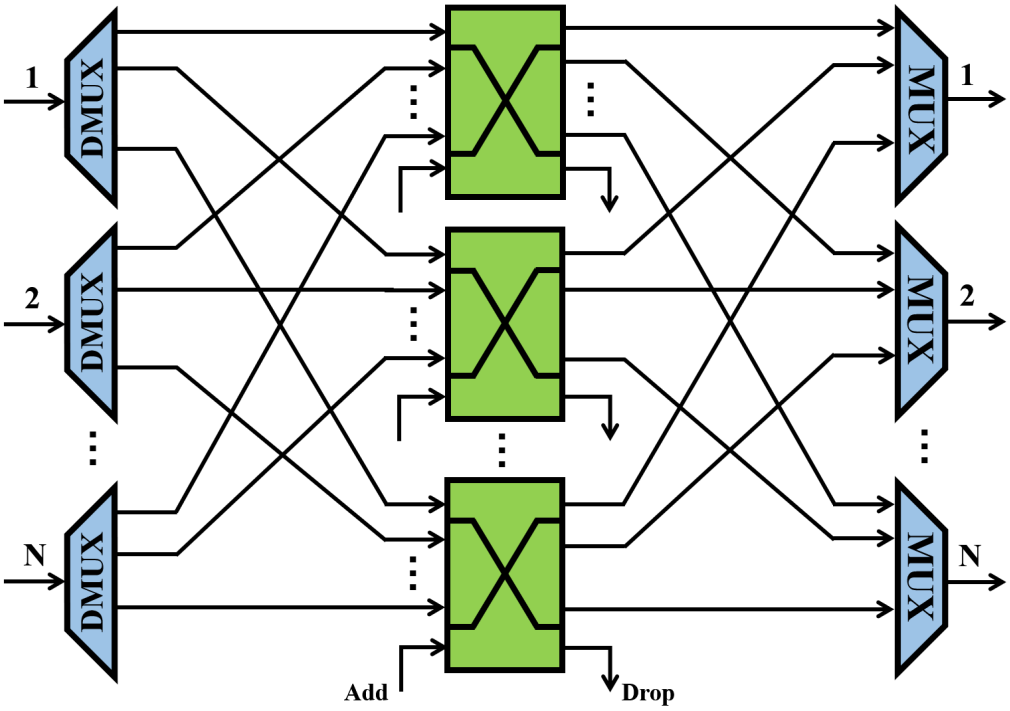

Figure 2.9: Architecture of a conventional N×N WXC.

A WSS is an integrated optical switches and multiplexer/demultiplexer (MUX/DMUX) subsys-

tem for wavelength switching. In other words, the WSS is considered a tunable MUX/DMUX that can handle the switching of wavelength sets with different numbers of wavelength [16]. Therefore, the implementation of WXC based on WSSs can simplify the complexity of its architecture. Figure 2.9 shows the architecture of a conventional WXC with N input ports and N output ports. The input WDM signal is separated into different wavelengths by a DMUX at each input port, then the wavelengths with the same index from different input ports are cross connected by an optical switch, and each set of different wavelengths are multiplexed by a MUX and finally sent to each output port.

Due to the internal switching characteristic of WSS, the WSS-based OXC can achieve simpler architecture and more flexible switching compared with the conventional WXC. An N×N WSS-based WXC is shown in Figure 2.10, where any wavelength set can be cross connected, added, or dropped between different WSS pairs. In addition, there are two main types of WSS: One is a micro electro-mechanical systems (MEMS) mirror based WSS with a fixed bandwidth (related to the mirror width) [17]; Another is a bandwidth variable WSS based on liquid crystal on silicon (LCoS) spatial light modulator [18].

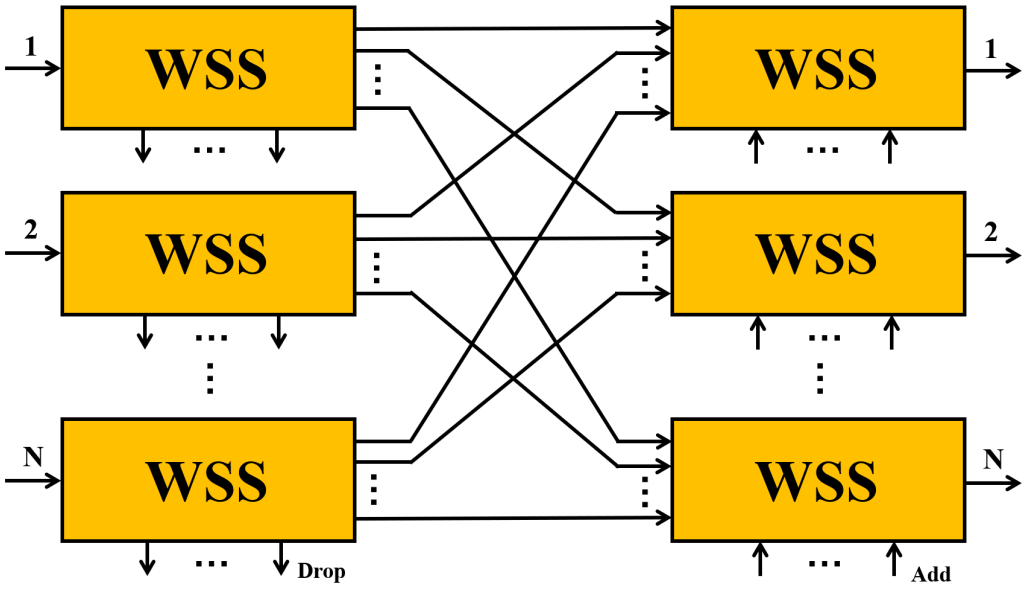

Figure 2.10: Architecture of a WSS-based N×N WXC.

2.3.3 Routing and Spectrum Assignment

Network designing typically includes specifying the network topology and determining the devices to be installed on network nodes to completely serve the connection requests while minimizing network capital expenditures (CAPEX) [19]. Before deploying a flexible grid EON-based optical network, the routing and spectrum assignment (RSA) problem is the main topic to be considered. Three primary constraints are necessary to be considered in the RSA problem: the spectrum conti-

nuity constraint, the spectrum contiguity constraint, and the spectrum non-overlapping constraint.

Figure 2.11 illustrates the three constraints of spectrum continuity, contiguity, and non-overlapping in EONs. The spectrum continuity constraint ensures that the same allocated FSs must be used along the links of the route for each connection request. The spectrum contiguity constraint ensures that the allocated FSs must be adjacent in the spectrum [20]. The spectrum non-overlapping guarantees that the FSs assigned for different connection requests along the same link should not overlap.

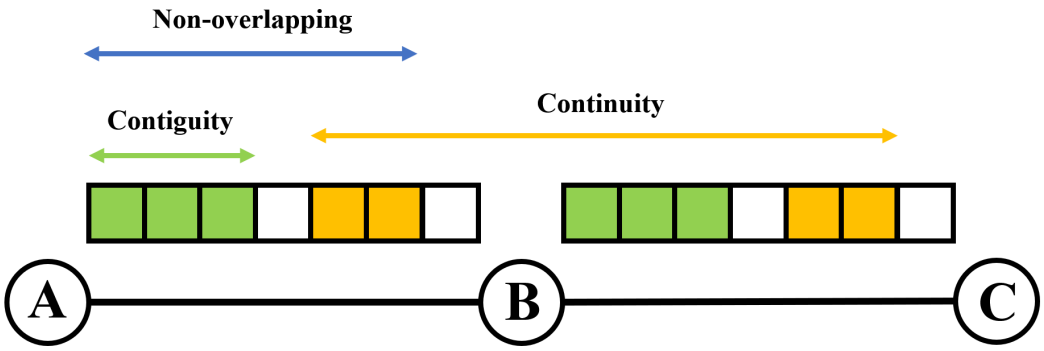

Figure 2.11: Constraints of spectrum continuity, contiguity, and non-overlapping in the RSA problem.

The RSA problem aims to find suitable lightpaths including routes and spectrum assignments for connection requests with the defined objective function. The RSA problem has been proved to be nondeterministic polynomial (NP)-complete so that the set of its solution can be verified in polynomial time [21, 22].

2.3.4 Grooming

With the growth of the types and quantity of network services, the traffic required rates are uncertain, and most of them occupy less than one wavelength for transmission [23]. Therefore, such a transmission approach carries a connection request using a full wavelength, resulting in a waste of spectrum resources. End-to-end multiplexing is considered an effective solution to carry multiple traffic demands with the same source and destination together in a single wavelength. Those demands are transmitted as an entity from source and destination. Such a multiplexing method improves the spectrum utilization efficiency but it can not make sense if the total traffic volume between the same node pairs is relatively small. Therefore, grooming is proposed as an improved end-to-end multiplexing method that allows the traffic demands to be aggregated at both the endpoints and intermediate points.

Grooming allows the traffic demands even with different endpoints to be carried at the same wavelength and is considered a feasible method to improve spectrum utilization efficiency.

As indicated in Figure 2.12, fourteen requests with different traffic demands are transmitted between different source-destination pairs: two requests with 10 Gbps from node A to node H, one request with 10 Gbps from node A to node I, four requests with 2.5 Gbps from node A to node K, two requests with 2.5 Gbps from node B to node H, four requests with 2.5 Gbps from node B to node I, and one request with 10 Gbps from node B to node K. With the assumption of a 40 Gbps line rate supported by each wavelength, we can find that one wavelength carrying two 10 Gbps traffic between node A and node H is only half used by end-to-end multiplexing. The average spectrum utilization of six wavelengths for the transmission of those requests is 27%. It is worth mentioning that if all the requests are transmitted by independent wavelengths without using multiplexing, the average spectrum utilization is 12% which is far less than using end-to-end multiplexing.

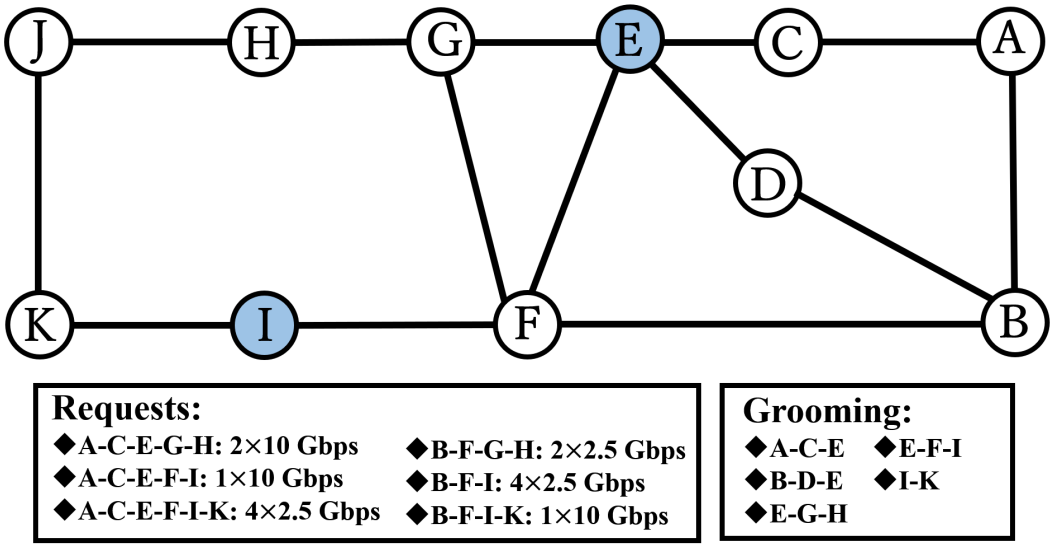

Figure 2.12: End-to-end multiplexing and intermediate grooming in a simple network topology.

Grooming attempts to form the wavelengths for transmission of connection requests passing through particular intermediate nodes. One of the possible grooming strategies that the wavelengths are groomed at intermediate nodes E and I, which is shown in Figure 2.12. Thus, there exist five wavelengths for those fourteen requests with grooming. A single wavelength carries the traffic requests passing from node A to node E. Similarly, the traffic demands at node B are transmitted to node E on another single wavelength. Besides, one wavelength at node E is used to carry traffic requests whose destination is node H regardless of source nodes. Two wavelengths left are used for transmissions of traffic requests from node E to node I and from node I to node K. Compared with end-to-end multiplexing, grooming has two main advantages: the first is that number of required wavelengths by grooming is less than that by end-to-end multiplexing; the second is that the average spectrum utilization using grooming is 75%, which is far more than 27% using end-to-end multiplexing.

Grooming is implemented by installing the switches of specific fabric on the nodes, which improves spectral efficiency and routing flexibility of optical transmission. The traffic demands added at the node are allowed to be compressed into wavelengths together with the traffic demands passing through that node in a grooming switch. [24, 25]. The architecture of a grooming switch is shown in Figure 2.13. A ROADM achieves optical bypass with no additional cost for photoelectric conversion by making the traffic demands remain in the optical domain. The grooming switch is an edge switch that is only used for traffic demands that need to be aggregated.

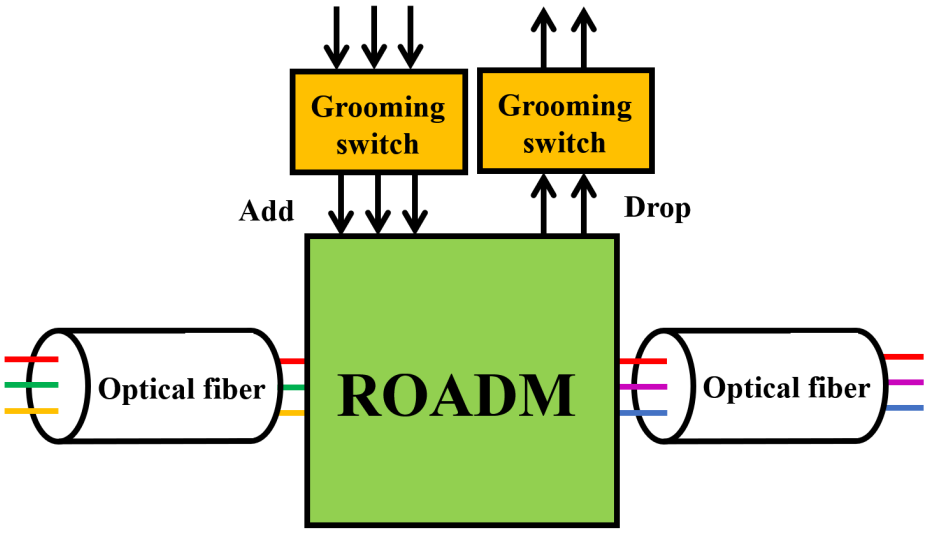

Figure 2.13: Grooming switch at the nodal edge.

2.4 Space Division Multiplexing-based Optical Networks

EON is considered a short-term solution to increase transmission capacity by maximizing spectral efficiency with finer grid spectrum resource usage [26]. However, as the traffic volume carried by OTNs is increasing at a high rate, extending fiber capacity beyond the C-band is regarded as a long-term approach to solving the problem of transmission capacity shortage. There are two possible solutions: increasing the telecommunication window such as other bands (L-band, S-band) beyond C-band [27] or introducing parallelism such as fiber overlays [28]; the expansion of space channels from one dimension to multiple dimensions by space division multiplexing (SDM) technology. However, increasing the telecommunication window or introducing parallelism is not a promising approach due to its low compatibility and high complexity. Therefore, SDM has emerged as an effective solution to overcome the capacity upper limit and keep up with rapidly increasing network traffic.

2.4.1 SDM Optical Fibers

To demonstrate the space expansion, different types of optical fibers can be used in SDM-based optical networks, such as multi mode fibers (MMFs), multi core fibers (MCFs), and single mode fiber bundles (SMFBs).

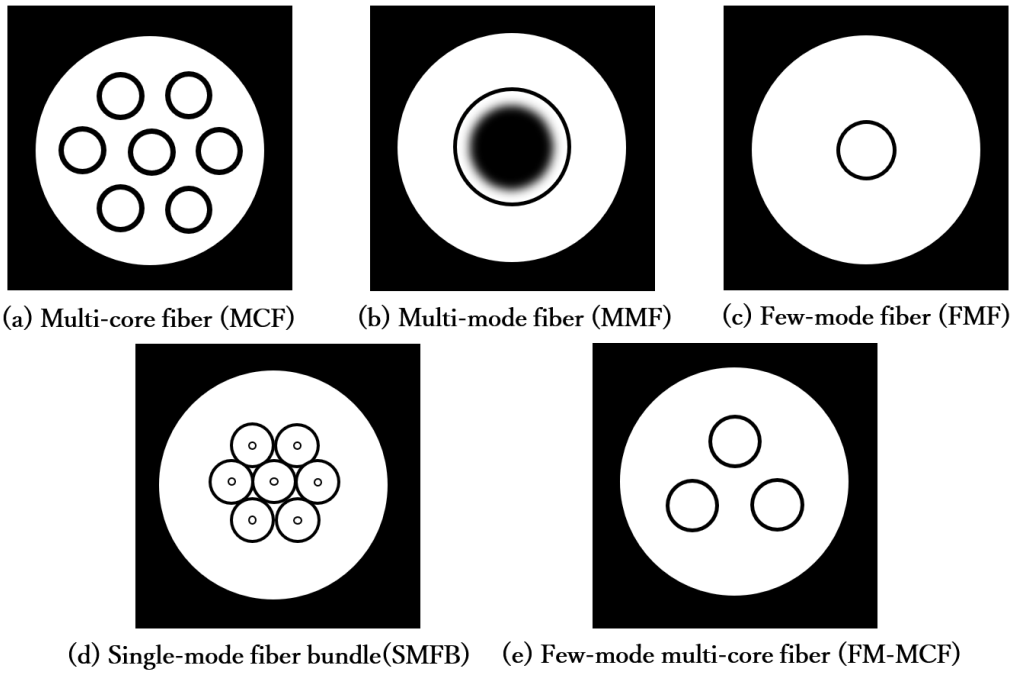

Figure 2.14: Different types of SDM fibers.

Figure 2.14 shows different types of SDM fibers. One of the most direct ways to realize SDM fibers is to bundle multiple SMFs together, which is called an SMFB. Another popular way to achieve SDM is with MCFs, which have various numbers of cores inside a single cladding [29]. Compared with the SMFB, the MCF has better space efficiency, but its transmission distance is shorter due to the effect of intercore XT. Moreover, mode division multiplexing (MDM) technology can also support SDM networks. MMFs and few-mode fibers (FMFs) are the two most common types of SDM fibers implemented by MDMs [30]. The MMF supports the transmission over a single core in tens of strongly coupled modes. The FMF is basically the same as the MMF but allows few-mode propagation. To realize such SDM fibers with multiple modes, an SDM MUX and DMUX which include specific mode conversion components are required. Both MMF and FMF are the most commonly used fiber types in short-distance transmissions, such as local area networks (LANs).

Additionally, another fiber concept, which is the combination of MCF and FMF, called few-mode multicore fiber (FM-MCF), is a promising SDM approach. The FM-MCF is an uncoupled MCF that has multiple few-mode cores, and it integrates the advantages of both. However, the

design of FM-MCF still has many issues to address, such as the optimization of core and mode count [31].

2.4.2 SDM Amplification

Amplification is an indispensable part of communication networks, especially for long-haul transmission networks such as the national backbone networks. The loss of the light passing through a long-distance transmission over the optical fiber (10 km or 100 km) can not be ignored so the installation of optical amplifiers at a regular distance (generally 80 km) ensures reliable transmission. Therefore, the integrated SDM amplifier is a crucial and necessary optical component for the deployment of future SDM-based optical networks [32].

The optical amplifier consists of two types including the optical fiber amplifier (OFA) and the semiconductor optical amplifier (SOA), and OFA can be further divided into two different optical amplifiers: the fiber raman amplifier (FRA) and erbium doped fiber amplifier (EDFA) [33]. An EDFA is an optical amplifier that adds erbium ions to the fiber core, which is shown in Figure 2.15. It has the characteristics of high gain, low noise, and polarization-independent. In addition, the optical signals can be amplified in the 1.55 μm band or 1.58 μm band. An FRA causes stimulated emission with the entry of strong excitation light into the optical fiber based on stimulated raman scattering (SRS). The optical signals amplified by the FRA can achieve a wavelength range that is about 100 nm longer than the excitation light wavelength. The FRA has advantages of a wide amplification wavelength region and free setting. The SOA is a semiconductor element whose size is more compact, leading to a lower cost compared with the OFA. In an SOA, by performing antireflective processing on the cleavage plane of a semiconductor laser and eliminating the resonator structure, light can enter from outside the semiconductor and be amplified through excitation.

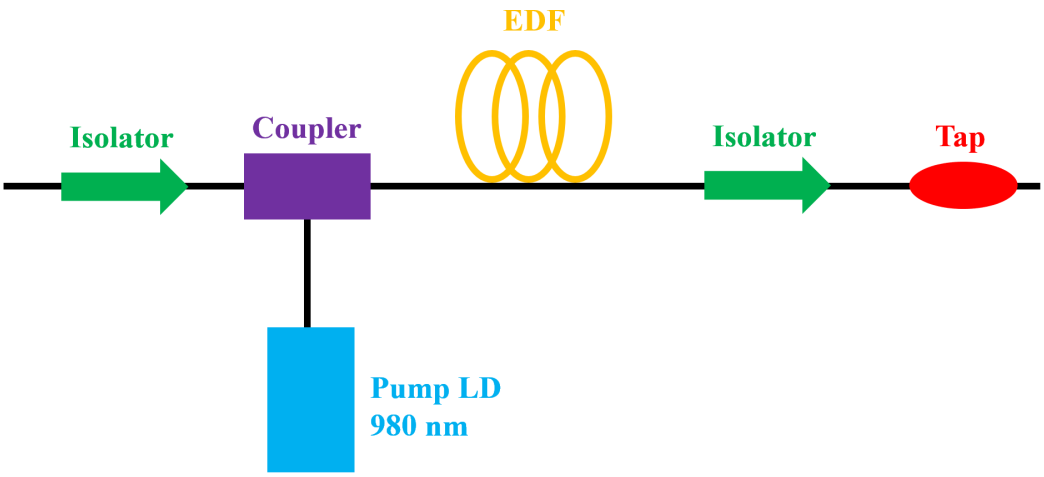

Figure 2.15: Block diagram of an EDFA.

Several SDM amplifiers are proposed for SDM networks with different architectures. 1) The pumped-distributed raman amplifier [34, 35] is proposed to support the transmission of long-haul FMF-based and MCF-based optical networks. 2) The fiber bundle EDFA [36] is proposed for SMFB-based optical networks with characteristics of low XT and uniform gain. 3) The multi-element EDFA for core or cladding pumping [37] such as the 7-core EDFA with a gain over 25 dB and the few mode EDFA with a gain over 20 dB.

2.4.3 SDM Multiplexer and Demultiplexer

The coupling of SDM fibers such as MCFs and MMFs is a critical and challenging issue that impacts the reliability, routing efficiency, and viability of SDM networks. The SDM fiber coupling can be divided into the direct coupling and indirect coupling. Indirect coupling is a free-space optical method that relies on a lens system [38]. A large number of MCFs can be extended and XT can be suppressed by indirect coupling. However, it has a huge scale and requires complex optomechanics. On the other hand, direct coupling implements a wavelength optical interface that directly connects multiple SMFs as an MCF. There are two main direct coupling approaches including tapered multi core connector (TMC) or known as simply tapered cladding [39] and waveguide coupling [40]. An MCF can be spliced with a bundle of tapered cladding SMFs, and the spacing of the cores inside the fiber taper is reduced to the same core spacing as the MCF. This approach is susceptible to phonographic interference and requires advanced slicing technology, but is compact and highly commercialized [41]. Another direct coupling approach is called waveguide coupling where several SMFs are connected to an MCF, and each SMF is coupled to a particular core of the MCF by inscribing spatially isolated waveguides. Waveguide coupling is such a low complexity, flexible and compact coupling approach that it has been commercialized by Optoscribe [42].

2.4.4 SDM Transceiver

The optical transceiver (TxRx) is implemented by the integration of the transmitter (Tx) and receiver (Rx). The block diagram of an optical TxRx is shown in Figure 2.16 [44]. In this figure, DSP denotes digital signal processing, LPF denotes low-pass filter, DAC/ADC denotes digital-to-analog converter/analog-to-digital converter, DRV denotes optical modulator driver amplifier, LS/LO denotes laser source/local oscillator, I/Q MZM denotes in-phase/quadrature Mach-Zehnder modulator, PBC/PBS denotes polarization beam combiner/polarization beam splitter, and PD denotes photodiode.

In a TxRx, a Tx aims to encode the data onto the optical carriers (OCs). The input discrete digital signal is converted to a continuous analog signal by a DAC. The modulator attaches the analog electrical signal to the OCs generated by an LS. A Rx decodes the data carried by OCs. The coherent receiver mixes the input optical signal with an LO to obtain an intermediate frequency

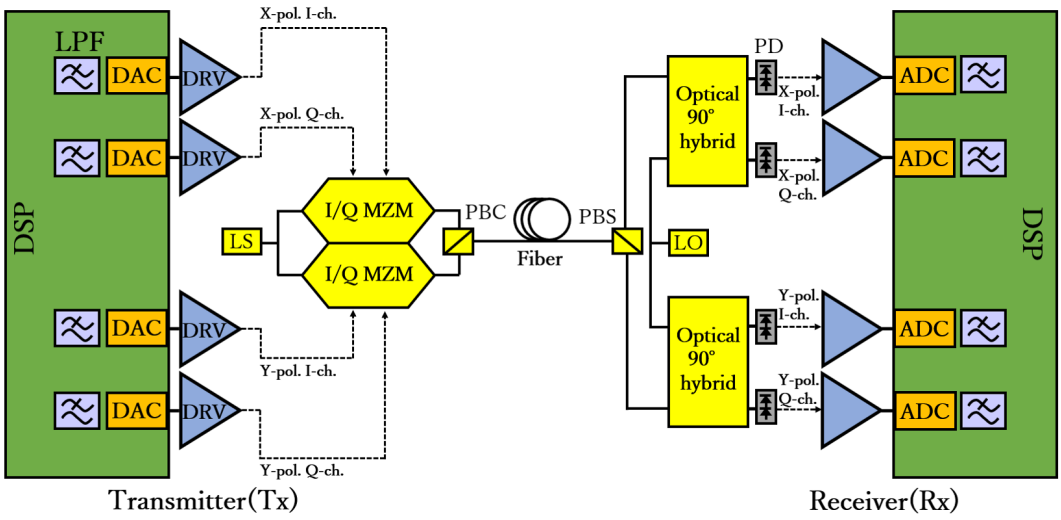

Figure 2.16: Block diagram of an optical transceiver.

analog signal. Then, an ADC converts the input analog signal into a digital signal. Finally, the information carried by the signal is obtained by the DSP module.

An SDM TxRx, also known as a spatial and spectral superchannel transceiver (Spa & Spe SpCh TxRx), is the integration of single-carrier optical TxRxs in spatial and spectral domains. A spatially and spectrally integrated SDM TxRx is composed of an integrated Tx and an integrated Rx, which is shown in Figure 2.17. An $S \times O$ SDM TxRx is generated by O continuous single-carrier TxRx distributed over S spatial dimensions.

2.4.5 SDM Reconfigurable Optical Add/Drop Multiplexer and Spatial Lane Change

To guarantee the successful application of SDM technology in optical fiber transmission networks, wavelength channel adding/dropping and flexible switching is essential for transmission systems. The reconfigurable optical add/drop multiplexer (ROADM) is considered to provide flexible switching in both the spectral and spatial domains which promote the realization of groups of optical channels carried by the same wavelength under different cores(modes) supported in an SDM fiber.

Generally, the ROADM can be classified into several types according to different standards. Firstly, a ROADM can be divided into two categories according to wavelength switching strategy: colored and colorless. A colored ROADM enables each port can only add or drop fixed wavelengths, conversely, wavelengths can be added or dropped through any port on a colorless ROADM board. Secondly, according to the constraint of transmission direction, a ROADM can be divided into a directional one and a directionless one. A directional or directionless ROADM enables wavelengths can be transmitted in specific directions or any direction, respectively. Furthermore, a contentionless ROADM refers to a ROADM where optical signals over different wavelengths can be received from

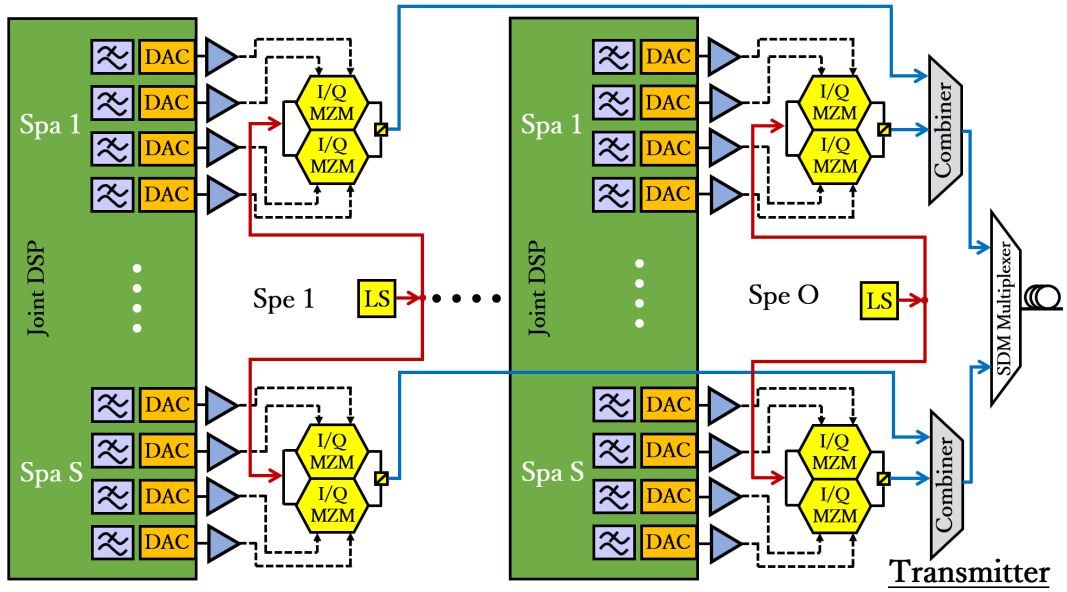

(a) An $S \times O$ SDM Tx

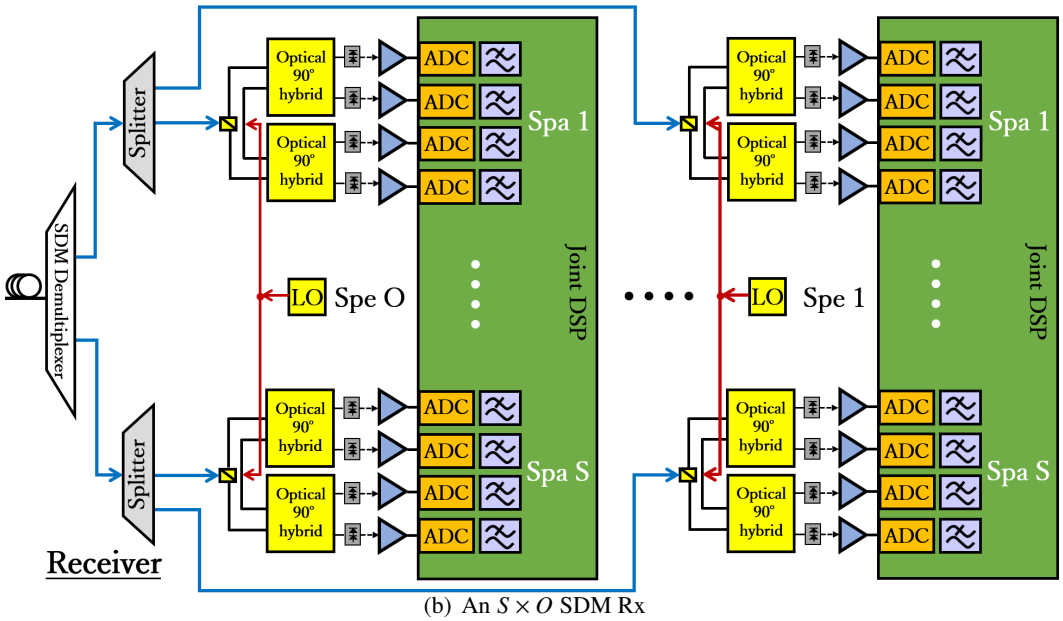

(b) An $S \times O$ SDM Rx

Figure 2.17: Architecture of an integrated $S \times O$ SDM transceiver.

any direction and added or dropped on the same module without being blocked.

SDM ROADMs provide flexible switching between the space domain and the spectral domain. Different ways are proposed to implement SDM ROADMs ranging from EON to SDM-EON with flexible mode allocation [45]. One way to achieve wavelength granularity switching is to switch the wavelength with the same index in fixed spatial superchannels along the cores of the SDM fiber. This can be easily achieved by using wavelength selective switches (WSSs) on the basis of each wavelength. Another way is more flexible that various combinations of wavelengths can be allocated in different cores of the SDM fiber instead of fixed spatial superchannels. In this way, the design of the switching nodes is more complex with requirements of multiple WSSs and optical cross connects (OXCs) with high port counts. A simple example of the SDM ROADM is shown in Figure 2.18.

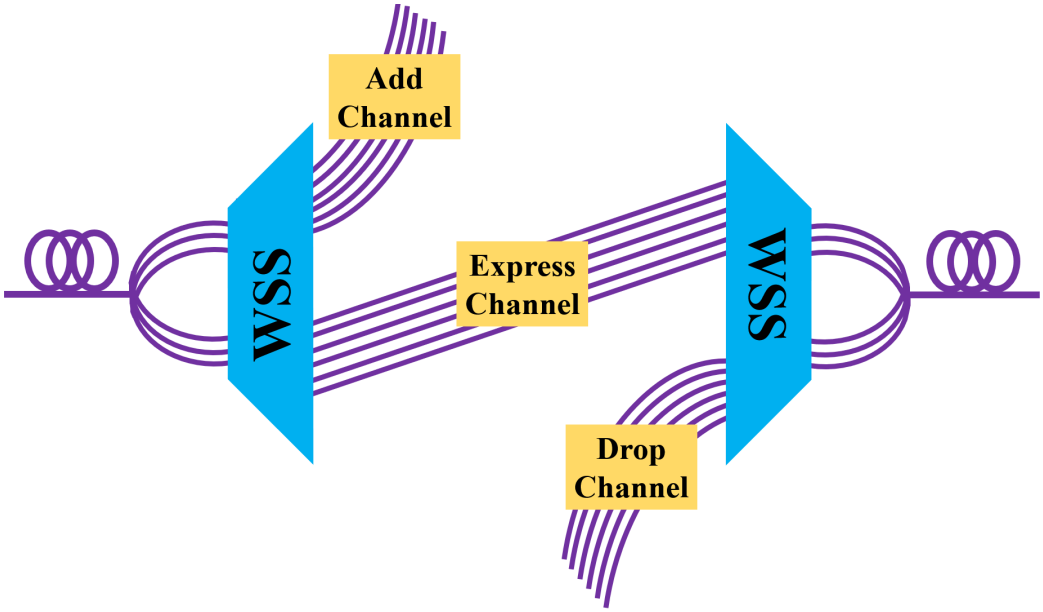

Figure 2.18: A simple example of the SDM ROADM.

As shown in Figure 2.19, two requests with different traffic demands are switched with 2×3 Spa & Spe SpCh transceivers through ROADMs. Multiple transceivers and a ROADM are installed on each node for transmission. For example, the request which needs two transceivers for transmission from the west side to the east side is output by transmitters of SDM transceivers 1 and 2 to the add/drop module in ROADM 1, then after traversing SDM fiber between ROADM 1 and 3, the request is finally dropped to the east side by the add/drop module in ROADM 3.

Another newly proposed technology called spatial lane change (SLC) can achieve higher flexibility and have an impact on the architecture of the ROADM. SLC technology enables the superchannel in each spatial group to be freely switched to any output port.

As indicated in Figure 2.20, to explain the SLC technology concretely, we give a simple exam-

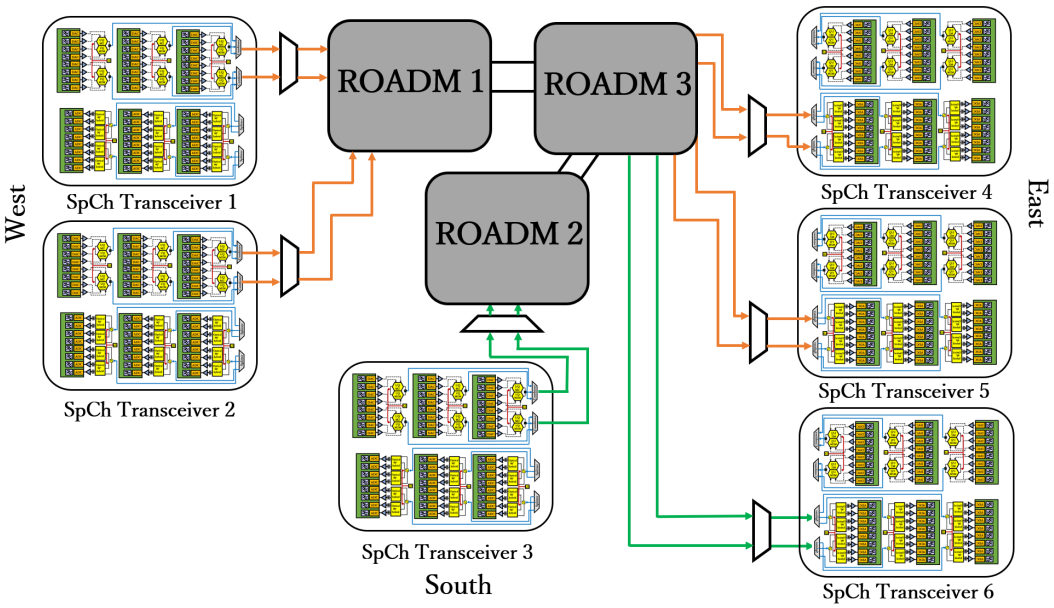

Figure 2.19: Illustration of switching between different nodes by 2×3 SDM transceivers.

ple of switching paradigms supported by SLC or not from west to the east. The dotted lines show the signals transmitted from east to west, and the solid lines represent the transmission in the opposite direction. Figure 2.20(a) indicates the switching paradigm without the support of SLC technology. The input channel in each subgroup of four spatial groups needs to be switched to the output port with the same group index as the input port. In contrast, as shown in Figure 2.20(b), switching with SLC technology support does not need to contain the spatial continuity constraint. Input from each spatial subgroup can be switched to any index of output ports independently. In particular, whether SLC technology is supported makes a difference in the switching paradigms of independent switching (InS) and fractional joint switching (FJoS). However, all the spatial dimensions are switched together in the joint switching (JoS) paradigm so that with or without SLC technology support is equivalent. Therefore, SLC technology can offer higher routing flexibility in general but increases the complexity and cost of the network architecture.

2.4.6 Spatial and Spectral Superchannel

Due to the limitation of current conversion technology, the supportable symbol rate of a transceiver is limited. To overcome this limitation and expand transmission capacity, spatial and spectral superchannel (Spa & Spe SpCh) transmission is proposed to gather multiple contiguous OCs as a superchannel.

As shown in Figure 2.21, a spectral superchannel consists of multiple OCs and there are no switching guard bands (GBs) between the adjacent OCs in a Spa & Spe SpCh. An OC generated under DP-BPSK modulation by a single carrier transceiver whose symbol rate is 32 Gbaud with

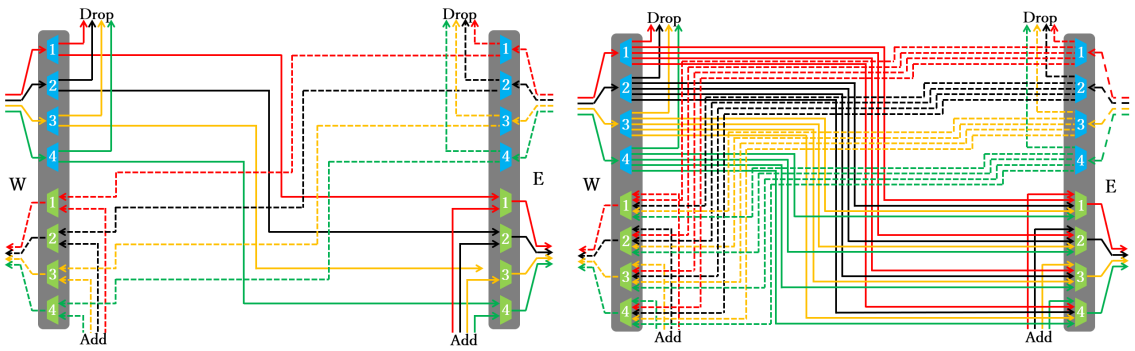

(a) NSLC (b) SLC

Figure 2.20: Illustration of two switching patterns for a 4-core MCF supported by SLC technology or not in the west-east direction.

considering 7 Gbaud ECC can support 50 Gbps net traffic volume. The assumption of 32 Gbaud symbol rate shaping with 3.125 GHz filter resolution in this research enables the relatively higher spectral efficiency, lower cost consumption and deployment complexity compared with high symbol rate transceivers [46]. According to ITU-T g.694.1, the spectral granularity is set as a 12.5 GHz grid. Therefore, the spectrum occupation of the OC must be an integer multiple of it, that is, 3 FSs. Moreover, the GB on both sides of the superchannel is 6.25 GHz.

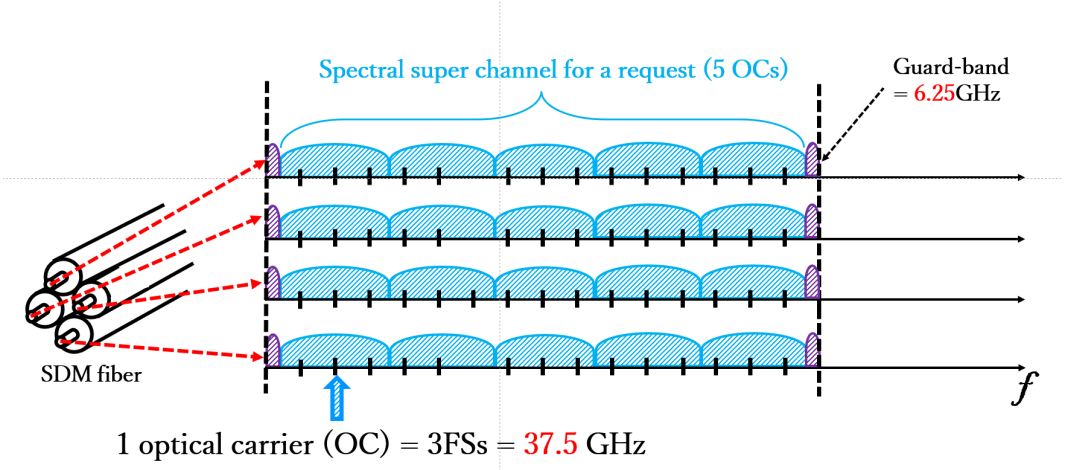

Figure 2.21: Spatial and spectral superchannel transmission.

In a N-core SDM fiber-based optical transmission, a group of spatial dimensions used for transmission is called the spatial granularity, denoted by S, and a group of adjacent OCs used is called spectral granularity, denoted by O [31]. Core number N must be an integer multiple of spatial granularity S.

As shown in Figure 2.22, a simple example of a 4-core MCF is given, where the spatial granularity S is set to 1, 2, and 4. The Spa & Spe SpCh are separated into three types according to different

switching strategies in SDM networks: 1) independent switching (InS), in which the Spe SpChs are transmitted independently in each spatial mode; 2) fractional joint switching (FJoS), in which the spatial modes are divided into groups, and the Spe SpChs in each spatial group are transmitted together; and 3) joint switching (JoS), where all the Spe SpChs in each spatial mode are treated as a whole to be transmitted.

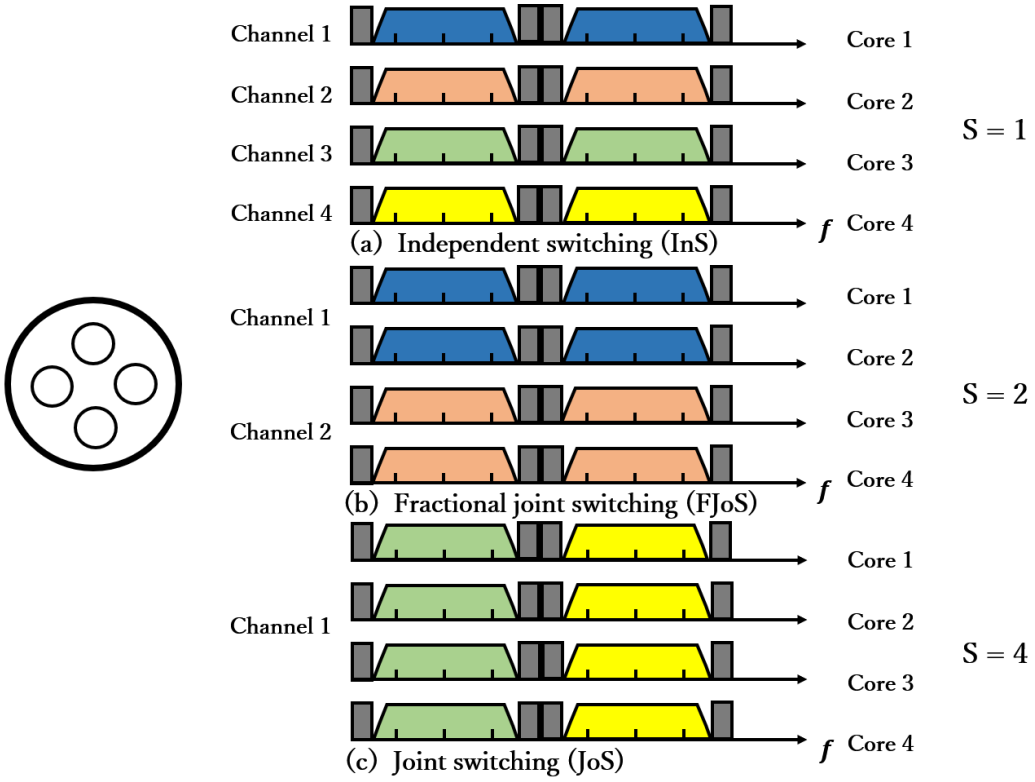

Figure 2.22: Different types of Spa & Spe SpCh with spatial granularity S equal to 1, 2, and 4.

2.4.7 Routing, Spectrum and Space/Core Assignment

The additional spatial dimensions enable extra space assignment considering in routing and resource assignment problems in SDN-EONs. Therefore, the routing and spectrum allocation problem in SDM-EONs becomes the problem of Routing, spectrum, and space/core assignment (RSSA/RSCA) problem [47,48]. In the RSSA/RSCA problem, for each connection request, except for the variables related to the selection of route and spectrum assignment, the additional variables of spatial dimension selection on each link along the lightpath to be decided make the RSSA/RSCA problem more complex.

Furthermore, SDM technology enables additional spatial granularity to be considered whose value should be the divisor of the core/SMF number. Different spatial granularities lead to different groupings of spatial resources in SDM-EONs, which will influence the routing decision and

spectrum assignment.

2.5 Spatial Channel Networks

According to [49], the massive SDM era is upcoming with the prediction of the requirement for commercial 10 Tb/s optical interfaces working in 1 Pb/s optical transport systems by 2024. With the assuming 40% compound annual growth rate (CAGR) of router interface speed, a 10 Tb/s DP-QPSK superchannel will occupy the entire 4.4 THz spectrum resource in the C-band by 2023 [50]. Such an entire C-band accommodating one superchannel eliminates the necessity of wavelength switching in this case. Therefore, a high cost efficiency designed OTN architecture called spatial channel network (SCN), where the optical layer is evolved to hierarchical SDM and WDM layers, is proposed to be in light of the forthcoming massive SDM era.

2.5.1 Spatial Channels and Hierarchical Optical Cross-connect

The main characteristic of an SCN is that the optical layer can be divided into a hierarchical SDM layer and a WDM layer, which is considered a realistic and cost-effective solution [51]. In an SCN, an SCh is supposed to carry the data stream with high demands that occupies the entire spectrum resource of a spatial lane (SL), which can be a core in an MCF or an SMF in a bundle of SMFs. As shown in Figure 2.23 (a), there are three main SChs to be considered in this dissertation: 1) Type I: an SCh transports a single optical channel (OCh) with large capacity. 2) Type II: an SCh transports multiple OChs with the same source-destination node pair. 3) Type III: an SCh transports multiple OChs with different source-destination node pairs. Figure 2.23 (b) shows the architecture of an SCN with two SChs with spatial bypassing (Type I and Type II) and two SChs with wavelength switching (Type III).

In the SDM layer, a spatial cross-connect (SXC) is served as the main switch of a hierarchical optical cross-connect (HOXC) and provides end-to-end optical routing. In the WDM layer, WXCs is served as edge switches of a HOXC and perform wavelength multiplexing and grooming [52].

2.5.2 Routing, Spatial Channel, and Spectrum Assignment

Compared to the RSSA problem in SDM-EONs, the routing, spatial channel, and spectrum assignment (RSCSA) problem focuses on the selection of SChs instead of the space or core searching in the RSSA problem. The objective of the RSCSA problem is to minimize the number of SLs used or numbers of SLs with wavelength switching used in the SCN-based optical networks. Minimizing the number of SLs used is equivalent to maximizing the number of SLs in the network that is not occupied, which is related to network resource consumption and network reliability. Minimizing the number of SLs with wavelength switching used is equivalent to minimizing the number of WXCs

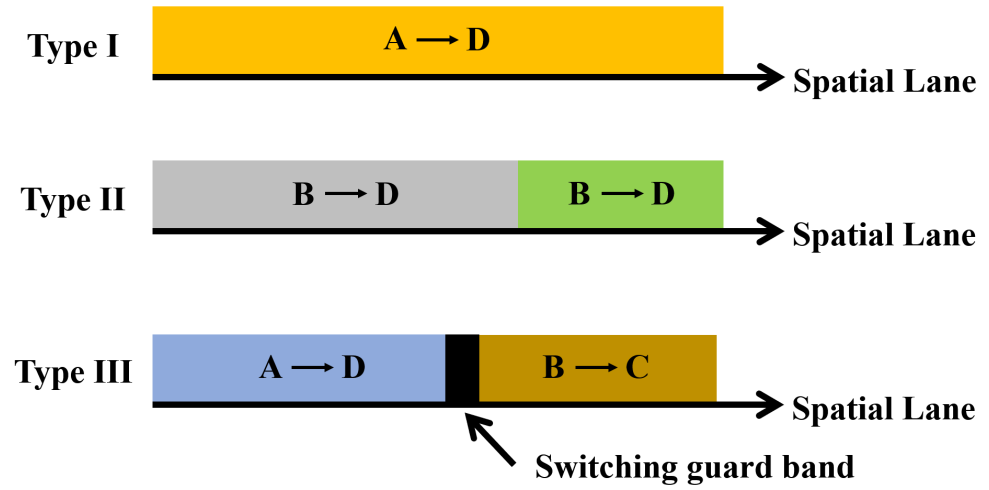

(a)

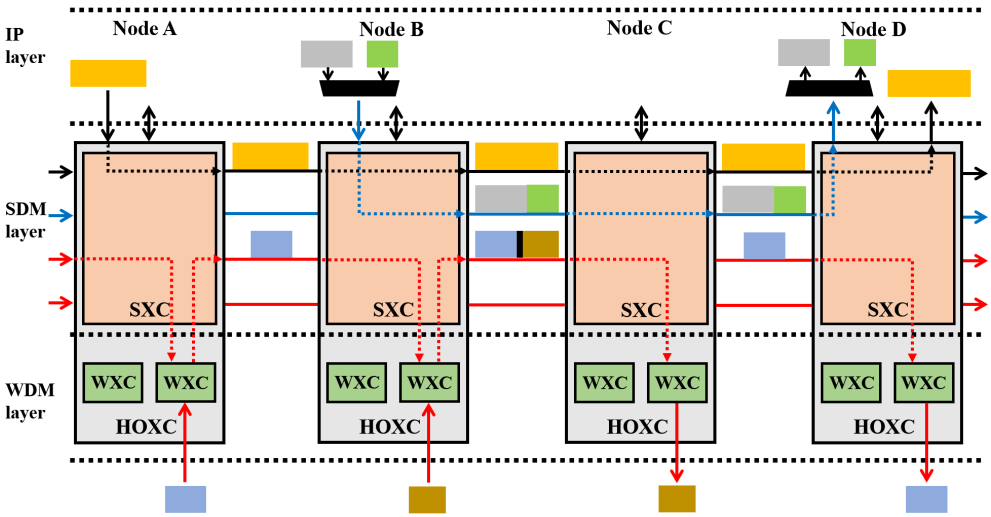

(b)

Figure 2.23: (a) Different types of SChs in SCNs. (b) Architecture of an SCN with one Type I SCh, one Type II SCh and two Type III SChs.

required for network deployment, which is related to the device cost consumption of network planning. Moreover, many possible types of SCN systems have different architectures of HOXCs, and different numbers of WXCs used. There exists a trade off in network architecture design. Concretely, if more WXCs are deployed on the nodes of the network, the switching is more flexible but costs more. Conversely, if fewer WXCs are deployed, the cost is lower, but the switching is more inflexible. Therefore, the evaluation of different architectures of SCN-based optical networks in terms of device cost and network performance is worth considering.

2.6 Conclusion

In this chapter, we give a detailed background of the evolution of optical networks and related technologies. We start with the introduction of the earliest optical networks based on TDM transmission technology. Then, we introduce the background technologies used in WDM-based optical networks. Next, we make an overview of the relevant technologies in EONs as well as the routing and spectrum assignment problem. Moreover, we introduce the supported device and technologies in SDM-based optical networks and the routing, spectrum, and space/core assignment problem. Lastly, we illustrate the architecture of SCNs and related technologies as well as the routing, spatial channel, and spectrum assignment problem.

Chapter 3

Evaluation of Optical Transport Unit Line-Card Integration in Spatially and Spectrally Flexible Optical Networks in Terms of Device Cost and Network Performance

In SDM-EONs, the spatial and spectral superchannel transmission technology can be supported by the Spa & Spe SpCh transceiver and the ROADM, allocating OCs in spatial and spectral domains simultaneously. The architectures of the manufactured transceivers and ROADMs installed in advance at each network node are fixed. This necessitates the determination of the appropriate spatial and spectral granularity combination that affects the transceiver and ROADM designs to efficiently utilize the switching capacity and reduce the implementation costs.

In this research work, we focus on the performance analysis for the N-core MCF-based network deployment issues under different granularity combinations. Detailed evaluation of a 4-core MCF-based network reveals that the device cost and network performance are influenced by spatial and spectral granularities and can provide guidance for real-world network planning and design. In particular, the trade-off between device cost and network performance based on different granularities should be taken into account in network design.

3.1 Our contributions in this research work

There exists a trade-off between device cost and network performance for different spatial and spectral granularities. Indeed, the integrated optical transport unit line cards, also known as the Spa & Spe SpCh transceivers, and ROADMs are installed in advance, implying that the architectures of both are fixed. Therefore, the appropriate spatial and spectral granularity setting is an important issue. In this study, we evaluate device cost and network performance with different granularities

and aim to find the optimal granularity combination ($S \times O$).

The main contributions of this work are as follows. 1) We proposed a method to design SDM networks considering both the spatial and the spectral granularities. We found that these two granularities have strong effects on the device cost (i.e. the total costs of transceivers and ROADMs) and network performance (i.e., the maximum average throughput, the average transceiver utilization and the spectral efficiency). 2) Furthermore, we also found that there are cases the device cost may increase even when the number of transceivers per node decreases. The reason for this result is that the cost of a transceiver is determined by the spatial and spectral granularities and the cost of transceivers may become dominating. 3) We found that low spatial and spectral granularities usually lead to good performance. Especially, lower granularity leads to better transceiver utilization and spectral efficiency but lower throughput. Furthermore, the ratio of device cost to maximum average throughput is not monotonically increasing with the increase of either the spatial or the spectral granularity, causing some difficulties to find the best granularities.

3.2 Space Divison Multiplexing-based Flexible Optical Networks

The proposed EON technology is regarded as a promising method to achieve the goal of high spectral efficiency. In addition, due to the capacity limitations of current SMF optical networks, SDM technology is implemented to satisfy the rapidly increasing network traffic demand. Therefore, SDM-based flexible optical networks not only improve the utilization of spectrum resources but also increase the transmission bandwidth.

3.2.1 Switching Paradigms with Different Optical Fibers and Spatial Granularities

Switching paradigms of an SDM network are significantly influenced by fiber type and spatial granularity. By increasing the number of spatial dimensions (cores/modes) and improving the corresponding core/mode distribution, the transmission capacity of an SDM fiber can be substantially enlarged. Furthermore, the capacity is also governed by mode coupling and fiber properties.

SDM fibers with distinct optical loss and physical impairments lead to different transmission reaches and bandwidths. MMFs are strongly influenced by mode coupling so that MMFs are generally suitable for short-haul transmission (i.e., 100 ~ 1000 meters) [31]. FMFs have been demonstrated as a compromise between MMFs and SMFs, and their transmission distance can reach 1050 kilometers under BPSK [55]. Transmission distance is inevitably limited by optical loss for the bundle packing fraction (BPF) in the bundles of SMF-based optical networks. BPF is related to the total diameter, total bundle area, and number of SMFs [56]. The transmission distance of the MCF-based optical transmission is mainly affected by intercore crosstalk. The crosstalk of an MCF

can be computed by Eq. (3.1) [57]:

$$XT(L) = \frac{n - n \cdot exp\{-(n+1)2hL\}}{1 + n \cdot exp\{-(n+1)2hL\}}, \tag{3.1}$$

where n is the number of cores adjacent to the target core, L is the transmission distance in kilometers and h is a parameter related to the physical features of the MCF. $h = 2k^2 r/\beta\Lambda$, where k is the coupling coefficient, Λ is the core pitch, β is the propagation constant and r is the bending radius. Note that modulation formats make a difference to the robustness of the signal with respect to crosstalk. For a given modulation format m and its corresponding crosstalk threshold xt_m, considering the crosstalk margin xt^* required for crosstalk oscillation, its transmission reach bounded by the threshold can be calculated as follows:

$$L_m = \max\{L | XT(L) \leq xt_m + xt^*\}. \tag{3.2}$$

Therefore, MCFs with different physical features such as layouts (i.e., ring layout, hexagonal layout or square layout) or the number of cores will affect the crosstalk and the transmission distance limit. For given physical characteristics of N-core MCF, we can calculate the crosstalks and transmission reaches under different modulation formats by Eq. (3.1) and (3.2), respectively.

3.2.2 Cost Analysis of The Spa & Spe SpCh Transceiver

As mentioned in Section 2.4.4, A Spa & Spe SpCh transceiver is the integration of single-carrier optical transceivers in the spatial and spectral domains. According to [53], we set the cost of a single-carrier transceiver as 1. The quantity required and unit cost of each component in a single-carrier transceiver are shown in Table 3.1.

Table 3.1: Costs and quantities of the components in a single-carrier transceiver [46, 53].

Component	Unit cost	Quantity required	Total cost
DSP[1]	0.36	1	0.36
LPF	0.004	8	0.03
4-Port DRV	0.07	1	0.07
LS/LO	0.05	2	0.10
IQ-MZM	0.22	1	0.22
DP Coherent RX	0.22	1	0.22
Single-OC Transceiver			1

[1] The DSP module includes ADCs, DACs and amplifiers.

A $S\times O$ Spa & Spe SpCh can be regarded as the Spe SpCh generated by O continuous single-carrier transceivers distributed over S spatial dimensions. In an SDM transceiver, an LS/LO can be shared in parallel spatial domains. In addition, DSPs can be replaced by a joint DSP leading to a 20% cost reduction [54, 58, 59], and other components replacement can lead to a 40% cost

reduction due to the line-card integration [46]. Therefore, the cost of an $S \times O$ SDM transceiver can be computed as follows:

- The cost of sharing LS/LO $C_{LS/LO}$:

$$C_{LS/LO} = 0.05 \times 2 \times O. \tag{3.3}$$

- The cost of (joint) DSP C_{DSP}:

$$C_{DSP} = (1 - 0.2 \times f(S)) \times 0.36 \times S \times O, \tag{3.4}$$

$$f(S) = \begin{cases} 1 & S > 1, \\ 0 & S = 1. \end{cases} \tag{3.5}$$

  The joint DSP module is used only if the spatial granularity $S > 1$.

- The cost of other components in the integration line-card C_{others}:

$$\begin{aligned} C_{others} &= (1 - 0.4) \times (1 - 0.05 \times 2 - 0.36) \times S \times O \\ &= 0.6 \times 0.54 \times S \times O. \end{aligned} \tag{3.6}$$

The total cost of a $S \times O$ Spa & Spe SpCh transceiver C_{Tran} is given by:

$$\begin{aligned} C_{Tran}(S, O) &= C_{LS/LO} + C_{DSP} + C_{others} \\ &= \begin{cases} 0.1 \times O + 0.612 \times S \times O & \text{if } S > 1, \\ 0.1 \times O + 0.684 \times S \times O & \text{if } S = 1. \end{cases} \end{aligned} \tag{3.7}$$

Transceivers are installed on the switching node in advance and the architecture of the transceiver is fixed. This implies that the maximum bit rate of an installed transceiver is constant. In the real-world case, the network traffic load is dynamic, and the size of each traffic request is variable. Due to different traffic volumes of connections, the preinstalled transceiver with an appropriate spatial-spectral granularity is important for SDM networks.

As shown in Figure 3.1, to illustrate the importance of granularity selection, we use a simple example that 2×3 SDM transceivers are installed on the network nodes. When a connection with a relatively small traffic volume arrives at a node in time, we can see from Figure 3.1 (a) that such a transceiver is activated but not fully utilized, increasing device cost and resource wastage. On the other hand, if the traffic volume of the arriving connection is relatively large, more than one transceiver is required to support it. As shown in Figure 3.1 (b), it results in low spectral efficiency due to the additional spectrum consumption of GBs between the transceivers. Overall, we focus on the evaluation of the device cost and network performance with different spatial and spectral granularities in this research.

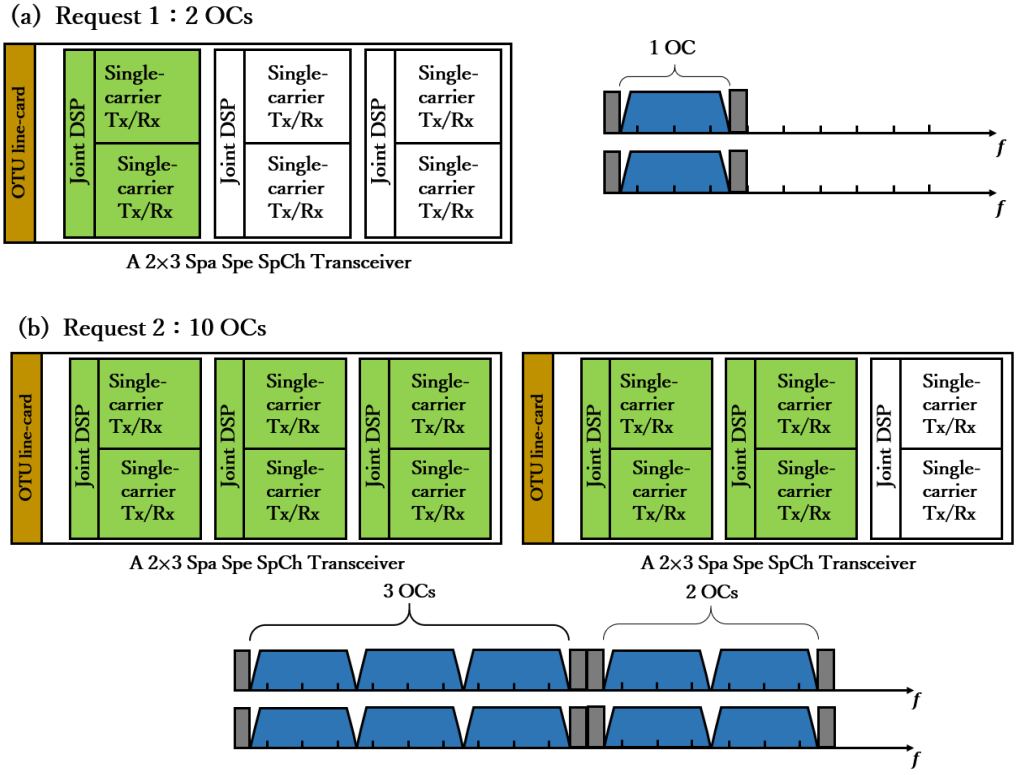

Figure 3.1: Illustration of 2×3 Spa & Spe SpCh transceiver(s) utilization of different requests: (a) Request 1: 2 OCs; (b) Request 2: 12 OCs.

3.2.3 Cost Analysis of The ROADM

A ROADM provides wavelength adding/dropping and flexible switching functionalities [41, 60], which is composed of two modules: an express module and an add/drop module. The express module can be a broadcast-and-select (B&S) module if splitters are used or a route-and-select (R&S) module if WSSs are used at ingress [46, 61]. Compared with the B&S-based ROADM, the R&S-based ROADM is more suitable for nodes with high degrees because it provides superior isolation on the blocking ports and has a low insertion loss regardless of the port count [62]. The add/drop module provides connectivity between the express module and transceivers which can be implemented by WSSs or multicast switches (MCSs). In this work, we treat the R&S module as the express module and the 16-port MCS module as the add/drop module.

For a N-core MCF, the architecture of a ROADM at an intermediate node with degree D is determined by the total number of spatial dimensions N, the spatial granularity S, the node degree D and whether or not SLC technology is used.

SLC technology enables the superchannel in each spatial group to be freely switched to any output port with different group indices. Clearly, whether SLC technology is supported influences the number of ports of WSSs. In particular, SLC technology only has an impact on independent

and fractional joint switching but not on joint switching strategies. Therefore, SLC technology can offer higher routing flexibility but increases the complexity of the ROADM architecture due to the requirement of high port count WSSs.

The architecture of a ROADM, including an express and an add/drop module, is determined by the number of installed transceivers at each node and to whether or not the SLC technology is supported. Figure 3.2 shows the three-degree ROADM architectures with the B&S express module and MCS- based add/drop module under different spatial granularities.

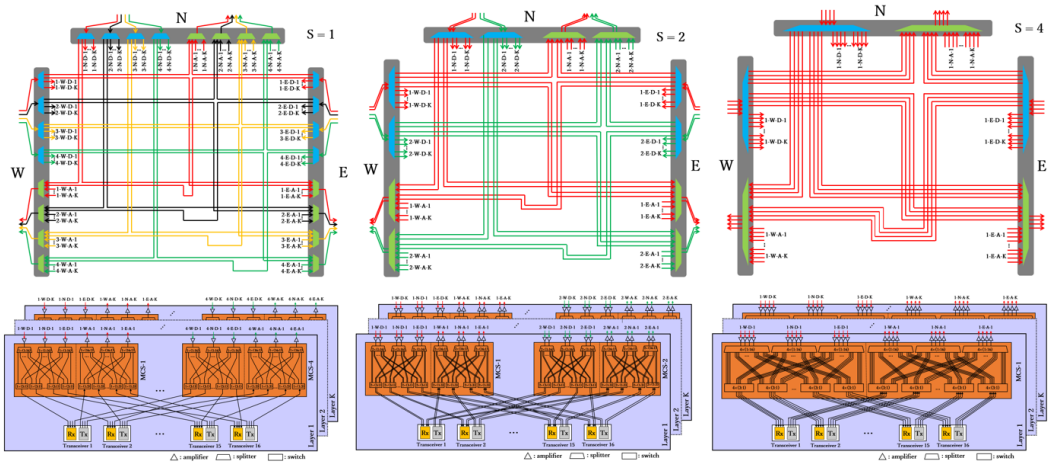

Figure 3.2: Three degree ROADMs with R&S express module and MCS-based add/drop module for a 4-core MCF for different spatial granularities (S = 1, 2, 4).

The usage of multicore erbium-doped fiber amplifiers (MC-EDFAs) and SDM fan-in/fan-out (FIFO) for SDM fiber-in/out are equivalent in the case of different spatial switching granularities. Therefore, we consider the R&S module cost in two parts of the variable-gain dual-stage amplifiers (VGDAs) (unit cost: 0.18) and WSSs, whose costs are dependent on the fiber spatial dimension N, the spatial granularity S, and the node degree D and on whether or not the SLC technology is applied. The cost of an R&S module for the ROADM at an intermediate node with degree D in a N-core MCF-based optical network is computed as follows:

- The cost of VGDAs C_{VGDA}: The number of VGDAs required is equal to the product of the node degree and core number.

$$C_{VGDA} = 0.18 \times N \times D. \tag{3.8}$$

- The cost of WSSs C_{WSS}: The number of WSSs used and the port count of each WSS are specified in Table 3.2. Any design of a $P \times (I \times Q)$ WSS can be implemented by the reconfiguration of a $1 \times N$ WSS with the same total port count [63]. For example, a 1×20 WSS can be reconfigured to $7 \times (1 \times 3)$. Therefore, the cost of a $P \times (I \times Q)$ WSS C_{wss} can be

Table 3.2: Number of WSSs used and port-count of each WSS with/without SLC supported in 4-core MCF.

	Num. of WSSs used	Port count per WSS
With SLC	$2 \times D \times \frac{N}{S}$	$S + [(D-1) \times S \times \frac{N}{S} + K \times S]$
Without SLC	$2 \times D \times \frac{N}{S}$	$S + S \times [\ (D-1) + K]$

calculated based on the data presented in Table 3.3 [46, 64]. The total cost of required WSSs

Table 3.3: Cost of WSS with different port counts.

WSS	1×320	1×160	1×80	1×40	1×20	1×9	1×5
C_{wss}	3.37	2.13	1.35	0.85	0.54	0.34	0.22

C_{WSS} for the express module in a ROADM is given as follows:

$$C_{WSS} = C_{wss} \times 2 \times D \times \frac{N}{S}. \tag{3.9}$$

Therefore, the cost of an R&S module $C_{R\&S}$ can be computed by the sum of costs of VGDAs and WSSs:

$$\begin{aligned} C_{R\&S} &= C_{VGDA} + C_{WSS} \\ &= 0.18 \times N \times D + C_{wss} \times 2 \times D \times \frac{N}{S}. \end{aligned} \tag{3.10}$$

Compared with the $R\&S$ module, the $B\&S$ module, as an express module suitable for small-scale networks, can reduce device cost and optical-electronic complexity. By replacing the WSSs at the ingress with splitters with the same port-counts, the $B\&S$ module reduces the number of WSSs by half. Because the cost of a splitter is basically negligible compared with other components [65], the device cost of an $B\&S$ module can be computed as follows:

$$\begin{aligned} C_{B\&S} &= C_{VGDA} + C_{WSS} \\ &= 0.18 \times N \times D + C_{wss} \times D \times \frac{N}{S}. \end{aligned} \tag{3.11}$$

The architecture of the MCS-based add/drop module is composed of low-cost single-stage amplifiers (LCSAs) and MCSs, which is determined by the fiber spatial dimension N, the spatial granularity S, the node degree D and the number of transceivers T arranged at each node. The cost of the add/drop module for the ROADM at an intermediate node with D degree in a N-core MCF-based optical network is computed as follows:

- The cost of LCSAs C_{LCSA}: LCSAs (unit cost: 0.06) connect WSSs and splitters/combiners to compensate for the losses during transmission in each MCS layer, and the total number

of required LCSAs for an add/drop module is related to the number of fiber cores, the node degree and the number of MCS layers:

$$\begin{aligned} C_{LCSA} &= 0.06 \times S \times D \times 2 \times \frac{N}{S} \times K \\ &= 0.12 \times D \times N \times K. \end{aligned} \tag{3.12}$$

- The cost of MCSs C_{MCS}: The cost of a 4×16 MCS is assumed to be 0.49, and the cost of an 8×16 MCS is 25 % higher [63]. Therefore, the costs of different types of MCSs are shown in Table 3.4. We consider the cost of a $S \times (D \times 16)$ MCS to be $S \times C_{D\times16mcs}$. The number

Table 3.4: Cost of MCS with different port counts.

D × 16 MCS	8×16	4×16	2×16	1×16
$C_{D\times16mcs}$	0.61	0.49	0.39	0.31

of layers of MCS K is determined by the number of transceivers T arranged per node:

$$K = \lceil \frac{T}{16} \rceil. \tag{3.13}$$

The cost of MCSs C_{MCS} is:

$$\begin{aligned} C_{MCS} &= \lceil \frac{T}{16} \rceil \times \frac{N}{S} \times S \times C_{D\times16mcs} \\ &= \lceil \frac{T}{16} \rceil \times N \times C_{D\times16mcs}. \end{aligned} \tag{3.14}$$

Therefore, the cost of an MCS-based add/drop module $C_{MCS-A/D}$ can be computed as the sum of the costs of LCSAs and MCSs:

$$\begin{aligned} C_{MCS-A/D} &= C_{LCSA} + C_{MCS} \\ &= \lceil \frac{T}{16} \rceil \times N \times (0.12 \times D + C_{D\times16mcs}). \end{aligned} \tag{3.15}$$

Compared with the MCS-based add/drop module, the WSS-based implementation causes much higher device cost. The number of WSSs required for add/drop cards is $\frac{N}{S}$, whose port-count of ingress and egress is $S \times D$ and $S \times T$, respectively [53]. The cost of an WSS-based add/drop module $C_{WSS-A/D}$ can be computed as follows ($C_{wss}{}^*$ is the cost of an $S\times(D\times T)$ WSS according to Table 3.3):

$$\begin{aligned} C_{WSS-A/D} &= C_{LCSA} + C_{WSS} \\ &= 0.12 \times D \times N + 2 \times \frac{N}{S} \times C_{wss}{}^*. \end{aligned} \tag{3.16}$$

Overall, the total cost of a ROADM C_{ROADM} with an $R\&S$ express module and an MCS-based add/drop module can be computed as follows:

$$\begin{aligned} C_{ROADM}(N,S,D,T) &= C_{R\&S} + C_{MCS-A/D} \\ &= \left(0.18 \times N \times D + C_{wss} \times 2 \times D \times \frac{N}{S}\right) \\ &+ \left[\lceil \frac{T}{16} \rceil \times N \times (0.12 \times D + C_{D\times16mcs})\right]. \end{aligned} \tag{3.17}$$

3.3 Simulation and Results

We conduct simulations with the network model using a 28-node European Optical Backbone Network (EOBN) and a 27-node American ATT Backbone Network (AABN), as shown in Figure 4.13. The assumptions in our simulation experiments are as follows:

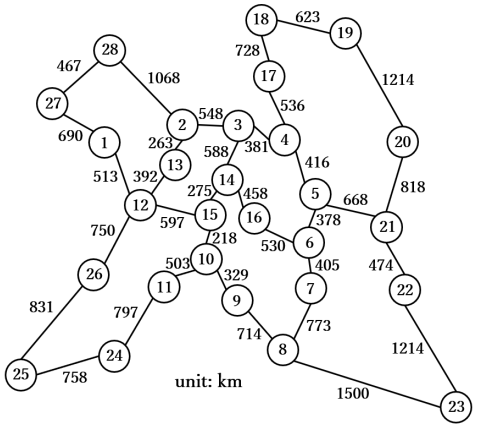

(a) European Optical Backbone Network (EOBN)

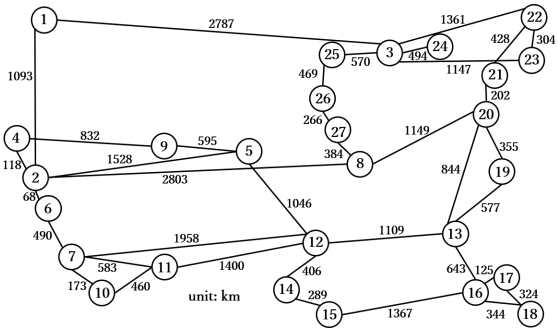

(b) American ATT backbone network (AABN)

Figure 3.3: Network topology: (a) EOBN with 28 nodes and 68 directed links; (b) AABN with 27 nodes and 74 directed links.

The assumptions in our simulation experiments are as follows:

(1) Each link in our simulated network model is a 4-core MCF because its crosstalk is lower than those in MMF or FMF fibers and no additional optical devices in MCF such as MIMO DSP module and mode conversion components are needed, reducing device cost [66–68]. Furthermore, due to light leakage (caused by the thin layer of the cladding between adjacent fibers) and reduction of the lateral optical resolution in the specimen plane (caused by the pixelation transmission) in the bundle of SMFs, transmission using MCF fibers is more efficient and resource saving than the bundle of SMFs [69,70]. Considering a -2 dB margin (xt^*), the crosstalk

Table 3.5: Transmission reaches limited by the OSNR and crosstalk for 4-core MCFs

Limitation factor	Transmission reach [km]			
	BPSK	QPSK	8-QAM	16-QAM
OSNR	6300	3500	1200	600
Crosstalk	38945	13872	7808	3111

thresholds (xt_m) are assumed to be -14, -18.5, -21, and -25 dB for BPSK, QPSK, 8-QAM and 16-QAM, respectively. The crosstalks and transmission reaches under different modulation formats can be computed by Eq.(3.1) and (3.2). Therefore, the transmission reaches limited by the optical signal-to-noise ratio (OSNR) or the crosstalk are shown in Table 3.5. Regardless of the modulation format, the influence of OSNR on the transmission reach is much greater than

that of crosstalk. Therefore, the 4-core MCF is weakly coupled so that its transmission reach is mainly limited by the optical signal-to-noise ratio (OSNR), which decreases by multistage optical amplification and optical physical impairments rather than crosstalk; the diameter of the 4-core MCF is approximately 125 μm [57], which is compatible with many current SMF-based network devices, such as interfaces and optical cables.

(2) We estimate the transmission reaches accounting for different modulation formats with consideration of the OSNR in the 4-core MCF (the influence of crosstalk is negligible) [71]. The transmission reaches in kilometers and modulation level in bit/symbol supported under different modulation formats [72] are shown in Table 3.6.

Table 3.6: Transmission reaches under different modulation formats in the 4-core MCF-based network.

Modulation format	Transmission reach	Modulation level
DP-BPSK	6300	2
DP-QPSK	3500	4
DP-8QAM	1200	6
DP-16QAM	600	8

(3) The total available spectrum resource of each core spanned by C-baud in the 4-core MCF is assumed to be 4 THz and can be divided into 320 FSs according to ITU-T G.694.1.

(4) An OC generated under DP-BPSK modulation by a single-carrier transceiver with a symbol rate of 32 Gbaud considering 7 Gbaud ECC can support 50 Gbps net traffic volume. The assumption of a symbol rate of 32 Gbaud shaping with 3.125 GHz filter resolution in this research enables higher spectral efficiency, lower cost consumption and deployment complexity compared with high symbol rate transceivers [46]. According to ITU-T g.694.1, the spectral granularity is set as 12.5 GHz grid. Therefore, the spectral occupation of the OC must be an integer multiple of the granularity, that is, 3 FSs. Moreover, the GB on both sides of the superchannel is 6.25 GHz.

(5) The number of requests in the simulation is 100,000, and the traffic volume of each request follows a uniform distribution ranging from 100 Gbps to 1,000 Gbps. The requests with a source-destination pair are supposed to arrive at each network node in accordance with a Poisson process with given average holding and arrival times, and both arrival and holding times follow a negative exponential distribution.

(6) In our 4-core MCF-based simulated network, the spatial granularity S for transceivers is considered to be 1, 2, and 4, and the spectral granularity O is assumed to be 1, 2, 3,... 20. The traffic volume reaches 1,000 Gbps, as shown in Table 3.6, and the request of 1000 Gbps requires at

most 20 OCs (under DP-BPSK) for transmission. Therefore, the maximum spectral granularity is set to 20.

(7) The routing path of each source-destination pair request is found by the K-shortest path algorithm (K = 3). The required FSs of each request is assigned by the first-fit allocation scheme.

3.3.1 Results for Device Cost

The device cost in optical networks is composed of the costs of transceivers, optical cables, ROADMs, etc. In this research, we define the device cost as the costs of SDM transceivers and ROADMs that are considered to be the two main components in SDM networks.

According to the transceiver cost analysis in Section 3.2.2, the cost of an $S \times O$ Spa & Spe SpCh transceiver in 4-core MCF-based optical networks can be computed as follows:

$$C_{Tran}(S,O) = \begin{cases} 0.1 \times O + 0.612 \times S \times O & \text{if } S > 1, \\ 0.1 \times O + 0.684 \times S \times O & \text{if } S = 1. \end{cases} \tag{3.18}$$

According to the ROADM cost analysis in Section 3.2.3, the cost of a ROADM in 4-core MCF-based optical networks can be computed as follows:

$$\begin{aligned} C_{ROADM}(S,D,T) = &\left(0.72 \times D + C_{wss} \times D \times \frac{8}{S}\right) \\ &+ \left[\lceil \frac{T}{16} \rceil \times 4 \times (0.12 \times D + C_{D \times 16mcs})\right]. \end{aligned} \tag{3.19}$$

Therefore, the device cost C considered in 4-core MCF-based optical networks is the total cost of SDM transceivers and ROADMs installed at the nodes of the entire network.

$$C = V \times T \times C_{Tran}(S,O) + V \times C_{ROADM}(S,D,T), \tag{3.20}$$

where V is the total number of network nodes, T is the number of transceivers installed at each node and is determined by network topology and spatial-spectral granularity ($S-O$), and S and O are the spatial and spectral granularities, respectively.

With a reasonable 1% BP, for different spatial and spectral switching granularities, we investigate the number of transceivers and the architecture of ROADM deployed at each node in AABN and EON. We assume that the number of transceivers installed at each node T in a network is the same with a certain spatial and spectral granularity. As shown by an examination of the data presented in Table 3.7, the number of transceivers installed per node for each granularity combination ($S \times O$) is obtained by the maximum number of required transceivers during the entire simulation experiment with the BP close to 1%.

The device costs (unit: 1) of the AABN and EOBN vary with spatial and spectral granularity, which are shown in Figure 3.4.

Table 3.7: Number of Spa & Spe SpCh transceivers installed per node for different spatial and spectral switching granularity designs in AABN vs. EOBN

O \ S	AABN with SLC			AABN without SLC			EOBN with SLC			EOBN without SLC		
	1	2	4	1	2	4	1	2	4	1	2	4
1	222	118	69	218	122	69	286	130	67	262	132	67
2	128	71	41	128	71	41	164	81	46	150	83	46
3	96	52	33	96	52	33	124	66	35	121	66	35
4	76	45	29	77	48	29	97	59	33	98	58	33
5	67	41	27	67	42	27	83	45	32	79	48	32
6	57	38	26	58	39	26	72	46	32	70	47	32
7	53	37	26	53	38	26	65	45	32	64	45	32
8	49	35	26	49	36	26	61	44	32	61	44	32
9	46	32	26	45	32	26	55	39	32	51	40	32
10	43	29	26	44	30	26	48	37	32	48	39	32
11	43	29	26	44	30	26	48	37	32	48	39	32
12	40	29	26	40	30	26	46	37	32	48	39	32
13	40	29	26	40	30	26	47	37	32	48	39	32
14	39	29	26	39	30	26	47	37	32	45	39	32
15	39	29	26	39	30	26	47	37	32	45	39	32
16	37	29	26	37	30	26	44	37	32	44	39	32
17	37	29	26	37	30	26	44	37	32	44	39	32
18	34	29	26	34	30	26	42	37	32	41	39	32
19	34	29	26	34	30	26	42	37	32	41	39	32
20	32	29	26	32	30	26	42	37	32	40	39	32

Overall, comparing the AABN and EOBN, the device cost of the EON is slightly higher than that of the AABN because the network nodes of the EOBN are more centralized than those of the AABN. Requests of the same size have shorter transmission distances in the EOBN and require fewer OCs, and source-destination pairs with a certain bandwidth can transmit more requests so that more transceivers are needed in the EOBN. Moreover, whether in the AABN or in the EOBN, for the same spatial granularity S, device cost grows with increasing spectral granularity O.

According to Eq. (3.20), for a given network topology, the device cost C is determined by spatial-spectral granularity S-O and the number of transceivers per node T. As shown in Eq. (3.18) and (3.19), the cost of a single SDM transceiver C_{Tran}, which is proportional to O and linear to S, is more affected by granularity than that of a ROADM C_{ROADM}. Therefore, C_{Tran} is the main factor affecting C that with increasing of S and O, T decreases while C increases.

In detail, for a given S, the reduction rate of T is lower than the increase rate of O, and the gap between the two is expanding as O increases. Therefore, C increases with increasing O due to the proportional relationship between C_{Tran} and O. On the other hand, for a given O, as indicated in Fig. 3.4, when O is relatively small, the difference of C under different S is not apparent. When O

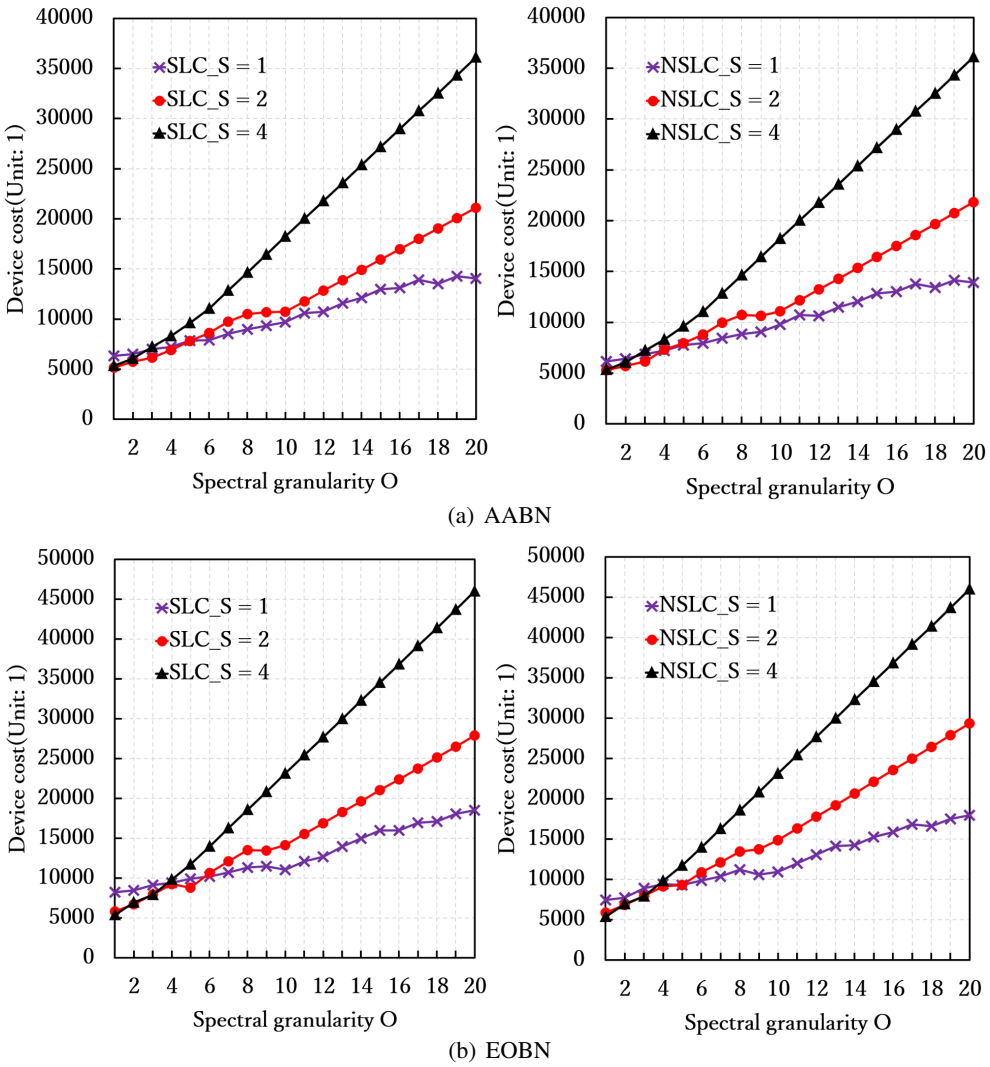

Figure 3.4: Device cost (DC) vs. the spectral switching granularity for different network topologies.

is enlarged, C increases significantly with the increase of S. This is because the gaps in the number of SDM transceivers under different S become small with the increase of O, while C_{Tran} increases linearly with the increase of S. Therefore, C increases with increasing S.

In addition, when O is limited to small values, a lower device cost is required for SDM networks with a higher S. Then, with the same high-value O, C increases with increasing S. In this case, the device cost when $S = 4$ is nearly twice that of other spatial granularities, which is not a good choice when only device cost is considered. As shown in Figure 3.4, it is clear that SLC switching technology achieves negligible improvements ($0.1\% \sim 3\%$) in device cost with various S and O.

3.3.2 Results for Network Performance

The network performance metrics used here include the maximum average throughput, the average transceiver utilization and spectral efficiency. The 100,000 requests arrive at the network at different times in a dynamic scenario with a fixed arrival rate, and we evaluate network performance when all 100,000 connections are torn from the network.

In detail, the connections are assigned to each source node following a Poisson distribution process with an average arrival rate λ. The average holding time of the connections follows a negative exponential distribution with parameter μ. The offered load which is defined as the number of connections loaded at points in time, follows an $Erlang(\frac{\lambda}{\mu})$ distribution. These performance metrics can be obtained until the blocking probability (BP) is close to 1% with increasing offered load. In the following, we give a detailed description of the above three performance metrics.

(1) Maximum average throughput

The maximum average throughput is defined as the average traffic load per second during the entire simulation. Along with the whole simulation of duration T_s, each unblocked request i with traffic demand tr_i in Gbps and holding time t_i is successfully assigned, and the maximum average throughput (MAT) in Tbps can be computed as follows:

$$MAT = \frac{\sum_i \frac{tr_i}{1000} \times t_i}{T_s}. \tag{3.21}$$

(2) Average transceiver utilization

The utilization of transceivers with fixed bit rates will be different for 100,000 different connections. The number of required OCs n_i of unblocked request i can be computed by traffic demand tr_i under a selected modulation format (DP-BPSK, DP-QPSK, DP-8QAM, DP-16QAM), so that the transceiver utilization of unblocked request i TU_i is given as follows:

$$TU_i = \frac{n_i}{\lceil \frac{n_i}{S \times O} \rceil \times S \times O}. \tag{3.22}$$

Hence, the average transceiver utilization (ATU) of j unblocked requests is given by:

$$ATU = \frac{\sum_{i=1}^{j} TU_i}{j} \times 100\%. \tag{3.23}$$

(3) Spectral efficiency

The spectral efficiency (SE) describes the amount of data transmitted over a given spectrum. SE is defined as the number of bits transmitted over a given frequency band per second. During the entire simulation, SE in Gbps/Hz can be calculated as follows:

$$SE = \frac{\sum_i tr_i}{\sum_i \left\{ \lceil \frac{n_i}{S \times O} \rceil \times [(S \times O \times 37.5) + (S \times 12.5)] \right\}}. \tag{3.24}$$

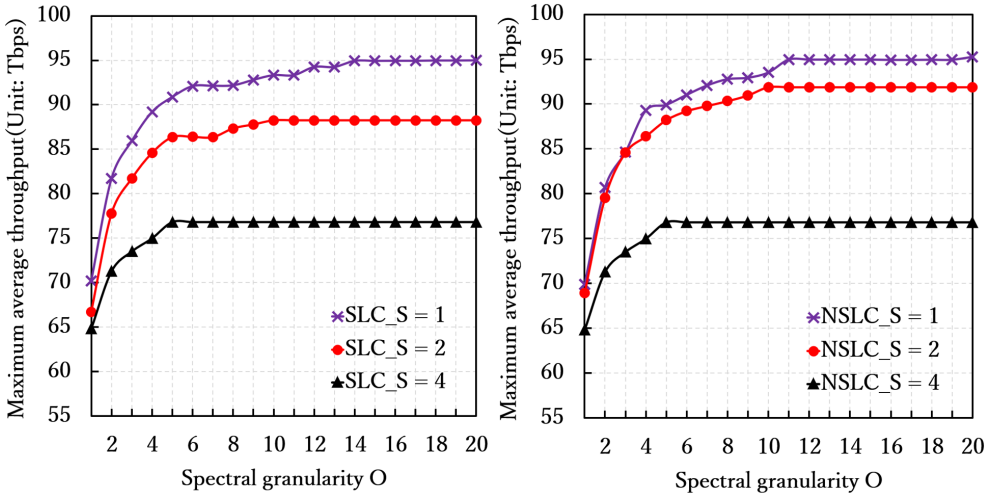

(a) AABN

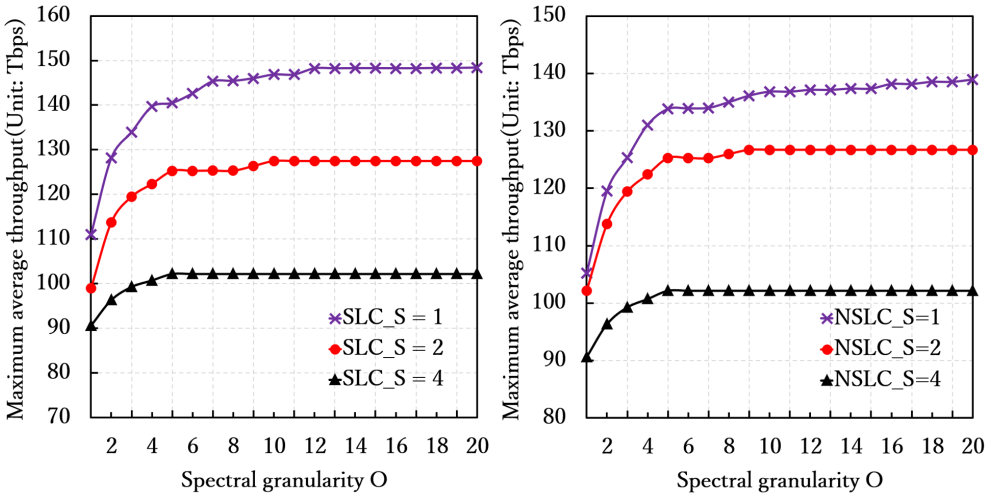

(b) EOBN

Figure 3.5: Maximum average throughput (MAT) vs. the spectral switching granularity for AABN and EOBN.

As indicated in Figure 3.5, MAT varies with granularities in the AABN and the EOBN. As mentioned above, more transceivers are required at nodes in the EOBN compared with the AABN, so MAT of the EOBN is approximately 40% higher than that of the AABN. For a given S, MAT initially increases with increasing O. When O reaches a high value, the growth of MAT tends to saturate.

Figure 3.5 shows that the network throughput is bounded due to the insufficiency of spectrum resources when enough transceivers are installed at each node. In addition, the network throughput is nearly unchanged when $S = 2$, $O > 10$ and $S = 4$, $O > 5$. This is because the maximum OCs required by a connection is 20 (1,000 Gbps traffic volume under DP-BPSK modulation format) so that even a single Spa & Spe SpCh transceiver is sufficient to support the transmission with different

traffic volume connections. We note that the transmission system with lower S can achieve higher network throughput for a given O. This is because the transceiver with a higher S needs more switching GBs to support an equivalent capacity.

Overall, SDM networks become more spectrally efficient with relatively higher O or lower S. The gap between scenarios with and without SLC technology support is narrow ($0.1\% \sim 8\%$). In particular, when $S = 2$, $O > 10$ or when $S = 4$, $O > 5$, which means that a single transceiver can support more than 20 OCs (the maximum OC requirement in our simulation) for transmission, MAT is nearly invariable but results in resource wastage due to overprovisioning.

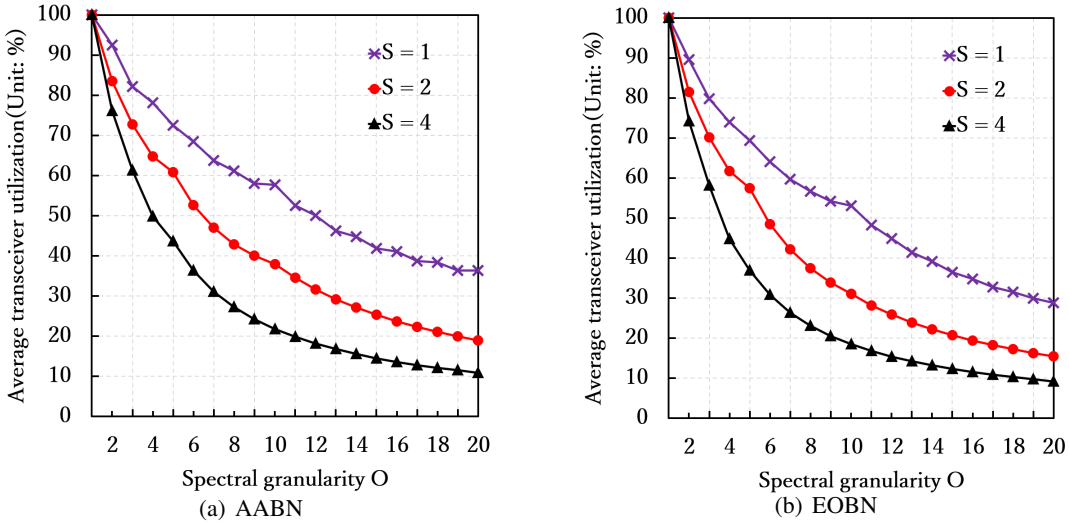

Figure 3.6: Average transceiver utilization (ATU) vs. the spectral switching granularity for AABN and EOBN.

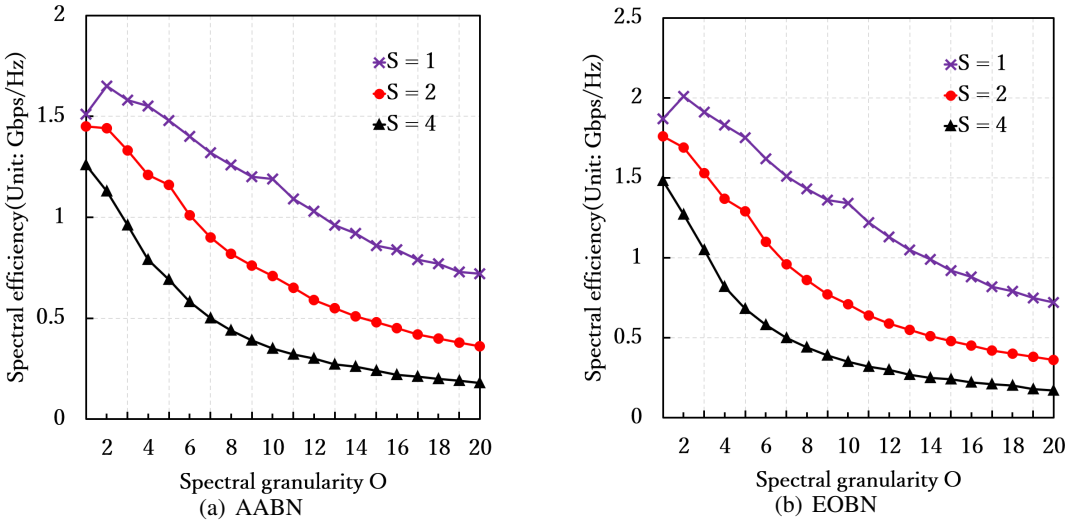

Figure 3.7: Spectral efficiency (SE) vs. the spectral switching granularity for AABN and EBON.

The overprovisioning of a transceiver can be quantified by transceiver utilization, and ATU is

the average utilization of transceiver support per request. Figure 3.6 shows ATU against different network topologies. When O equals 1, regardless of S, the $1 \times O$ Spa & Spe SpCh transceiver is completely used. An increase in either S or O leads to a decrease in ATU. In addition, SLC technology has little impact on ATU.

Figure 3.7 shows SE for different network topologies plotted versus S and O. For a given S, SE decreases with the growth of O because that overprovisioning is more likely in transceivers with higher spectral granularity, leading to spectrum resource wastage. In addition, SDM networks with higher S cause lower SE in view of greater switching GB utilization and transceiver overprovisioning. Overall, the SE of a Spa & Spe SpCh transceiver is improved when S and O decrease.

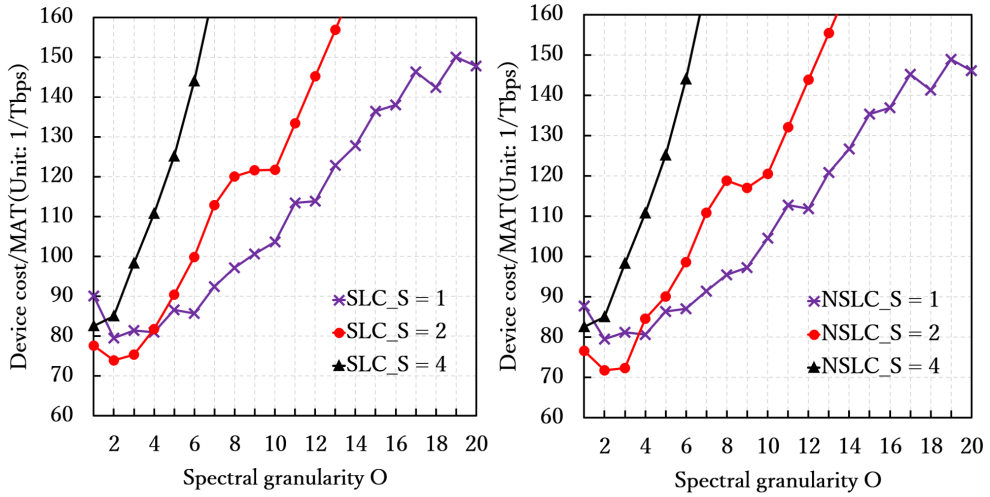

(a) AABN

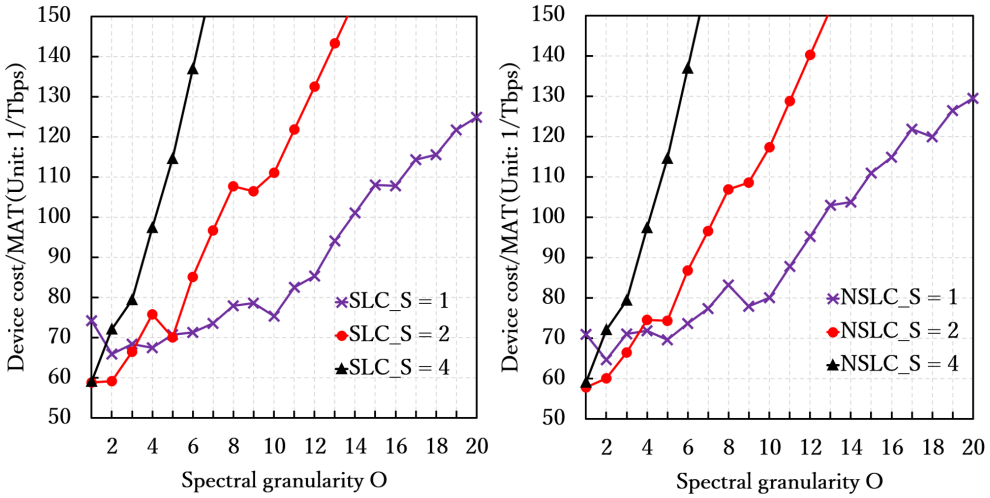

(b) EOBN

Figure 3.8: Ratio of device cost to MAT vs. the spectral switching granularity for AABN and EOBN.

There exists a trade-off between the device cost and network performance. For a given S, device cost and MAT show opposite trends with ATU and SE when plotted versus O. Focusing on different

performance evaluation indicators, we can obtain various optimal choices of $S \times O$ for different network topologies. Specifically, as the two most critical factors considered by network operators, device cost and MAT must be given more attention in actual commercial network deployment.

We introduce the ratio of device cost to MAT as a new performance metric to evaluate SDM networks with different granularity combinations. Figure 3.8 shows the ratio of device cost to MAT for different transmission systems plotted versus S and O. We only show some of the results in Figure 3.8 that show better performance on the ratio of device cost to MAT. We can see that the shape of the curve for each network topology is locally convex. Overall, the ratio of device cost to MAT increases whether with the growth of S and O but with some variations. These results show that there exists an optimal choice of $S \times O$ for each transmission system. For both EOBN and AABN, the combinations of 2×2 ($S = 2, O = 2$), 4×1 ($S = 4, O = 1$) and 1×2 ($S = 1, O = 2$) perform relatively well with regard to device cost and MAT.

Since there exists a large difference in the data scale among device cost, MAT, ATU and SE, each of these variables has different units. Therefore, we use the min-max normalization method to guarantee that all of the metrics have the exact same scale between 0 and 1, and the top 5 values of each metric are presented in Table 3.8. An SDM network with lower device cost, higher MAT, higher ATU, and higher SE is considered to be a better choice for network deployment. However, no granularity combination can achieve the above requirements in reality. Considering all of the metrics, under a 4-core MCF-based optical transmission we can obtain that for the AABN, regardless of whether or not the SLC technology is supported, the two most suitable granularity combinations are 1×4 ($S = 1, O = 4$) and 2×2 ($S = 2, O = 2$). For the EON, the two most suitable granularity combinations are 2×2 ($S = 2, O = 2$ and 1×2 ($S = 1, O = 2$). Moreover, for a 4-core MCF-based SDM network, the recommended spatial granularities are 1 and 2, and the recommended spectral granularities are $1 \sim 6$.

On the other hand, in actual commercial network deployment, in addition to device cost, network operators pay attention to resource consumption due to the increasingly urgent shortage of resources, that is, device cost and SE mentioned in our research. Therefore, considering only device cost, regardless of whether or not the SLC is supported, the best granularity combination for AABN and EON is 4×1 ($S = 4, O = 1$) and 2×1 ($S = 2, O = 1$), respectively. Similarly, 1×2 ($S = 1, O = 2$)is the best choice when only considering SE for both AABN and EON. Taking both device cost and SE into account, we obtain that 2×1 ($S = 2, O = 1$) is optimal. In addition, the best granularity combination is 1×20 ($S = 1, O = 20$) and 1×1 ($S = 1, O = 1$) when only considering MAT or ATU, respectively.

Table 3.8: Device cost, maximum average throughput, average transceiver utilization and spectral efficiency power for different spatial and spectral switching granularity designs.

	$S \times O$	With SLC				without SLC			
		device cost	MAT	ATU	SE	device cost	MAT	ATU	SE
AABN	2×1	1×20	1×1	1×2	2×1	1×20	1×1	1×2	
	4×1	1×19	1×2	1×3	4×1	1×19	1×2	1×3	
	2×2	1×18	1×3	1×4	2×2	1×18	1×3	1×4	
	4×2	1×17	1×4	1×1	4×2	1×17	1×4	1×1	
	2×3	1×16	1×5	1×5	2×3	1×16	1×5	1×5	
EOBN	4×1	1×20	1×20	1×2	4×1	1×20	1×1	1×2	
	2×1	1×19	1×2	1×3	2×1	1×19	1×2	1×3	
	2×2	1×18	1×3	1×1	2×2	1×18	1×3	1×1	
	4×2	1×17	1×4	1×4	4×2	1×17	1×4	1×4	
	4×3	1×16	1×5	2×1	1×1	1×16	1×5	2×1	

3.4 Conclusion

In this research work, we comprehensively analyze the network architectures, including the transceiver and ROADM, according to different granularity combinations. We propose detailed models for N-core MCF-based SDM networks considering the device cost, MAT, ATU and SE. According to the simulation results under a specific 4-core MCF-based SDM network, we find that the spatial and spectral granularity (S and O) will strongly influence the number of Spa & Spe SpCh transceivers installed at each node and the architecture of the ROADM and transceiver, resulting in different device costs and performance of network deployment. Moreover, whether or not SLC technology is supported also has an impact on the network cost/performance, but the impact is not prominent. With a trade-off relationship between the device cost and network performance, network operators need to choose the most suitable transmission system according to their objectives. If the network operators focus on device cost reduction, an SDM network with higher S and lower O but without SLC support is recommended. Conversely, focusing on the maximization of the whole network throughput, an SDM network with lower S and higher O and with SLC support is preferred. In addition, an SDM network with lower S and O improves transceiver utility and spectral efficiency. Furthermore, different types of SDM fibers, such as 7-core MCF, 12-core MCF and 4-SMFB connected simulation networks, and new switching techniques, such as FSSS and SCNs, should be explored further.

Chapter 4

Robust Design against Network Failures of Shared Backup Path Protected SDM-EONs

SDM-EONs can provide higher capacity, higher spectral efficiency, and more flexible optical transmission to address future explosive data growth. However, the key challenge for the widespread deployment of such complex networks is how to ensure their survivability against different types of network failures.

In this research, we consider the robust design of a N-SMFB-based SDM-EON with shared backup path protection (SBPP). Considering the network reliability against different failures and the uncertainty in traffic volume, we focus on RSSA problems of working and backup path determination. We formulate the problems as two mixed integer linear programming (MILP) models with the objective of minimizing the maximal FS index used and the total number of backup FSs. In this scenario, we propose heuristic algorithms for routing decision and spectrum assignment, and we compare the spectrum efficiency and execution time among MILP models, our proposed algorithms and the existing algorithm. Finally, we employ the Γ-robust optimization technique to handle traffic with uncertainties and compare the simulation results obtained in deterministic and nondeterministic scenarios.

4.1 Our contributions in this research work

In this research, we focus on robust design for an SBPP-based SDM-EON considering reliability against the different occurrences of network failures and uncertainty in traffic volume. We formulate the related problems as MILP models with the objectives of minimizing the total number of reserved FSs and the maximum number of FSs used.

The main contributions of this paper are summarized as follows. 1) We consider multiple possible network failures in SBPP-based SDM-EONs, which is different from the previous works that

only consider a single type of failure (link failure or SRLG failure). 2) The working path of each request is not given in advance. We first determine the working paths for requests and then determine their backup paths based on the results of the working path determination. 3) We formulate the RSSA problems using node-arc-based MILP models to minimize used and backup spectrum resources in SBPP-based SDM-EONs facing various types of network failures. We find that the number of requests and network topology affect the spectrum resources used, while different types of network failures present different requirements for backup spectrum resources. 4) We propose a heuristic best-fit FS assignment algorithm that can reduce spectrum fragmentation and improve searching efficiency. 5) We propose two heuristic routing algorithms for working path and backup path determination. We find that our proposed algorithms outperform the existing algorithm in terms of spectrum resource usage. Compared with the MILP models, the gaps between the solutions obtained with our proposed algorithms and the optimal solution in terms of used and backup spectrum resources are within an acceptable range, while the execution time is greatly reduced. 5) Furthermore, we introduce a Γ-robust optimization technique to develop a network design that is robust against various network failures while considering the uncertainty in traffic volume. We find that the amount of backup spectrum resources needed initially increases as the request size uncertainty increases and then tends to remain constant. It is worth mentioning that the corresponding values of Γ at which the amount of backup spectrum resources saturates are different for various types of network failures.

4.2 Network Failures and Protection Techniques in SDM-EONs

4.2.1 Network Failures in SDM-EONs

Network survivability and reliability are essential and challenging issues in network design. The introduction of SDM technology can solve the problem of increasing network capacity requirements. However, the greater complexity of the communication infrastructure that is supported by this technology increases the possibility of network failures. Therefore, the design of a reliable and high-capacity optical network that can withstand various types of network failures is of vital importance for supporting future transmission.

In SDM-EONs, network protection is more complicated and failures in the physical layer are more difficult to detect [73]. Therefore, a reliable design based on network protection techniques is a complex task in SDM-EONs when considering all possible network failures. In this section, we introduce four main types of network failures, core failure, node failure, link failure and SRLG failure, in SDM-EONs as follows.

(1) ***Core failure:*** Core failure refers to the failure of an SMF or a core in SMFB-based or MCF-based SDM-EONs. The breakdown of a single SDM optic fiber or one of the parallel SDM

transceivers will cause core failure.

(2) ***Node failure:*** Node failure refers to the failure of a node in the network layer that affects the lightpaths passing through that node. Without node redundancy, a lightpath that starts or terminates at the failed node cannot be protected [74]. Therefore, we consider the path protection issue only in the case of intermediate node failure. Specifically, the transceivers used for transmission in an SDM-EON are multiple single carrier transceivers or integrated single carrier transceivers. A malfunction of the SDM transceiver or its internal optical elements, such as lasers or DSP elements, will cause node failure. In addition, as shown in Figure 4.1, the breakdown of intermediate stations for SDM-based all-optical transmission, including optical line amplifiers (OLAs), optical add/drop multiplexers (OADMs) and regeneration stations (REGs), is related to node failure.

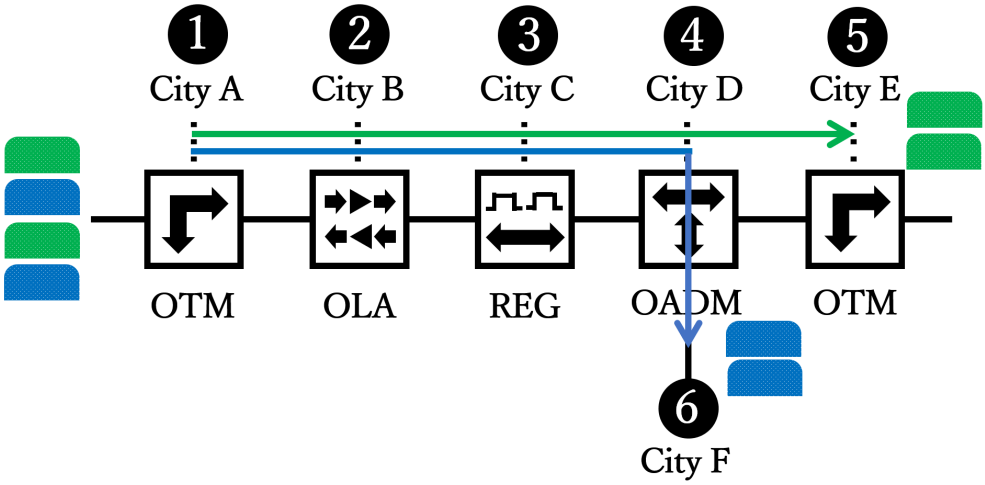

Figure 4.1: Different types of stations in node-arc optical transmission.

(3) ***Link failure:*** Link failure refers to a failure of a virtual link that influences the lightpaths traversing it. The breakdown of the fiber optic cable responsible for a virtual link is one of the main causes of link failure. In addition, failures of some optical components, such as SDM MUX/DMUX, SDM FIFO or MC-EDFA components, will also cause link failure [73].

(4) ***SRLG failure:*** SRLG failure refers to the breaking of multiple links due to the failure of a common resource [75], and is mainly caused by the breakdown of fiber optic cables. As shown in Table 4.1, dig-ups are the dominant cause of fiber optic cable failures that can lead to the disruption of all SMFBs or MCFs in an SDM-EON. A fiber optic cable in a physical layer realized by means of SMFBs or MCFs may control transmission on multiple links in the network layer that can serve as an SRLG.

Table 4.1: Causes of historical fiber optic cable failures [76].

Cause	Proportion (%)
Dig-ups	57
Craftsperson/Worker Error	7
Rodents	4
Fire	4
Vehicles	4
Defective Cable	3
Firearms	2
Intrinsic Electronic Failure	2
Flooding	2
Lightning	1
Extreme Temperature	1
Ice	1
Stream Damage	1
Other	5
Unknown	5

4.2.2 Protection Techniques in SDM-EONs

To design a reliable SDM-EON, network protection techniques are critical. Dedicated path protection (DPP) and SBPP are two simple but efficient protection techniques [47, 77].

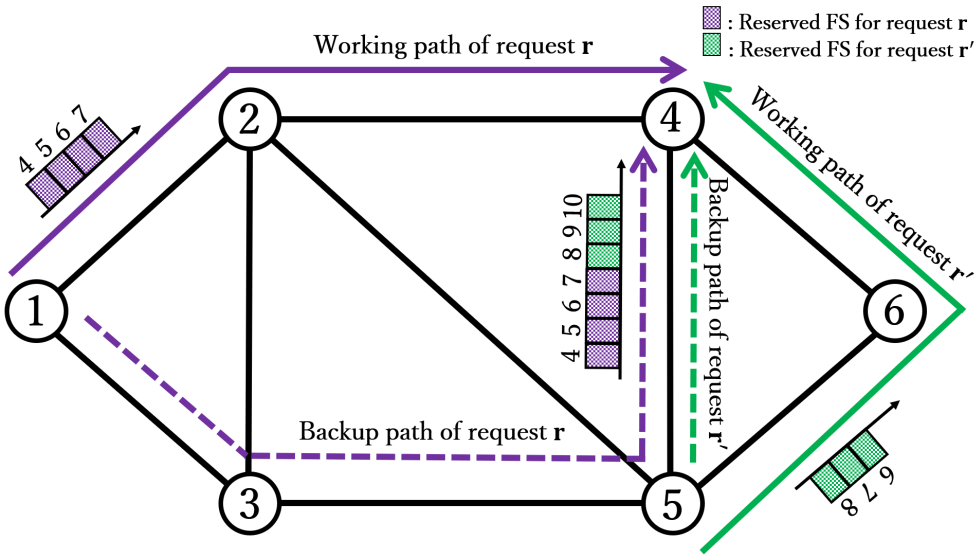

Figure 4.2: Example of network protection against link failures using DPP.

DPP is regarded as a reliable static path protection method because of its short restoration time and ability guarantee. DPP is also called 1+1 path protection, which means that the working path and the backup path of each source-destination node pair are one-to-one. This makes DPP a faster pro-

tection scheme because the optics along both paths are activated and no signaling between ingress and egress node pairs is involved. However, DPP is a relatively expensive and resource-intensive approach due to the need for additional optical elements and provisioned capacity.

A simple example of DPP is shown in Figure 4.2. If the working path of request r (1-2-4) is affected by a network failure, then the traffic flow of request r is directly switched to a predefined backup path with the same FS index range [4, 7], i.e., (1-3-5-4). Similarly, the affected working path of request r' (5-6-4) is switched to a backup path (5-4) for failure recovery.

There is a common link between the backup paths for requests r and r', and their working paths share the same FSs (6 and 7). However, the spectrum resources cannot be shared on the common link of their backup paths in DPP. To avoid overlapping with the backup FSs used by request r on the common link (5-4), the FSs [6, 8] assigned for the backup path of request r' must be tuned to [8, 10] by deploying tunable transponders. Therefore, although DPP is fast and simple to operate, it still has the disadvantages of high device cost and resource consumption.

With the ability to share spare protection capacity on common links, SBPP is considered a better technique for network protection. As indicated in Figure 4.3, the key feature of SBPP is that when the working paths for multiple requests do not have any common links, their corresponding backup paths can share spectrum resources on their common links.

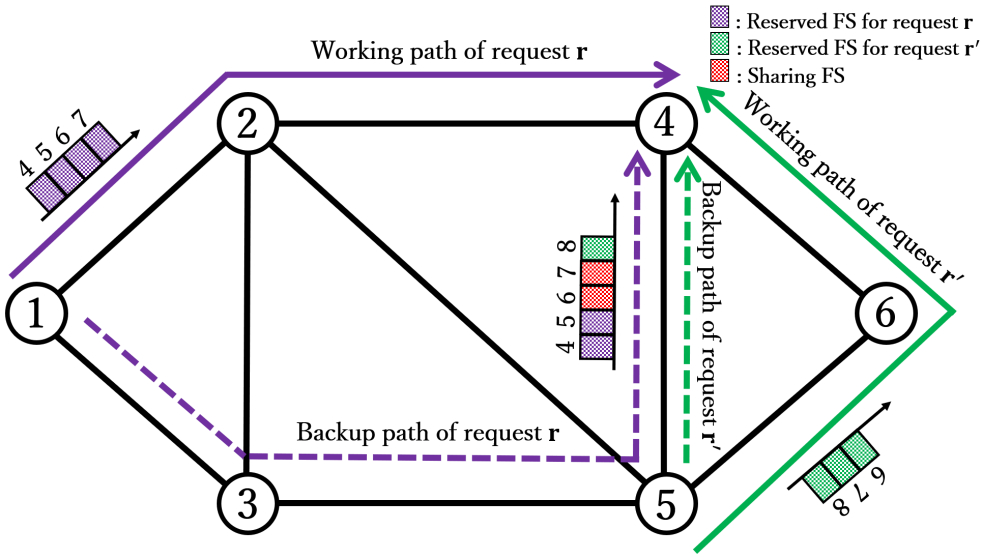

Figure 4.3: Example of network protection against link failures using SBPP.

Similar to the DPP scheme, link (4-5) is traversed by the backup paths of requests r and r' simultaneously, whose corresponding working paths (1-2-4) and (5-6-4) do not have any common links. However, backup paths (1-3-5-4) and (5-4) can share spare capacity [6, 7] on their common link (5-4). Therefore, the indices of the FSs assigned in each backup path have the same range as the corresponding working path in SBPP. Consequently, in contrast to the 7 FSs needed or spectrum

reservation in DPP, only 5 backup FSs are required in SBPP. Overall, SBPP has the same advantages of speed and simple operation as DPP, but achieves higher spectrum efficiency and lower device cost than DPP.

4.2.3 XT Estimation in SDM-EONs

XT is an important issue in SDM-EONs. MCFs and SMFBs, which are the two most commonly used types of SDM fibers, suffer from distinct types of interference caused by XT. In SMFB-based SDM-EONs, the impact of XT is negligible; instead, the maximum transmission distances for different modulation formats are limited by the optical signal-to-noise ratio (OSNR) [43,44,46]. Conversely, in MCF-based SDM-EONs, as the number of MCF fiber cores increases, the interference of inter-core XT on transmission becomes more apparent. Therefore, the maximum transmission distances in MCF-based SDM-EONs are limited by both OSNR and XT. According to [**?**], the XT caused by two adjacent cores c and c' can be computed as follows:

$$XT_{c,c'}(L) = \frac{1 - exp(-2hL)}{1 + exp(-2hL)}, \tag{4.1}$$

where L is the transmission distance and h is a parameter related to the fiber type. Based on the set of FSs used by both cores c and c', whose number is denoted by $F_{c,c'}$, the total XT of core c with adjacent cores $c' \in A_c$ can be computed as follows:

$$XT_c = \sum_{c' \in A_c} F_{c,c'} XT_{c,c'}. \tag{4.2}$$

4.3 SBPP against Various Network Failures in a N-SMFB-Based SDM-EON

Spectrum resource sharing, as the most attractive aspect of SBPP, can be achieved for multiple backup paths when their corresponding working paths are link disjoint. In Figure 4.4, three requests, Request 1, Request 2, and Request 3, are assigned between different node pairs with pairs of link-disjoint working and backup paths.

In Figure 4.4, the solid lines indicate working paths, and the dotted lines represent backup paths. Concretely, (1-2-4) and (1-3-5-4) are the working path and backup path, respectively, for Request 1, (5-6-4) and (5-4) are the corresponding paths for Request 2, and (1-2) and (1-3-2) are the corresponding paths for Request 3. The working paths for Request 1 and Request 2 are link disjoint, so their corresponding backup paths can share spectrum resources on the common link (5-4). Conversely, the backup paths of Request 1 and Request 3 cannot share spectrum resources due to link (1-2) sharing on their working paths.

Given a set of traffic requests to be assigned in a N-SMFB-based SDM-EON, we formulate two MILP models: an MILP model for working path determination with the objective of minimizing the

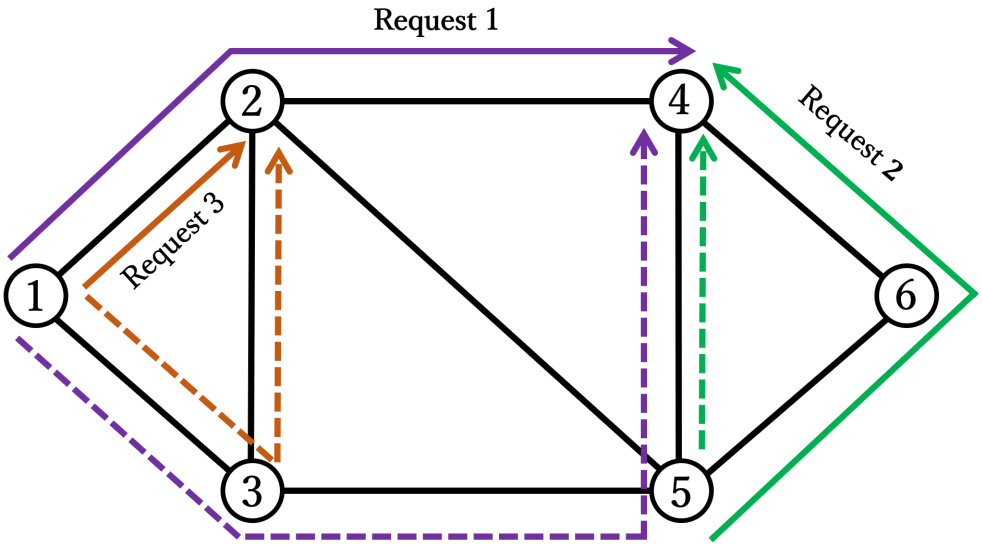

Figure 4.4: Example of SBPP in the case of a common link existing in working paths or not.

spectrum resources used; and an MILP model for backup path determination in the face of different network failures, with the objective of minimizing both used and backup spectrum resources.

4.3.1 Problem Description

In this subsection, we consider the routing, space, and spectrum assignment (RSSA) problems in a N-SMFB-based SDM-EON protected with SBPP.

The network topology is represented by a graph $G(V, E)$, where V is the set of nodes and E is the set of links. The set of spatial domains in each link of N-SMFB is denoted $C = \{1, 2, ..., N\}$. The set of SRLGs is represented by U, and each SRLG is composed of several links. The set of requests assigned in the network is denoted by R, and the traffic demand of each request is given in advance. The set of network failure types is represented by $X = \{1, 2, 3, 4\}$, where the different failure types x are defined as follows: $x = 1$ denotes core failure, $x = 2$ denotes node failure, $x = 3$ denotes link failure, and $x = 4$ denotes SRLG failure.

The objectives of the RSSA problems are to minimize the maximum number of FSs used and the total number of backup FSs for connection requests. In RSSA, the spectrum contiguity and continuity constraints should be satisfied. Spectrum contiguity means that the spectrum resources assigned to each request must be adjacent FSs. Furthermore, spectrum continuity means that the contiguous adjacent FSs allocated to the path of each request must be the same on all of the links traversed by the lightpath. FSs used in the common SMF of the same link cannot overlap; this is defined as spectrum nonoverlap. In this work, we consider the routing decision and spectrum assignment for both working and backup paths. Since the problem of working and backup paths determination is complicated and the RSSA of the working path has an impact on backup path

determination, we solve it in two steps. We first solve the RSSA problem of the working path decision, and then solve the RSSA problem of the backup path decision based on the solution of the working path determination problem. The working path and backup path of each request are not intersecting with each other. Only one backup path can be established for each request, and only one type of network failure and one location of network failure occurrence are considered for the problem.

4.3.2 Working Path Determination Based on the Node-Arc-Based MILP Formulation for the RSSA Problem

We aim to find the working paths for requests with a node-arc-based MILP formulation for an RSSA problem. The MILP formulations for working determination are as follows.

- ***Parameters:***

  V : Set of network nodes.

  E : Set of network links.

  C : Set of SMFs in a N-SMFB.

  R : Set of requests assigned in the network, $r = \{s_r, d_r, t_r\} \in R$, where s_r and d_r are source and destination nodes of request r, respectively, and t_r is the traffic demand in FSs (including guard bands) of request r.

  L_v : Set of network links whose egress node is $v \in V$.

  $L_v{}'$: Set of network links whose ingress node is $v \in V$.

  $XT^e_{c,c'}$: XT between SMF c and c' on link e.

  F : Set of available FSs.

  Ω : XT threshold.

  M : A large value.

- ***Variables:***

  $a_r^{e,c}$: A binary variable that is equal to 1 if SMF c of link e is selected for the working path of request r; otherwise, it is 0.

  b_r^v : A binary variable that is equal to 1 if node v is traversed by the working path for request r; otherwise, it is 0.

  w_r : An integer variable that denotes the initial FS index of the working path for request r.

  $o_r^{r'}$: A binary variable that is equal to 1 if the initial FS index of the path for request r is larger than that for request r', i.e., if $w_r > w_{r'}$; otherwise, it is 0.

$l_r^{e,c,k}$: A binary variable that is equal to 1 if the kth FS in SMF c of link e is assigned to the working path for request r; otherwise, it is 0.

$x_r^{e,k}$: A continuous variable that indicates the XT on FS k of link e for the working path of request r.

F_{max}^{w} : An integer variable that indicates the maximal FS index used for working paths.

- ***Objective:***

$$\min \quad F_{max}^{w}. \tag{4.3}$$

Our objective is to minimize the spectrum resources used as represented by the maximal FS index used in the network.

- ***Constraints:***

Constraint for the Final FS Index Used

$$w_r + t_r - 1 \leq F_{max}^{w} \quad \forall r \in R. \tag{4.4}$$

Constraint (4.4) ensures that the final FS index of the working path for each request is less than the maximal FS index used.

Constraints for Route Selection

$$\sum_{c \in C} a_r^{e,c} \leq 1 \; \forall r \in R, \; \forall e \in E, \tag{4.5}$$

$$\sum_{c \in C} \sum_{e \in L_{s_r}} a_r^{e,c} = 1 \; \forall r \in R, \tag{4.6}$$

$$\sum_{c \in C} \sum_{e \in L_{d_r}{}'} a_r^{e,c} = 1 \; \forall r \in R, \tag{4.7}$$

$$\sum_{c \in C} \sum_{e \in L_v} a_r^{e,c} - b_r^v = 0 \; \forall r \in R, \; \forall v \in V \backslash \{s_r, d_r\}, \tag{4.8}$$

$$\sum_{c \in C} \sum_{e \in L_v{}'} a_r^{e,c} - b_r^v = 0 \; \forall r \in R, \; \forall v \in V \backslash \{s_r, d_r\}, \tag{4.9}$$

$$2 \sum_{c \in C} a_r^{e,c} - (b_r^{v_1} + b_r^{v_2}) \leq 0 \; \forall r \in R, \; \forall e = (v_1, v_2) \in E. \tag{4.10}$$

Constraint (4.5) ensures that at most one SMF c is selected on link e for each request r. Constraint (4.6) ensures that the egress node of the first link of the working path for each request r is its source node s_r. Constraint (4.7) ensures that the ingress node of the last link of the working path for each request r is its destination node d_r. Constraint (4.8) ensures that

for each intermediate node v traversed by the working path for request r, only one link can end at this node. Constraint (4.9) ensures that for each intermediate node v traversed by the working path for request r, only one link can start from this node. Constraints (4.8) and (4.9) together ensure that the out-degree and in-degree of each intermediate node traversed by the working path for each request are equal, and are both equal to 1. Constraint (4.10) ensures that if the working path for request r traverses link $e = (v_1, v_2)$, then it must also traverse nodes v_1 and v_2.

Constraints for the Elimination of Cycles and Subtours

$$\sum_{c \in C} a_r^{e_1,c} + \sum_{c \in C} a_r^{e_2,c} \leq 1$$
$$\forall r \in R,\ \forall e_1 = (v_1, v_2) \in E,\ \forall e_2 = (v_2, v_1) \in E, \tag{4.11}$$

$$\sum_{c \in C} \sum_{e \in L_{d_r}} a_r^{e,c} = 0\ \forall r \in R, \tag{4.12}$$

$$\sum_{c \in C} \sum_{e \in L_{s_r}{}'} a_r^{e,c} = 0\ \forall r \in R. \tag{4.13}$$

Constraint (4.11) ensures that cycles are avoided on the working path for each request r. Constraints (4.12) and (4.13) ensure that subtours are avoided on the working path for each request r.

Constraints for Spectrum Nonoverlap

$$w_{r'} - w_r \leq M(1 - o_r^{r'} + 2 - (a_r^{e,c} + a_{r'}^{e,c})) - 1$$
$$\forall e \in E,\ \forall c \in C,\ \forall r, r' \in R,\ r \neq r', \tag{4.14}$$

$$w_r + t_r - w_{r'} \leq M(o_r^{r'} + 2 - (a_r^{e,c} + a_{r'}^{e,c}))$$
$$\forall e \in E,\ \forall c \in C,\ \forall r, r' \in R,\ r \neq r'. \tag{4.15}$$

Constraints (4.14) and (4.15) ensure that the FSs allocated to a common SMF on the same link on working paths for different requests cannot overlap. Figure 4.5 illustrates the case in which the working paths for requests r and r' share a common SMF and link. If the initial FS index assigned to the working path for request r is larger than that assigned to the working path for request r', then the initial FS index assigned to the working path for request r must also be larger than the final FS index assigned to the working path for request r'.

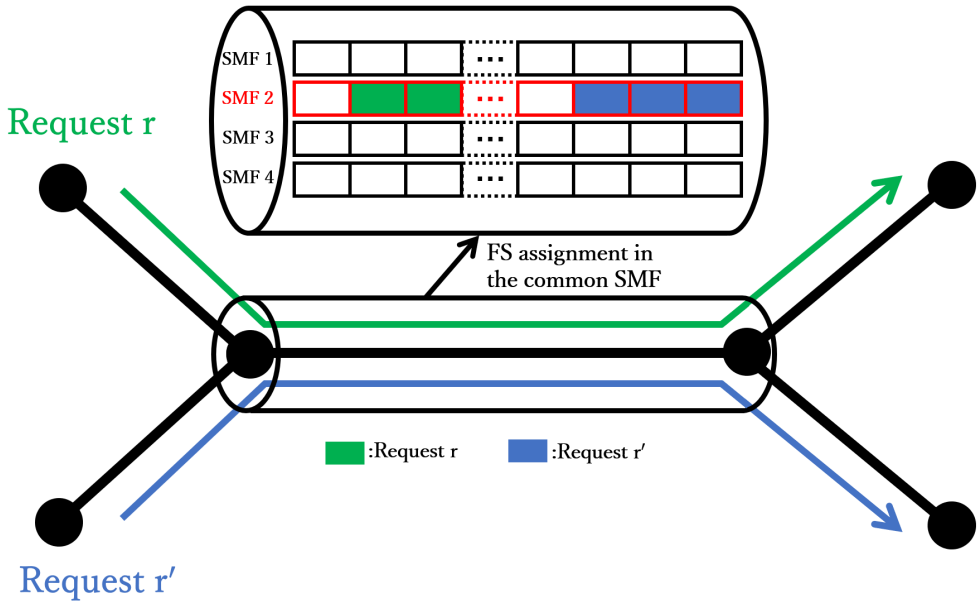

Figure 4.5: Case in which the working paths of two distinct requests share a common SMF on the same link.

Constraints for Spectrum Contiguity and Continuity

$$\sum_{k \in F} l_r^{e,c,k} - t_r a_r^{e,c} = 0 \qquad \forall r \in R, \forall e \in E, \ \forall c \in C, \tag{4.16}$$

$$M\Big(\sum_{c \in C} l_r^{e,c,k} - 1\Big) \leq k - w_r \qquad \forall r \in R, \ \forall e \in E, \ \forall k \in F, \tag{4.17}$$

$$M\Big(\sum_{c \in C} l_r^{e,c,k} - 1\Big) \leq w_r + t_r - 1 - k \qquad \forall r \in R, \ \forall e \in E, \ \forall k \in F. \tag{4.18}$$

Constraint (4.16) ensures that when SMF c of link e is selected for the working path for request r, a number of FSs with capacity equal to its traffic demand t_r are assigned. Constraints (4.17) and (4.18) ensure that the indices of the FSs assigned to SMF c of link e for request r are between the starting FS index w_r and the ending FS index $w_r + t_r - 1$, that is, $f \in [w_r, w_r + t_r - 1]$. Thus, spectrum contiguity and continuity are satisfied.

Constraints for XT

$$\sum_{c' \in A_c} \sum_{r' \in R} XT_{c,c'}^{e} l_{r'}^{e,c',k} - M(1 - l_r^{e,c,k}) \ \leq x_r^{e,k} \qquad \forall r \in R, \forall e \in E, \ \forall c \in C, \forall k \in F, \tag{4.19}$$

$$\sum_{e \in E} x_r^{e,k} \leq \Omega$$
$$\forall r \in R,\ \forall k \in F. \tag{4.20}$$

Constraint (4.19) ensures that if the kth FS on SMF c of link e is assigned to the working path for request r, that is, $l_r^{e,c,k} = 1$, then the XT on the kth FS of link e for request r should be greater than the sum of the XTs caused by other requests assigned to the same FS on adjacent cores of this common link in the case of link sharing. Constraint (4.20) ensures that the XT on the working path selected for request r should be less than the XT threshold Ω.

4.3.3 Backup Path Determination in the Face of Various Network Failures Based on the Node-Arc-Based MILP Formulations for the RSSA Problem

After obtaining the assigned working path, SMFs, and spectrum interval for each request, we present an extended MILP optimization model for backup path determination in the face of different types of network failures.

- ***Parameters:***

  The backup path determination problem can be solved based on the results of working path determination as described in Section **??**. Therefore, the parameters marked with asterisks are based on the output of the MILP formulation for working path determination. The additional parameters beyond those introduced in Section **??** are listed as follows:

  U : Set of network SRLGs.

  $w_r{}^*$: Initial FS index selected to serve the working path for request r.

  $a_r^{e,c*}$: A binary parameter that is equal to 1 if the working path for request r traverses SMF c of link e; otherwise, it is 0.

  b_r^{v*} : A binary parameter that is equal to 1 if the working path for request r traverses node v; otherwise, it is 0.

  g_r^{e*} : A binary parameter that is equal to 1 if the working path for request r traverses link e; otherwise, it is 0.

  h_r^{u*} : A binary parameter that is equal to 1 if the working path for request r traverses SRLG u; otherwise, it is 0.

  $l_r^{e,c,k*}$: A binary parameter that is equal to 1 if the working path for request r traverses the kth FS on SMF c of link e; otherwise, it is 0.

  WL_r : Set of network links traversed by the working path for request r.

  WC_r : Set of network links traversed by the working path for request r and the corresponding SMF used on each link, $WC_r = \{(e \in E, c \in C\ ) |\ a_r^{e,c*} = 1\}$.

WV_r : Set of network nodes traversed by the working path for request r, $WV_r = \{v \in V, v \neq s_r, d_r \mid b_r^{v*} = 1\}$.

WF_r : Set of FS indices used by the working path for request r, $WF_r = \{k \in F \mid l_r^{e,c,k^*} = 1(\forall e \in E, \forall c \in C)\}$

WU_r : Set of network SRLGs traversed by the working path for request r.

X : Set of network failure types, $x \in X = \{1, 2, 3, 4\}$.

ω : A weight factor.

M : A large value.

- ***Variables:***

ζ_x : A binary variable that is equal to 1 if a network failure of type x occurs; otherwise, it is 0.

$\eta_r^{e,c}$: A binary variable that is equal to 1 if the backup path for request r traverses SMF c of link e; otherwise, it is 0.

p_r : An integer variable that denotes the initial FS index of the backup path for request r.

$m_r^{r'}$: A binary variable that is equal to 1 if the initial FS index of the path for request r is larger than that for request r', i.e., if $w_r > p_{r'}$; otherwise, it is 0.

$n_r^{e,c,k}$: A binary variable that is equal to 1 if the kth FS on SMF c of link e is assigned to the backup path for request r; otherwise, it is 0.

$t_r^{e,k}$: A continuous variable that represents XT on FS k of link e for the backup path of request r.

f_e^c : An integer variable that indicates the total number of backup FSs on SMF c of link e.

F_{max}^b : An integer variable that indicates the maximal FS index used for backup paths.

- ***Objective:***

$$\min \quad \sum_{e \in E} \sum_{c \in C} f_e^c + \omega F_{max}^b. \tag{4.21}$$

Given the working paths for the requests, our objective is to minimize the total amounts of used and backup spectrum resources (expressed in units of FSs) for the backup paths, which are computed as the maximal FS index used and the sum of the backup FSs on all SMFs of the links in the network, respectively.

- ***Constraints:***

Constraint for Network Failure Occurrence:

$$\sum_{x \in X} \zeta_x = 1. \tag{4.22}$$

Constraint (4.22) ensures that only one type of network failure exists in the network. $\zeta_1 = 1$ indicates the occurrence of core failure, $\zeta_2 = 1$ indicates the occurrence of node failure, $\zeta_3 = 1$ indicates the occurrence of link failure, and $\zeta_4 = 1$ indicates the occurrence of SRLG failure.

Constraint for the Final FS Index Used

$$p_r + t_r - 1 \leq F^b_{max} \quad \forall r \in R. \tag{4.23}$$

Constraint (4.23) ensures that the final FS index of the backup path for each request is less than the maximal FS index used.

Constraints for Backup FSs

$$\sum_{r \in R} a_r^{e,c*} \eta_r^{e',c'} t_r \leq f_{e'}^{c'}$$
$$\forall e, e' \in E,\ \forall c, c' \in C,\ \zeta_1 = 1, \tag{4.24}$$
$$\sum_{r \in R} b_r^{v*} \eta_r^{e,c} t_r \leq f_e^c$$
$$\forall v \in V,\ \forall e \in E,\ \forall c \in C,\ \zeta_2 = 1, \tag{4.25}$$
$$\sum_{r \in R} g_r^{e*} \eta_r^{e',c} t_r \leq f_{e'}^c$$
$$\forall e, e' \in E,\ \forall c \in C,\ \zeta_3 = 1, \tag{4.26}$$
$$\sum_{r \in R} h_r^{u*} \eta_r^{e,c} t_r \leq f_e^c$$
$$\forall u \in U,\ \forall e \in E,\ \forall c \in C,\ \zeta_4 = 1. \tag{4.27}$$

Constraints (4.24)~(4.27) count the total numbers of backup FSs on SMF c of link e that are reserved against core failure, node failure, link failure, and SRLG failure, respectively.

Constraints for Route Selection

The constraints for backup path route selection are similar to those for working path selection given in Section 4.3.2. For different types of network failures, the differences lie in the sets of available nodes and links.

Concretely, when core or link failure occurs ($\zeta_1 = 1, \zeta_3 = 1$), the sets of available nodes and links for each request r are V and $E - WL_r$, respectively; when node failure occurs ($\zeta_2 = 1$),

the sets of available nodes and links for each request r are $V - WV_r$ and $E - WL_r$, respectively; and when SRLG failure occurs ($\zeta_4 = 1$), the sets of available nodes and links for each request r are V and $E - WU_r$, respectively.

Constraints for XT

The XT constraints for backup path determination are the same as those for working path determination given in Section 4.3.2.

Constraints for the Elimination of Cycles and Subtours

The constraints for cycle and subtour elimination in backup path determination are the same as those for working paths in Section 4.3.2.

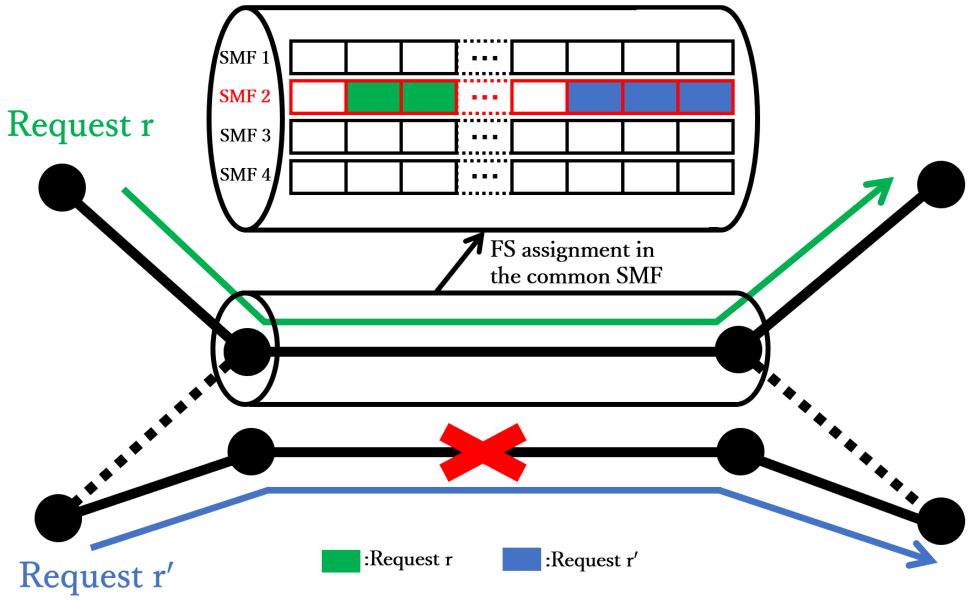

Figure 4.6: Case in which the working path for request r and the backup path for request r' share a common SMF on the same link.

Constraints for Spectrum Nonoverlap between Working and Backup Paths

$$p_{r'} - {w_r}^* \leq M(1 - m_r^{r'} + 2 - (a_r^{e,c*} + \eta_{r'}^{e,c})) - 1$$
$$\forall e \in E,\ \forall c \in C,\ \forall r, r' \in R,\ r \neq r', \tag{4.28}$$

$${w_r}^* + t_r - p_{r'} \leq M(m_r^{r'} + 2 - (a_r^{e,c*} + \eta_{r'}^{e,c}))$$
$$\forall e \in E,\ \forall c \in C,\ \forall r, r' \in R,\ r \neq r', \tag{4.29}$$

$$p_{r'} + t_{r'} - {w_r}^* \leq M(1 - m_r^{r'} + 2 - (a_r^{e,c*} + \eta_{r'}^{e,c}))$$
$$\forall e \in E,\ \forall c \in C,\ \forall r, r' \in R,\ r \neq r'. \tag{4.30}$$

Constraints (4.28)~(4.30) ensure that the spectrum resources allocated to a common SMF on a link that is shared between a working path for one request and a backup path for another request cannot overlap. Figure 4.6 shows an example in which the working path for request r shares a common SMF and link with the backup path for request r'; in this case, the allocated FSs should not overlap.

Constraints for Spectrum Nonoverlap between Backup Paths

• When the working paths for requests r and r' pass through a common SMF c on the same link e, as indicated by $a_r^{e,c*} = 1$ and $a_{r'}^{e,c*} = 1$, the following constraints apply.

$$p_{r'} - p_r \leq M(1 - m_r^{r'} + 2 - (\eta_r^{e',c'} + \eta_{r'}^{e',c'})) - 1$$
$$\forall e, e' \in E,\ \forall c, c' \in C,\ \forall r, r' \in R,\ \zeta_1 = 1, \tag{4.31}$$
$$p_r + t_r - p_{r'} \leq M(m_r^{r'} + 2 - (\eta_r^{e',c'} + \eta_{r'}^{e',c'}))$$
$$\forall e, e' \in E,\ \forall c, c' \in C,\ \forall r, r' \in R,\ \zeta_1 = 1. \tag{4.32}$$

Figure 4.7 shows a case in which an SMF fails and the backup path for request r shares a common span with the backup path for request r'. Constraints (4.31) and (4.32) ensure that the spectrum resources allocated to a common SMF of a shared link between the backup paths for requests r and r' do not overlap in the case of a failure occurring in a common SMF of their working paths.

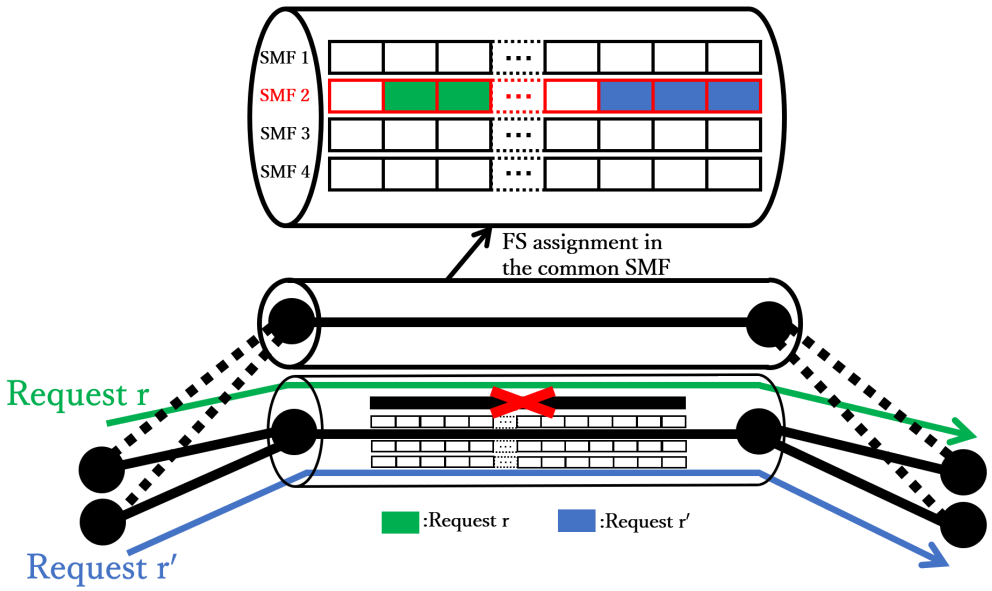

Figure 4.7: Case in which the backup paths for two distinct requests share a common SMF on the same link and SMF failure affects their working paths.

• When the working paths for requests r and r' pass through a common node v, as indicated by $b_r^{v*} = 1$ and $b_{r'}^{v*} = 1$, the following constraints apply.

$$p_{r'} - p_r \leq M(1 - m_r^{r'} + 2 - (\eta_r^{e,c} + \eta_{r'}^{e,c})) - 1$$
$$\forall e \in E,\ \forall c \in C,\ \forall v \in V,\ \forall r, r' \in R,\ \zeta_2 = 1, \tag{4.33}$$
$$p_r + t_r - p_{r'} \leq M(m_r^{r'} + 2 - (\eta_r^{e,c} + \eta_{r'}^{e,c}))$$
$$\forall e \in E,\ \forall c \in C,\ \forall v \in V,\ \forall r, r' \in R,\ \zeta_2 = 1. \tag{4.34}$$

A situation in which node failure simultaneously affects the working paths for requests r and r', both of which pass through the failed node, is shown in Figure 4.8. Constraints (4.33) and (4.34) ensure that the spectrum resources allocated to a common SMF of a shared link between the backup paths for the different requests do not overlap when node failure affects both of their working paths.

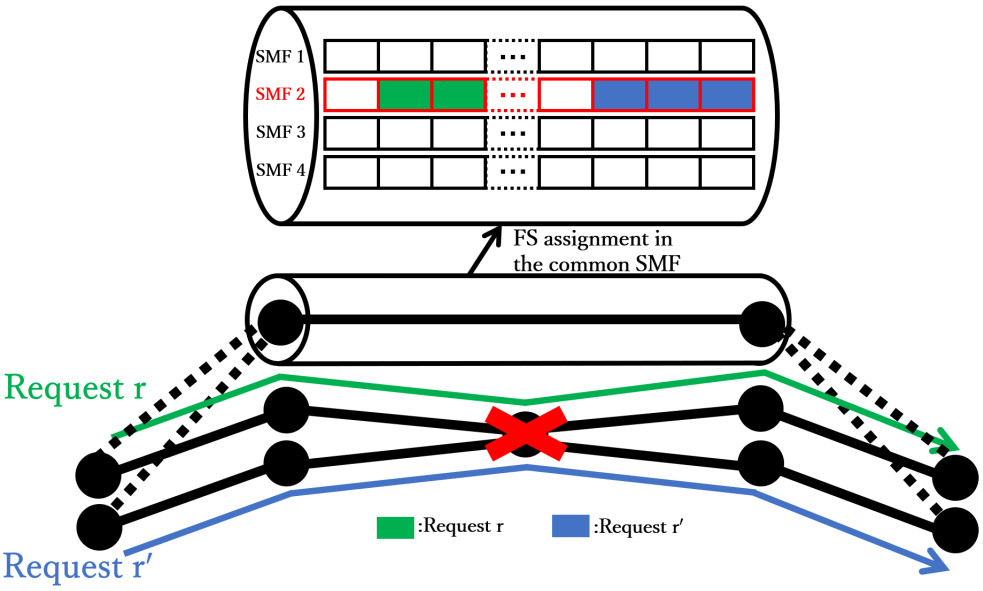

Figure 4.8: Case in which the backup paths for two distinct requests share a common SMF on the same link and node failure affects their working paths.

• When the working paths for requests r and r' pass through a common link e, as indicated by $g_r^{e*} = 1$ and $g_{r'}^{e*} = 1$, the following constraints apply.

$$p_{r'} - p_r \leq M(1 - m_r^{r'} + 2 - (\eta_r^{e',c} + \eta_{r'}^{e',c})) - 1$$
$$\forall e, e' \in E,\ \forall c \in C,\ \forall r, r' \in R,\ \zeta_3 = 1, \tag{4.35}$$
$$p_r + t_r - p_{r'} \leq M(m_r^{r'} + 2 - (\eta_r^{e',c} + \eta_{r'}^{e',c}))$$

$$\forall e, e' \in E,\ \forall c \in C,\ \forall r, r' \in \beta_e,\ \zeta_3 = 1. \tag{4.36}$$

Similarly, Figure 4.9 shows the case of SMF and link sharing between the backup paths for requests r and r', whose corresponding working paths share a common link. Specifically, constraints (4.35) and (4.36) ensure that when a link failure interrupts the working paths for both requests r and r' and their selected backup paths share a common SMF and link, spectrum nonoverlap is guaranteed in their common span.

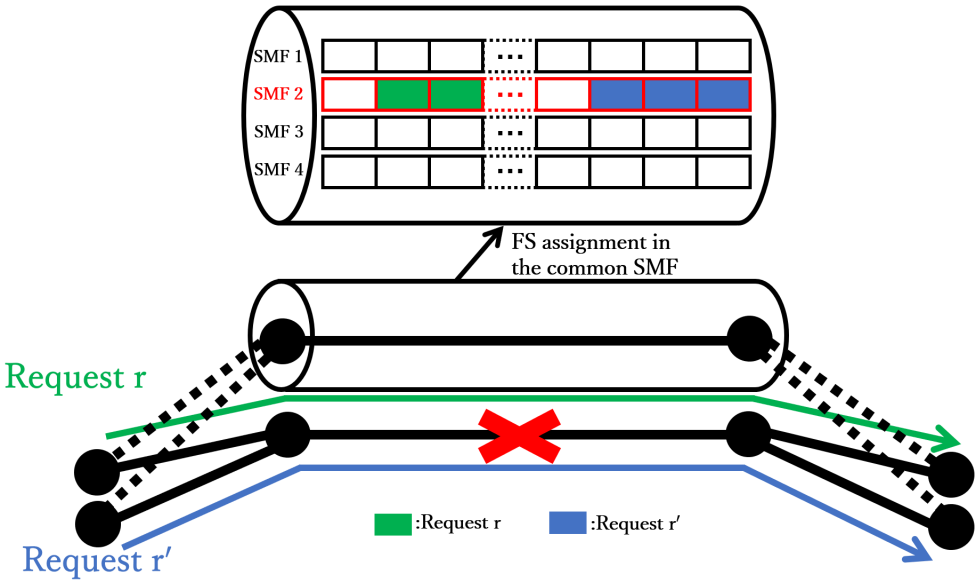

Figure 4.9: Case in which the backup paths for two distinct requests share a common SMF on the same link and link failure affects their working paths.

• When the working paths for requests r and r' pass through a common SRLG u, as indicated by $h_r^{u*} = 1$ and $h_{r'}^{u*} = 1$, the following constraints apply.

$$p_{r'} - p_r \leq M(1 - m_r^{r'} + 2 - (\eta_r^{e,c} + \eta_{r'}^{e,c})) - 1$$
$$\forall e \in E,\ \forall c \in C,\ \forall u \in U,\ \forall r, r' \in R,\ \zeta_4 = 1, \tag{4.37}$$
$$p_r + t_r - p_{r'} \leq M(m_r^{r'} + 2 - (\eta_r^{e,c} + \eta_{r'}^{e,c}))$$
$$\forall e \in E,\ \forall c \in C,\ \forall u \in U,\ \forall r, r' \in R,\ \zeta_4 = 1. \tag{4.38}$$

In the case shown in Figure 4.10, the working paths for requests r and r' are simultaneously affected by SRLG failure because the links that they traverse belong to the same SRLG. For this case, constraints (4.37) and (4.38) ensure that the spectrum does not overlap in a common SMF of a shared link between the backup paths for requests r and r' when the same SRLG failure influences their corresponding working paths.

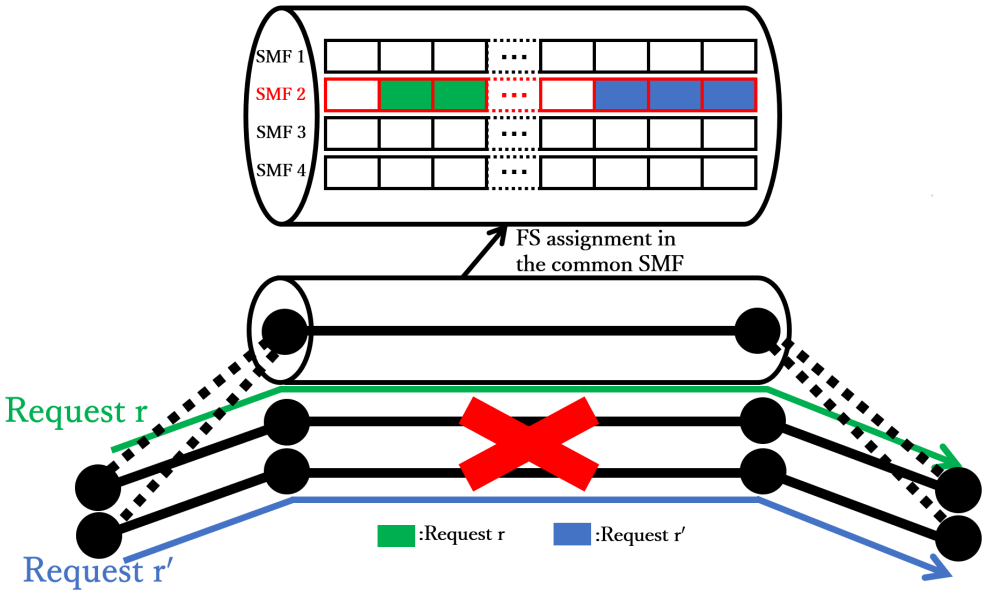

Figure 4.10: Case in which the backup paths for two distinct requests share a common SMF on the same link and SRLG failure affects their working paths.

4.4 Γ-Robust Optimization for Nondeterministic Traffic demand

The network traffic may become unpredictable in future networks due to diverse demands. In this work, network design considering the uncertainty in traffic volume is addressed.

We introduce a robust optimization technique called Γ-robust optimization [78, 80]. Suppose that the size uncertainty of request r, denoted $\widetilde{t_r} = \left[t_r - \hat{t}_r, t_r + \hat{t}_r\right]$, follows a symmetric distribution. Without loss of generality, Γ is a parameter (not necessarily an integer) whose value is in the interval $[0, |R|]$. The role of parameter Γ is to adjust the robustness of the proposed system against the conservation level of its solution [81]. Because Γ is not necessarily an integer, at most $|Q| = \lfloor \Gamma \rfloor$ requests are allowed to vary in size, and one request t_q $(q \in R \backslash Q)$ changes by $(\Gamma - \lfloor \Gamma \rfloor)\hat{t}_q$.

To demonstrate how to achieve Γ robustness, constraint (4.24) is rewritten as follows:

$$\sum_{r \in R} \eta_r^{e,c} t_r + \max_{\{Q \cup \{q\} | Q \subseteq R, |Q| = \lfloor \Gamma \rfloor, q \in R \backslash Q\}} \{\sum_{r \in Q} H_r^{e,c} \hat{t}_r + (\Gamma - \lfloor \Gamma \rfloor) H_q^{e,c} \hat{t}_q\} \leq f_e^c$$
$$\forall v \in V,\ \forall e \in E,\ \forall c \in C,\ -\eta_r^{e,c} \leq H_r^{e,c} \leq \eta_r^{e,c}. \tag{4.39}$$

If Γ is an integer, then the left side of constraint (4.24) is protected by

$$F(\boldsymbol{\eta}, \Gamma) = \max_{\{Q | Q \subseteq R, |Q| = \Gamma\}} \{\sum_{r \in Q} |\eta_r| \hat{t}_r\}.$$

Concretely, when $\Gamma = 0$, the size of all requests is deterministic. Otherwise, if $\Gamma = |R|$, then the size of all requests is uncertain. Therefore, the robustness of the proposed model is ensured by adjusting the parameter $\Gamma \in [0, |R|]$.

We can see that the left-hand side of constraint (4.39) is nonlinear since it contains two different variables, $\boldsymbol{\eta}$ and $\boldsymbol{H}$. To make it linear, we introduce the following proposition.

Proposition 1 Given vectors $\boldsymbol{\eta}^*$ and $\hat{\boldsymbol{t}}$, the uncertain part of constraint (4.24), given by (4.40),

$$F(\boldsymbol{\eta}^*, \Gamma) = \max_{\{Q \cup \{q\} | Q \subseteq R, |Q| = \lfloor \Gamma \rfloor, q \in R \setminus Q\}} \{ \sum_{r \in Q} |\eta_r^{e,c*}| \hat{t}_r + (\Gamma - \lfloor \Gamma \rfloor) |\eta_q^{e,c*}| \hat{t}_q \}, \tag{4.40}$$

can be obtained as the optimal solution to the following linear problem (LP) (4.41):

$$\begin{aligned} max \quad & \sum_{r \in R} |\eta_r^{e,c*}| \hat{t}_r z_r, \\ subject\ to \quad & \\ & \sum_{r \in R} z_r \leq \Gamma, \\ & 0 \leq z_r \leq 1 \qquad \forall r \in R. \end{aligned} \tag{4.41}$$

Proof *For the binary variable of each request r, denoted by $z_r \in [0, 1]$, the optimal solution to LP (4.39) can be obtained when $\lfloor \Gamma \rfloor$ variables z_r are equal to 1 and one variable is equal to $\Gamma - \lfloor \Gamma \rfloor$. Therefore, the optimal solution to LP (4.39) is equivalent to the cost function $\sum_{r \in Q} |\eta_r^{e,c*}| \hat{t}_r + (\Gamma - \lfloor \Gamma \rfloor) |\eta_q^{e,c*}| \hat{t}_q$ with subset $\{Q \cup \{q\} | Q \subseteq R, |Q| = \lfloor \Gamma \rfloor, q \in R \setminus Q\}$, which is equal to $F(\boldsymbol{\eta}^*, \Gamma)$.* □

Then, constraint (4.39) can be rewritten as a linear formulation in accordance with Theorem 1.

Theorem 1 Given the robustness parameter Γ, constraint (4.39) can be reformulated as follows:

$$\sum_{r \in R} \eta_r^{e,c} t_r + \Gamma \pi + \sum_{r \in R} \omega_r \leq f_e^c \qquad \forall v \in V, \forall e \in E, \forall c \in C, \tag{4.42}$$

$$|\eta_r^{e,c*}| \hat{t}_r - (\pi + \omega_r) \leq 0 \qquad \forall v \in V, \forall r \in R, \forall e \in E, \forall c \in C, \tag{4.43}$$

$$0 \leq \omega_r, \forall r \in R, \tag{4.44}$$

$$0 \leq \pi. \tag{4.45}$$

Proof *The dual of LP (4.41) is given as follows:*

$$\begin{aligned} \min \quad & \sum_{r \in R} \omega_r + \Gamma \pi, \\ \text{subject to} \quad & \\ & \pi + \omega_r \geq |\eta_r^{e,c*}| \hat{t}_r \qquad \forall r \in R, \\ & \omega_r \geq 0 \qquad \forall r \in R, \\ & \pi \geq 0. \end{aligned} \tag{4.46}$$

Obviously, the objective function of LP (4.41), $f(r) = |\eta_r^{e,c^*}|\hat{t}_r z_r$, is a convex function; $g(r) = z_r$ is also a convex function, and $h(r) = \sum_{r \in R} z_r$ is an affine function. Therefore, LP (4.41) has feasible solutions, and the solutions are bounded. Due to the strong duality, the dual of LP (4.41), given by (4.46), is also feasible, and its optimal solution is the optimal solution to the original LP (4.41). Therefore, constraint (4.24) can be replaced by constraints (42)~(45) in Theorem 1.□

Similarly, constraints (4.25), (4.26) and (4.27) can be reformulated in the same way as constraint (4.24).

4.4.1 Computational Complexity Analysis

In this part, we examine the computational complexity of optimization models by counting the number of variables and constraints. For the working path determination MILP model, the number of variables is bounded by the greater of $O(|R|^2)$ and $O(|R| \cdot |E| \cdot |C| \cdot |F|)$, and the number of constraints is bounded by the greater of $O(|R|^2 \cdot |E| \cdot |C|)$ and $O(|R| \cdot |E| \cdot |C| \cdot |F|)$. $|R|$ is the number of requests, $|E|$ is the number of network links, $|C|$ is the number of SMFs in each SMFB, and $|F|$ is the number of required FSs. For the backup path determination MILP model, the available links, nodes, and cores are fewer, so the upper bound of the number of variables and constraints in the backup path determination MILP model can be derived as the bounds in the working path determination MILP model. However, if we solve the working path and the backup path determination problems jointly in a MILP model, the lower bound for the number of variables and constraints are $O(|R|^4)$ and $O(|R|^4 \cdot |E|^2 \cdot |C|^2)$, which are far more than solving the problems separately.

4.5 Heuristic Algorithms for the Working and Backup Path Determination Problems

The RSSA problem has been proven to be NP-complete and the MILP model cannot be solved within a reasonable time as the transmission request matrix and the network itself increase in size. Therefore, in this section, we propose three heuristic algorithms for solving the working and backup paths determination problems: a best-fit FS assignment algorithm, a working path determination algorithm and a backup path determination algorithm.

4.5.1 Best-Fit FS Assignment Algorithm

In this subsection, we focus on the spectrum allocation problem and aim to find the best spectrum selection for the working and backup paths of a request. To reduce spectrum fragmentation and improve search efficiency, we propose a best-fit spectrum allocation algorithm whose pseudocode is shown in Algorithm 1.

Algorithm 1 Best-Fit FS Assignment Algorithm

Input: Number of required FSs for request r in each SMF of the link; available path p_r for request r
Output: Set of SMF of each link $e \in p_r$ selected for request r AG_r; available range of FSs for request r F_r

1: Set the initial FS index $f_{start} = 1$
2: Set the FS usage table $T[e, c, f] = \{e : c : f : 0\}(e \in E, c \in C, f \in F)$
3: Set the FS occupied list O
4: Set $flag = 1$, $flag_1 = 1$, $flag_2 = 1$
5: **while** $flag$ **do**
6: Set $flag = 0$
7: **for** each link e in available path p_r **do**
8: Obtain the output $(flag_3, info_3)$ from Phase 1
9: **if** $flag_3$ **then**
10: Update the selected core of link e for request r
$AG_r[e] = info_3$ and available range of FSs for request r
$F_r = [f_{start}, f_{start} + t_r - 1]$
11: **else**
12: Set $flag = 1$ and update $f_{start} = info_3 + 1$
13: **break** (go to line 5)
14: **end if**
15: **end for**
16: **end while**

Phase 1 SMF Selection

Input: Link e
Output: $(flag_3, info_3)$
17: **for** each SMF c in available SMF set C **do**
18: Obtain the output $(flag_2, info_2)$ from Phase 2
19: **if** $flag_2$ **then**
20: Update $flag_3 = 1$ and $info_3 = s$
21: **break** (go to line 7)
22: **else**
23: Add FS $info_2$ to the FS occupied list O
24: **end if**
25: **end for**
26: All of the SMFs $c \in C$ are unavailable. Update $flag_3 = 0$ and $Info_3 = min(f \; \forall f \in O)$

Phase 2 FS Range Selection

Input: SMF c of link e
Output: $(flag_2, info_2)$
27: **for** each FS f in the range of FSs $[f_{start}, f_{start} + t_r - 1]$ **do**
28: Check the FS usage table T to determine whether each FS f
29: in SMF c of link e is used (if $T[e, c, f] = 1$, FS f is used)
30: **if** $T[e, c, f]$ **then**
31: Update $flag_2 = 0$ and $info_2 = f$
32: **break** (go to line 17)
33: **end if**
34: **end for**
35: FSs in the range $[f_{start}, f_{start} + t_r - 1]$ are unused; update $flag_2 = 1$ and $info_2 = f$ (here, $Info_2$ is equal to $f_{start} + t_r - 1$)

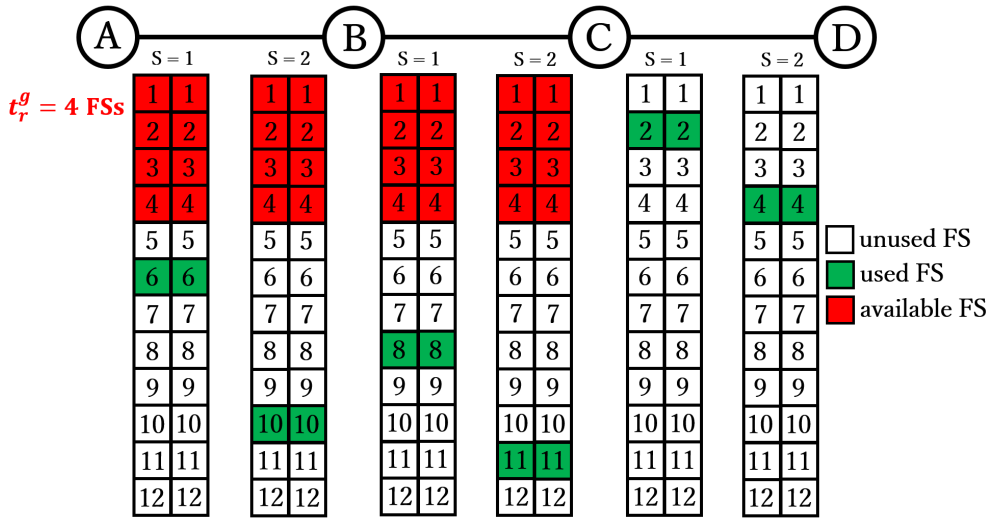

Figure 4.11: Example of our proposed best-fit FS assignment algorithm ($f_{start} = 1$).

In the example shown in Figure 4.11, a connection request r with a traffic demand of $t_r = 4\ FSs$ is transmitted in a chain network from node A to node D, where each link has a 2-SMFB. To simplify the problem for a better understanding, we assume that there are two available SMFs on each link. Some FSs are already used for other connection requests, as shown in green.

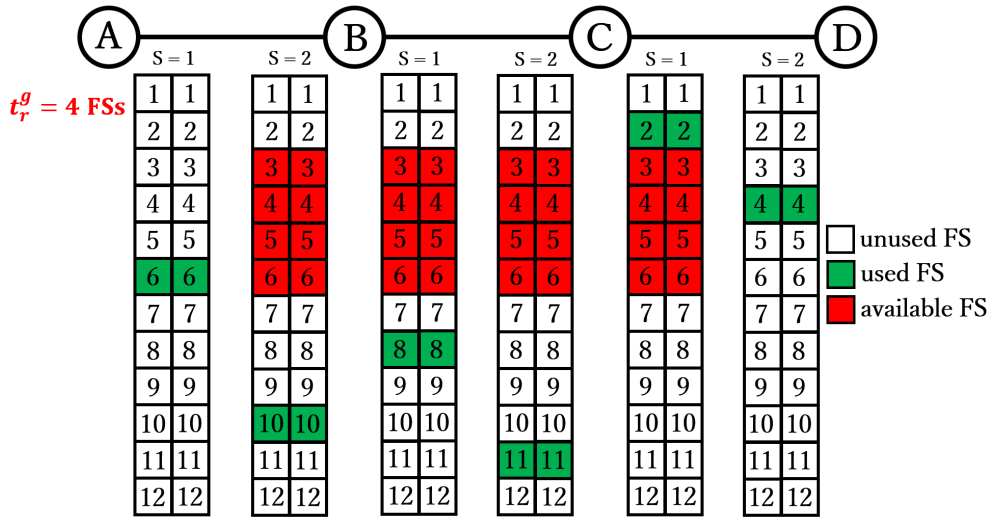

Figure 4.12: Example of our proposed best-fit FS assignment algorithm ($f_{start} = 3$).

We now show how our proposed FS assignment algorithm works. To meet the requirements of spectrum contiguity and continuity, the available ranges of the FSs in each SMF on the links with the initial FS index $f_{start} = 1$ are identified, as shown in red in Figure 4.11. First, we check whether continuous FSs exist in each SMF on each link for request r. For example, for link AB, the FSs [1, 2, 3, 4] in SMFs 1 and 2 can be assigned such that the output of Phase 2 (lines 27-35)

is (1, 4) for both SMFs 1 and 2, where the flag for judging whether there exists a continuous range of FSs is $flag_2 = 1$ and the maximal occupied index in the assigned range of FSs [1, 2, 3, 4] is $info_2 = 4$. With the output obtained from Phase 2, we can select one available SMF in Phase 1. If more than one such group exists, as in the case of link AB, we choose the first SMF with the output of $(flag_3 = 1, info_3 = 1)$. Conversely, if $flag_2 = 0$, which means that we cannot find 4 continuous FSs in any SMF, as in the case of link CD, then we set the initial FS index f_{start} equal to 3 as the minimal occupied FS, and the output of Phase 1 is $(flag_3 = 0, info_3 = 3)$. Then, we aim to find the available ranges of FSs for request r on each link with initial FS index $f_{start} = 3$, similar to the above process. As shown in Figure 4.12, the range of FSs [3, 4, 5, 6] in SMF 2 of link AB, SMF 1 of link BC and SMF 1 of link CD is assigned for request r.

4.5.2 Working Path Determination Algorithm

For a given transmission request sequence, we first sort the requests in descending order of their traffic demand sizes t_r. Then, we determine the RSSA for these requests one by one, starting with the request with the largest traffic demand.

We now introduce how the working path determination algorithm works. First, we calculate k shortest paths based on the K shortest path (KSP) algorithm as the working path candidates for each request r. Then, for each request r in the sorted traffic request sequence, we first choose the shortest path (ksp_r, $k = 1$) as the working path and select one SMF of each link along ksp_r with a range of FSs based on Algorithm 1. If a set of the available set of SMF AG_r and an available range of FSs F_r are successfully obtained by Algorithm 1, then the FSs $F_r = [f_s, f_s + t_r - 1]$ in the selected SMF of each link along ksp_r are assigned to the working path for each request r. After the assignment of the working path, SMFs and FSs for each request r, we need to update the FS usage table $T[e, c, f]$ and the maximal FS index used f^w_{max}. In addition, the working path determination table $W[r]$, including ksp_r, AG_r, and F_r, must be recorded for reference during the allocation of the backup paths.

After the working paths for all requests have been determined by the corresponding shortest paths, we find the most congested SMF among the links, i.e., the SMF with the maximum FS index used, according to the FS usage table $T[e, c, f]$. Then, we check the working path for each request r that traverses this most congested SMF and to find the one r^* that can maximally reduce the FS usage and reroute it to the second shortest path ($k_{r^*} + 1$). Finally, we update the FS usage table, the working path determination table $W[r]$ and the maximal FS index used f^w_{max}. Additionally, we update the KSP table $K[r]$ to keep track of whether all k shortest paths for a request have been allocated. The above process is repeated until we cannot find a request that can reduce the maximal FS index used f^w_{max} or the k shortest paths have all been selected for a request. The pseudocode of our proposed working path determination algorithm is shown in Algorithm 2.

Algorithm 2 Working Path Determination Algorithm

Input: Traffic request sequence R ($r = \{s_r, d_r, t_r\} \in R$)

Output: Working path determination table $W[r]$; maximal FS index used f^w_{max}

1: Arrange request sequence R in descending order according to the traffic demands of the requests t_r
2: Calculate the k shortest routing paths as the working path candidates for each request with the given source-destination pair based on the KSP algorithm [79]
3: Set the maximal FS index used f^w_{max} equal to 0
4: Set the FS usage table $T[e, c, f] = \{e : c : f : 0\}(e \in E, c \in C, f \in F)$
5: Set the working path determination table for requests $W[r] = \{r : (e, AG_r[e], F_r)\}(r \in R, e \in p_r)$
6: Set the KSP table $K[r] = \{r : k_r = 1\}(r \in R)$
7: **while** True **do**
8: **for** each request r in R **do**
9: Select one SMF of each link along the ksp_r based on Algorithm 1 with the available range of FSs
10: **if** AG_r and $F_r \neq \emptyset$ **then**
11: Assign the FSs $F_r = [f_s, f_s + t_r - 1]$ in the selected SMF along lightpath ksp_r to the working path for request r
12: Update the FS usage table $T[e, c, f]$ and the maximal used FS index f^w_{max}
13: Update the working path determination table $W[r]$ with the assigned ksp_r, AG_r and F_r
14: **end if**
15: **end for**
16: According to the FS usage table $T[e, c, f]$, find the most congested SMF among the links, with the maximum spectrum usage
17: Check the working path for each request that traverses SMF c of link e, find the one r^* that can maximally reduce f^w_{max} and reroute it
18: Set $k_{r^*} += 1$
19: Use set $\{r^*\}$ instead of R and return to line 8
20: **if** f^w_{max} decreases or $k_{r^*} < 5$ for request r^* **then**
21: Update the FS usage table $T[e, c, f]$ and the maximal FS index used f^w_{max}
22: Update the working path determination table $W[r]$ with the assigned ksp_r, AG_r and F_r
23: **else**
24: **break while**
25: **end if**
26: **end while**

4.5.3 Backup Path Determination Algorithm

In accordance with the working path determination table $W[r]$ obtained by Algorithm 2, we can determine the backup paths for requests to ensure robustness against different network failures based on Algorithm 3.

Algorithm 3 Backup Path Determination Algorithm

Input: Network failure type $x \in X$; traffic request sequence R ($r = \{s_r, d_r, t_r\} \in R$); working path assignment table obtained by Algorithm 2 $W[r]$
Output: maximal FS index used f^b_{max}; total number of backup FSs f_{bp}

```
Arrange request sequence R in descending order according to the traffic demands of requests
Calculate the k shortest routing paths as the backup path candidates for each request based on the KSP algorithm,
    with different available link and node sets for different types of network failures
Set the assigned request set R', and path comparison set for each request r P'_r
for each request r in R do
    if r = 1 then
        Select the shortest path as the backup path for request r and assign
        the FSs based on Algorithm 1
        if AG_r and F_r ≠ ∅ then
            Assign the FSs F_r = [f_s, f_s + λ_r − 1], lightpath ksp_r and
            the selected SMF to the backup path for request r
            Update the maximal FS index used f^b_max and total backup
            FSs f_bp and add request r to R'
        end if
    else
        for each request r' in R' do
            Check whether a common link/node/SRLG exists
            between the working paths for requests r' and r
            if such a link/node/SRLG exists then
                Select the shortest path p and assign the FSs based on
                Algorithm 1
                Add the maximal FS index used f^b_max, the backup FSs
                f_bp and path p into P'_r
            else
                Select the path p among the k = {1, 2, 3, 4, 5} shortest
                paths that coincides with the most links on the backup
                path of request r'
                Assign the FSs based on Algorithm 1 and add the maximal
                FS index used f^b_max, the backup FSs f_bp and path p
                to P'_r
            end if
        end for
    end if
    Compare the paths in P'_r, select the path with the minimal f_bp or
    f^b_max as the backup path for request r; then, add request r to R'
end for
```

Similar to the procedure for working path determination, the request sequence for backup path determination is arranged in descending order according to the traffic demands of requests. The k candidate shortest paths for the backup path for each request are calculated by means of the KSP algorithm. The available link and node sets for backup path determination are different for different types of network failures.

Our proposed backup path determination algorithm, for which the pseudocode is shown in Al-

gorithm 3, proceeds as follows. For each request in the sorted sequence R, we first choose the shortest path ($k = 1$) as the backup path for the first request with the largest demand and assign the FSs in the selected SMF of each link along this path based on Algorithm 1. Then, we update the maximal FS index used f^b_{max} and the backup FSs f_{bp}. For each request whose backup path has been determined, we add it to the assigned request set R'.

When allocating a request r after the first request, for each request r' in the assigned request set R', we check whether any common span (link/node/SRLG) exists between the working paths for requests r and r'. If such a common span exists, the shortest path ($k = 1$) p is selected, and the FSs in the SMF of each link along path p are assigned based on Algorithm 1. Then, we compute the maximal FS index used f^b_{max} and the backup FSs f_{bp} when path p is selected and add them to the path comparison set for request r P'_r. If there is no common span, then we select the path p among the k shortest paths that has the most links coinciding with the backup path for request r'. Similarly, we add f^b_{max}, f_{bp} and the path p to P'_r after allocating the FSs based on Algorithm 1. Finally, we compare the paths in P'_r, select the path with the minimal f_{bp} or f^b_{max} as the backup path for request r, and we add request r to R'.

4.6 Numerical Results and Performance Analysis

To obtain a robust design of SBPP-based SDM-EONs against different types of network failures and uncertainty in request size, we perform simulation experiments considering two network topologies: (1) a 14-node 21 dual-link NSFN, as shown in Figure 4.13(a), and (2) a 28-node 34 dual-link EOBN, as shown in Figure 4.13(b).

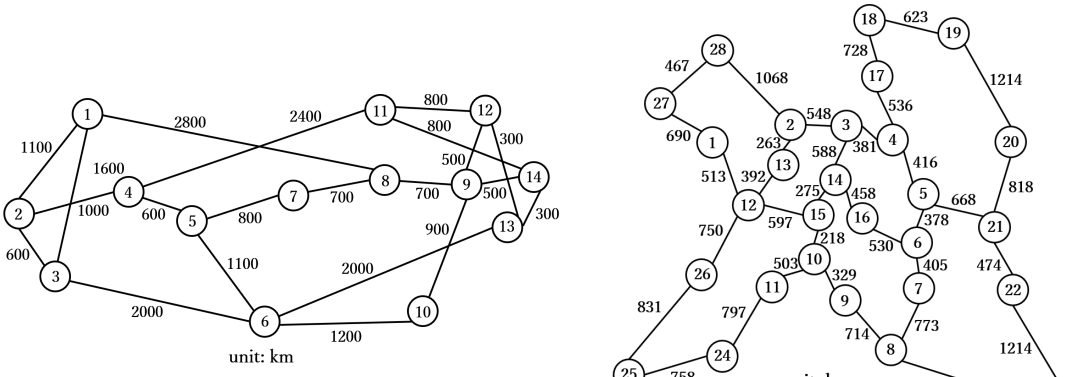

(a) NSFN

(b) EON

Figure 4.13: Network topology: (a) NSFN with 14 nodes and 42 directed links; (b) EOBN with 28 nodes and 68 directed links.

The assumptions of our simulation experiments are as follows:

(1) Among the numerous available types of SDM optical fibers, we choose parallel SMFs for our experimental scenarios. MMFs and MCFs are suitable only for short-range transmission because of the impact of the high intercore XT and the cladding diameter. By comparison, SMFBs are more appropriate for long-distance transmission in backbone networks due to their almost nonexistent intercore XT. Moreover, constructing SMFBs as bundles of parallel SMFs makes the migration from existing SMF-based networks easier and less expensive, as this type of SMFB is compatible with existing optical elements. In addition, the optical fibers of a backbone network are mainly laid under railways or on the seabed, so the low space efficiency of the SMFB can be ignored. Overall, SMFBs appear preferable to other types of SDM fibers in optical transmission and network scenarios [69].

(2) The predefined traffic size of each request is randomly selected from the set $\{$100 Gbps, 200 Gbps, 400 Gbps, 800 Gbps, 1 Tbps$\}$. The nondeterministic request size is defined via Γ-robust optimization [78].

(3) The number of connection requests for the simulation experiments of small-scale instances ranges from 20 to 50 at a step of 5; the number of requests for the simulation experiments of large-scale instances is set to 500 and 1,000. For each traffic matrix with a certain number of requests, their average request size is equivalent. To ensure generality, the source-destination node pair for each request is randomly chosen, and the final result reported under each number of requests is obtained by performing 50 iterations with independent inputs of randomly generated traffic matrices and taking the average.

(4) Each FS occupies 12.5 GHz of spectrum resources according to ITU-T G.694.1 [82]. We assume that an optical carrier (OC) is composed of 3 FSs, which can support the transmission of 50 Gbps of traffic under DP-BPSK [46].

(5) We assume that the backup paths for node failure are selected to be node-disjoint with respect to the corresponding working paths, that the backup paths for core and link failure are selected to be link disjoint with respect to the corresponding working paths, and that the backup paths for SRLG failure are selected to be SRLG disjoint with respect to the corresponding working paths.

(6) The previously proposed k shortest path and first fit spectrum assignment algorithm (KSP + FFSA) for working path and backup path determination is assumed that between each node pair there exist three shortest paths for working path establishment, and three another shortest path which are node/link/SRLG disjoint from its working path can be selected to determine the backup path.

4.6.1 Results for Maximal FS Index Used

We first evaluate the performance of the MILP model and our proposed heuristic algorithm for working path determination in a 4-SMFB-based optical network as examples.

The left part of Table 4.2 shows the maximal FS index used and execution time for working path determination of the MILP model, our proposed heuristic algorithm, and a previously proposed algorithm. As shown in Table 4.2, when the number of requests is small ($|R| \in [20, 50]$), the optimal solution for the maximal FS index used obtained by the MILP model is constant and equals 21.0 with an increasing number of requests in different network topologies. The execution time of the MILP model increases with the increase in the number of requests, and the execution time of the MILP model in the EOBN is much longer than that in the NSFN. This is because the feasible solution spaces of the MILP model expand with an increasing number of requests and network size, leading to long execution times.

Table 4.2: Performance evaluations for working and backup path determination in different network topologies

		Working path								Backup path							
		MILP-RSCA		Heuristic			KSP + FFSA			MILP-RSCA		Heuristic			KSP + FFSA		
r	NT	Req. FSs	Time	Req. FSs	Av.Gap	Time	Req. FSs	Av.Gap	Time	Req. FSs	Time	Req. FSs	Av.Gap	Time	Req. FSs	Av.Gap	Time
20	NSFN	21.0	25.2s	21.0	0.0%	1.4s	21.0	0.0%	1.6s	21.0	25.2s	21.8	3.8%	2.4s	22.1	5.2%	1.8s
	EOBN	21.0	62.7s	21.0	0.0%	1.7s	21.9	4.3%	2.4s	21.3	62.7s	22.0	4.8%	3.7s	22.8	8.6%	2.3s
25	NSFN	21.0	33.6s	21.0	0.0%	1.4s	22.7	8.1%	1.7s	21.0	33.6s	22.0	4.8%	2.4s	24.1	10.0%	1.8s
	EOBN	21.0	191.9s	21.0	0.0&	1.7s	24.0	14.3%	2.4s	22.8	191.9s	23.7	3.9&	3.7s	25.9	23.3%	2.3s
30	NSFN	21.0	60.1s	21.0	0.0%	1.4s	22.5	7.1%	1.7s	21.9	60.1s	22.8	4.1%	2.4s	24.5	11.9%	1.8s
	EOBN	21.0	238.3s	21.3	1.4%	1.7s	24.8	18.1%	2.4s	26.0	238.3s	27.1	4.2%	3.7s	28.7	10.4%	2.3s
35	NSFN	21.0	86.0s	21.0	0.0%	1.4s	25.3	20.5%	1.7s	23.3	86.0s	25.1	7.7%	2.5s	27.5	18.0%	1.8s
	EOBN	21.0	481.4s	21.5	2.4%	1.7s	28.3	34.8%	2.4s	30.4	481.4s	33.0	8.6%	3.7s	37.7	24.0%	2.5s
40	NSFN	21.0	136.3s	21.4	1.9%	1.4s	27.3	30.0%	1.7s	24.8	136.3s	26.9	8.5%	2.4s	30.3	22.2%	1.8s
	EOBN	21.0	1208.7s	22.2	5.7%	1.8s	30.0	42.9%	2.4s	36.6	1208.7s	38.9	6.3%	3.9s	48.5	32.6%	2.5s
45	NSFN	21.0	345.5s	21.8	3.8%	1.4s	29.7	41.4%	1.7s	28.8	345.5s	31.4	9.3%	2.4s	38.8	34.7%	1.8s
	EOBN	21.0	2863.5s	22.7	8.1%	1.8s	34.9	66.2%	2.4s	37.8	2863.5s	40.5	7.1%	3.7s	57.2	51.3%	2.5s
50	NSFN	21.0	377.7s	22.1	5.2%	1.4s	31.9	51.9%	1.7s	33.3	377.7s	36.8	10.5%	2.4s	53.3	60.1%	2.1s
	EOBN	21.0	4746.0s	22.9	9.1%	1.8s	36.5	73.8%	2.5s	38.8	4746.0s	41.6	10.1%	4.0s	65.4	68.6%	2.5s
500	NSFN	-	-	144.0	-	12.5s	196.3	-	1.9s	-	-	254.9	-	15.3s	302.7	-	2.4s
	EOBN	-	-	193.3	-	17.0s	220.0	-	2.9s	-	-	326.5	-	28.1s	372.9	-	4.1s
1000	NSFN	-	-	287.1	-	78.4s	368.5	-	2.8s	-	-	478.6	-	86.7s	589.3	-	4.7s
	EOBN	-	-	365.7	-	125.1s	415.2	-	5.1s	-	-	572.5	-	110.5s	667.1	-	8.9s

Compared with the optimal solution, the gap between the solution obtained by our proposed heuristic algorithm and the optimal solution increases with the number of requests, ranging from 0%~9.1%. However, our proposed heuristic algorithm can solve the problem in less than 2 seconds, which is much less than the case of the MILP model. In addition, our proposed heuristic algorithm performs better than the previous KSP + FFSA algorithm in both the maximal FS index used and execution time. When the number of requests enlarges to 500 and 1,000, the MILP model is hard to be solved due to the limitation of memory so that the optimal solution can not be found. Compared with the previous KSP + FFSA algorithm, our proposed heuristic algorithm requires more execution time but performs better in the maximal FS index used. Furthermore, similar to the case of a small number of requests, more spectrum resources are used in the EOBN than in the NSFN.

The backup path determination problem is based on the output of the working path determination WP^*, including the routes, SMFs, and FSs assigned. Therefore, the maximal FS index used for the backup path of requests against different network failures $x \in X$ can be obtained by the following equation:

$$F^p_{max}{}^* = \max\{WP^*, x \in X | F^p_{max}(WP^*, x)\}. \tag{4.47}$$

Table 4.3: The maximal FS index used in different network topologies

	NSFN			EOBN		
	MILP-RSCA	Heuristic	KSP + FFSA	MILP-RSCA	Heuristic	KSP + FFSA
20	21.0	21.8	22.1	21.3	22.0	22.8
25	21.0	22.0	24.1	22.8	23.7	25.9
30	21.9	22.8	24.5	26.0	27.1	28.7
35	23.3	25.1	27.5	30.4	33.0	37.7
40	24.8	26.9	30.3	36.6	38.9	48.5
45	28.8	31.4	38.8	37.8	40.5	57.2
50	33.3	36.8	53.3	38.8	41.6	65.4
500	-	254.9	302.7	-	254.9	372.9
1000	-	478.6	589.3	-	478.6	667.1

The right part of Table 4.2 shows the maximal FS index used and execution time for backup path determination obtained by the MILP model and heuristic algorithms in the NSFN and the EOBN. The maximal FS index used increases with an increasing number of requests, and two main reasons are as follows. 1) As the number of requests increases, the working paths of different requests are more likely to have a common core/node/link/SRLG, which leads to their corresponding backup paths being unable to share spectrum resources in the common SMF of the same link. 2) More requested backup paths share a common SMF on the same link as the number of requests increases, resulting in an increase in the FS index used due to the spectrum nonoverlap constraint. Moreover, the characteristics of the EOBN nodes and links are numerous and centralized, which leads to the utilization of more FSs than in the NSFN.

Therefore, the maximal FS index used for both working and backup path determination F_{max}

can be computed as follows:

$$F_{max} = \max\{F^{w}_{max}, F^{p}_{max}\}. \tag{4.48}$$

The results of the maximal FS index used in different network topologies are shown in Table 4.3.

4.6.2 Results for Minimum Total Number of FS Reserved

We evaluate the minimum total number of units in FSs for the establishment of all backup paths reserved on SMFs of links in the network. The four cases, node failure, SRLG failure, core failure, and link failure, are separately considered for backup path determination.

Figure 4.14 shows the results of the total number of backup FSs against different types of network failures and network topologies obtained via the MILP method and our heuristic algorithm. The x axis shows the number of transmission requests, and the y axis shows the number of FS reserved. The solid lines represent the optimal results obtained by the MILP model, and the dotted lines represent our heuristic results.

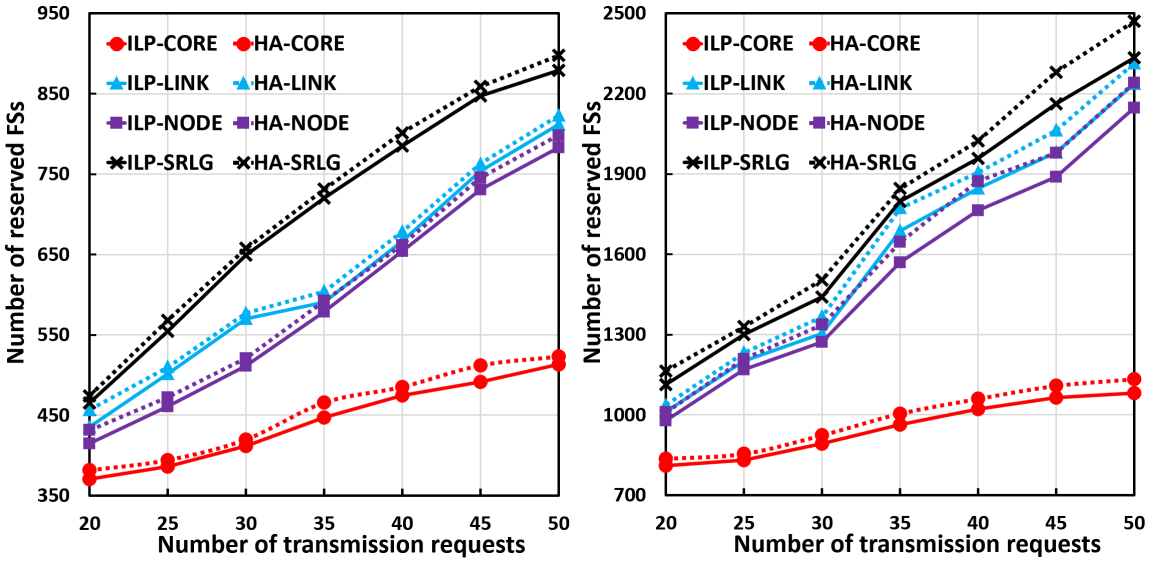

(a) NSFN (b) EON

Figure 4.14: Number of FS reserved vs. number of transmission requests against different network failures for the NSFN and EOBN.

As shown in Figure 4.14, regardless of the network failure or network topology, the total reserved spectrum resources increase as the number of requests increases. In detail, the network needs to reserve the sparest spectrum resources when SRLG failure occurs. In contrast, the least spare spectrum resources are required to be reserved for backup paths against core failure. This is because for the same traffic request matrix assigned in a certain network, the failure of an SRLG will affect the working paths of the largest number of requests, while the failure of a core will have the least impact. Moreover, the impacts of link failure and node failure on the working paths of requests,

which are more significant than the impact of core failure but inferior to the impact of SRLG failure, are almost equivalent. It is worth mentioning that more spectrum resources are reserved in case of link failure than in case of node failure. This is because the number of links in the network is more than the number of nodes, resulting in a single link failure affecting more requests. In addition, the number of FS reserved of the EOBN is much greater than that of the NSFN because the number of network nodes and links in the EOBN is greater and their distribution is more concentrated. In both the NSFN and the EOBN, the difference between the solution obtained by our proposed algorithm and the optimal solution of the MILP is 1.3%~5.8%.

4.6.3 Results for Γ-Robust Optimization with Nondeterministic Traffic

For a robust network design under request size uncertainty, the Γ-robust optimization technique is introduced.

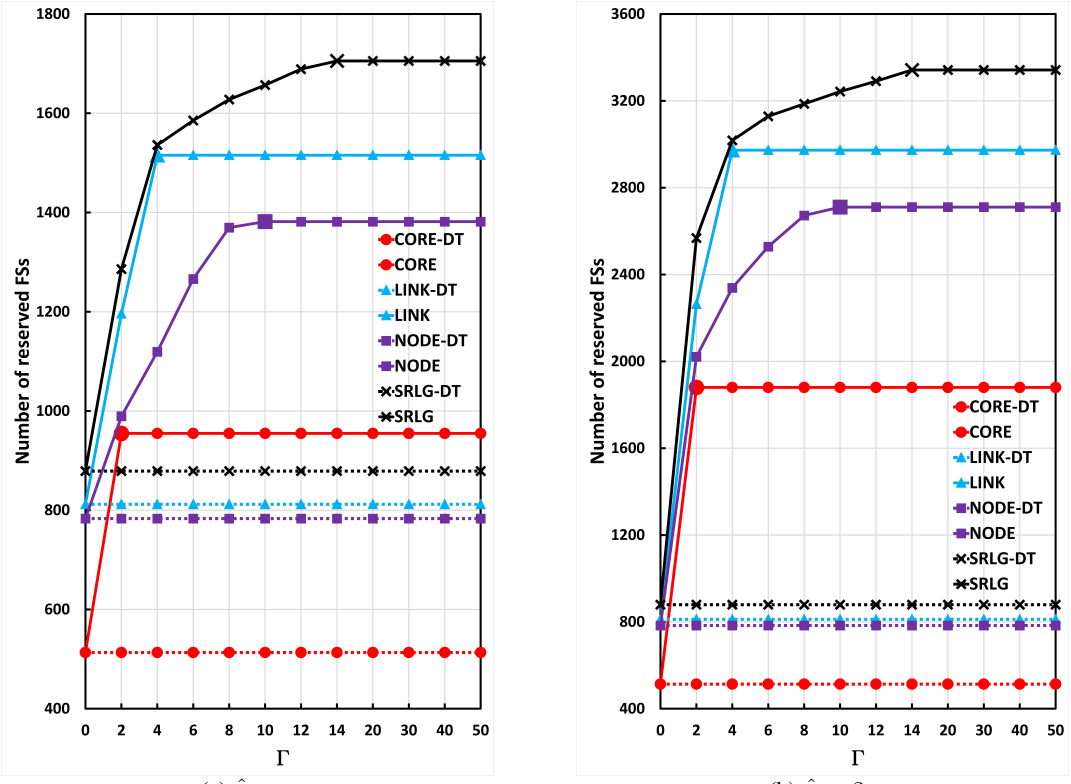

(a) $\hat{t}_r = t_r$ (b) $\hat{t}_r = 3t_r$

Figure 4.15: Number of FS reserved vs. Γ against different network failures for the NSFN with nondeterministic traffic.

In this part, we assume a value of request size uncertainty $\widetilde{t_r} = t_r + \hat{t}_r$. The values of parameter $\hat{t}_r$ are set to be t_r and $3t_r$ in our simulation experiments, which means that the nondeterministic request size deviates by 2 and 4 times the original size. The number of transmission requests is set to 50 so that the value of parameter Γ is in the interval $[0, 50]$, in which $\Gamma = 0$ indicates that the

size of all the requests in the network is deterministic and $\Gamma = 50$ indicates that the size of all the requests is equal to $t_r + \hat{t}_r$.

Figure 4.15 shows how the number of reserved spectrum resources changes with the value of Γ in the NSFN. The x axis shows the value of parameter Γ, the y axis shows the number of FS reserved. The solid lines represent the results with uncertainties in traffic volume and the dotted lines represent the results with deterministic traffic (DT). Regardless of the value of $\hat{t}_r$, when the size of requests fluctuates from t_r to $t_r + \hat{t}_r$, the total number of FS reserved for backup paths increases for small values of Γ and then saturates to a particular value as Γ increases.

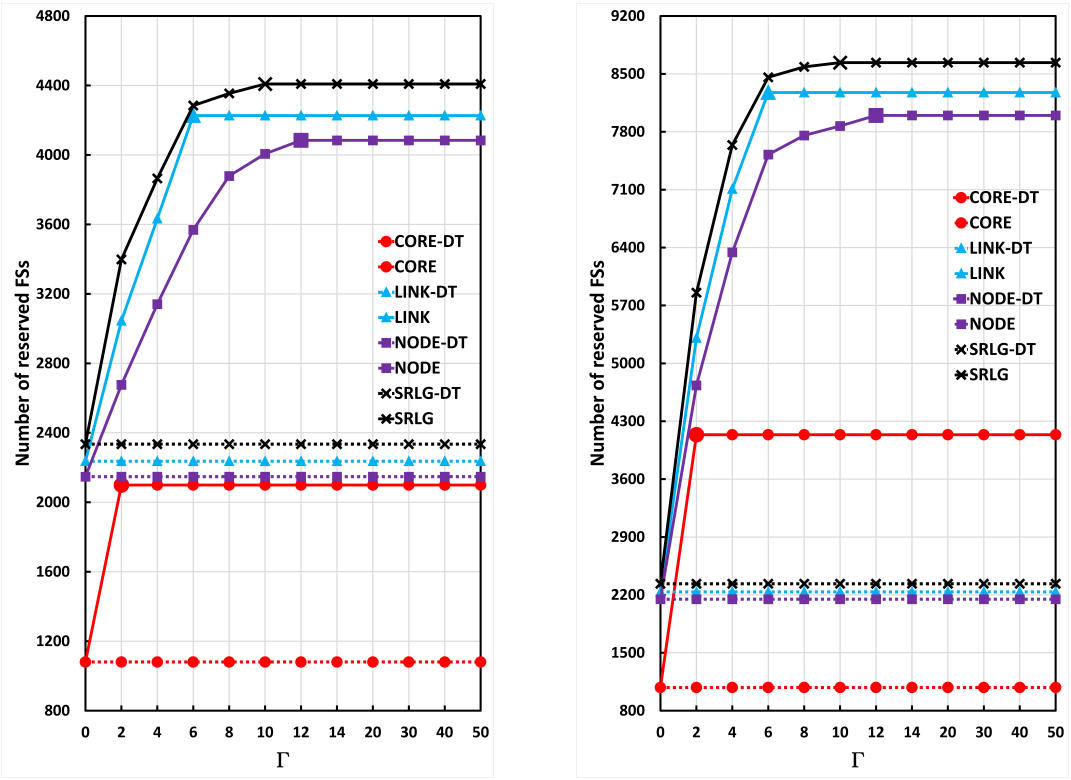

(a) $\hat{t}_r = t_r$ (b) $\hat{t}_r = 3t_r$

Figure 4.16: Number of FS reserved vs. Γ against different network failures for the EOBN with nondeterministic traffic.

The top and bottom halves of Figure 4.15 indicate the trend of reserved spectrum resources when $\hat{t}_r = t_r$ and $\hat{t}_r = 3t_r$, respectively. When $\Gamma = 0$, the curves of deterministic and nondeterministic traffic coincide at one point. As Γ increases, the spectrum resources in FSs to be reserved under different network failures generally increase, but the growth trends are inconsistent. The corresponding values of Γ are different when the numbers of FS reserved against different network failures converge. Concretely, the number of FS reserved against core, link, node, and SRLG failure becomes constant when Γ equals 2, 4, 10 and 14, respectively. Moreover, under any kind of network failure, the maximum increase in the number of FS reserved is approximately twice and four times

the original value when $\hat{t}_r$ equals to t_r and $3t_r$, respectively.

As indicated in Figure 4.16, the number of FS reserved varies with different values of Γ against different network failures in the EOBN. Similar to what is shown in Figure 4.15, the number of FS reserved first increases and then converges as Γ increases. Compared to the NSFN, the values of Γ when the numbers of FS reserved against each network failure converge are different. In detail, the number of FS reserved no longer changes when Γ is greater than or equal to 2, 6, 12, and 10 for core, link, node, and SRLG failure, respectively. In addition, more reserved spectrum resources are required for backup paths in the EOBN than in the NSFN regardless of the value of Γ. This is because the numbers of nodes and links in the EOBN are larger than those in the NSFN and the distribution of nodes in the EOBN is relatively concentrated.

4.7 Conclusion

In this research work, we address the RSSA problem for working and backup path determination in SDM-EONs implemented with bundles of SMFs. We propose a node–arc-based MILP model that determines the working path for each connection request so as to minimize the maximal FS index used while considering the assignment of routes, SMFs, and spectrum resources. Simulation results show that the gap between the solution obtained by our proposed heuristic algorithm and the optimal solution obtained by the MILP model is smaller than the gap between the solution found by the previous KSP+FFSA algorithm and the optimal solution. Based on the output from the working path determination problem, we also propose a node–arc-based MILP model and a heuristic algorithm for determining the backup paths against various types of network failures such that the total number of backup FSs is minimized. Simulation results show that the amounts of backup spectrum resources against various types of network failures are different. Moreover, in addition to considering the robustness of the network against failures, we also introduce a Γ-robust optimization technique to design a network that is robust against uncertain traffic volume. Simulation results demonstrate that the total number of backup FSs initially increases and then saturates as Γ increases regardless of the type of network failure considered. The corresponding values of Γ at which the backup spectrum resources saturate are different for various types of network failures.

Chapter 5

Conclusion and Future Works

This doctoral dissertation addressed the routing and resource allocation problems in space division multiplexing elastic optical networks. The conclusion of this dissertation per chapter is summarized as follows.

In Chapter 1, We proposed a brief introduction to research topics in the field of communication. We introduced the main research directions in optical communication networks and listed the corresponding topics of the research works in this dissertation.

In Chapter 2, we introduced five generations of optical networks with the development of Internet traffic including early TDM-based optical networks, WDM-based optical networks, EONs, SDM-EONs, and SCN-based optical networks. We introduced the core technologies of each generation of optical networks, performance improvements, and challenges of each generation of optical networks. In addition, we discussed the routing and resource assignment problems based on the characteristics of each generation of optical networks. We summarized the opportunities and challenges of routing and resource assignment problems brought by the evolution of optical networks.

In Chapter 3, we introduced our research work "Evaluation of Optical Transport Unit Line-Card Integration in Spatially and Spectrally Flexible Optical Networks in Terms of Device Cost and Network Performance". In this research, we comprehensively analyze the network architectures, including the transceiver and ROADM, according to different granularity combinations. We propose detailed models for N-core MCF-based SDM networks considering the device cost, MAT, ATU, and SE. According to the simulation results under a specific 4-core MCF-based SDM network, we find that the spatial and spectral granularity (S and O) will strongly influence the number of Spa & Spe SpCh transceivers installed at each node and the architecture of the ROADM and transceiver, resulting in different device costs and performance of network deployment. Moreover, whether or not SLC technology is supported also has an impact on the network cost/performance, but the impact is not prominent. With a trade-off relationship between the device cost and network performance, network operators need to choose the most suitable transmission system according to their objectives. If the network operators focus on device cost reduction, an SDM network with higher S and

lower O but without SLC support is recommended. Conversely, focusing on the maximization of the whole network throughput, an SDM network with lower S and higher O and with SLC support is preferred. In addition, an SDM network with lower S and O improves transceiver utility and spectral efficiency.

In Chapter 4, we introduced our research work "Robust Design against Network Failures of Shared Backup Path Protected SDM-EON". In this research, we address the RSSA problem for working and backup path determination in SDM-EONs with bundles of SMFs. We propose a node-arc-based MILP model that determines working paths for each connection request considering the assignment of routes, SMFs, and spectrum resources to minimize the maximal FS index used. The experiment and simulation results show that the gap between our proposed heuristic algorithm and the optimal solution obtained by the MILP model is smaller than the gap between the previous KSP+FFSA algorithm and the optimal solution. Based on the working path determination output, we propose a node-arc-based MILP model and a heuristic algorithm for backup path determination against different network failures to minimize the total number of backup FSs. The experiment and simulation results show that the backup spectrum resources for backup path establishment under different network failures are different. Moreover, in addition to considering the network robustness against failures, we also introduce the Γ-robust optimization technique to design a robust network under uncertainty of traffic volume. The experiment and simulation results demonstrate that the total number of backup FSs first increases and then converges as Γ increases regardless of the network failure. The corresponding values of Γ are different when the backup spectrum resource converges against different network failures.

Future works can be inferred based on the research lines stated in this dissertation. On the one hand, we will focus on the routing and spectrum assignment problem in terms of device cost and resource utilization in next-generation SCN-based optical networks. The main characteristic of an SCN is that the optical layer can be divided into a hierarchical SDM layer and a WDM layer, which is considered as a realistic and cost-effective solution. In an SCN, an SCh is supposed to carry a high-capacity optical data stream that occupies the entire spectrum resource of an SL, which can be a core in an MCF or an SMF in a bundle of SMFs. In the SDM layer, an SXC is served as the main switch of a HOXC and provides end-to-end optical routing. In the WDM layer, WXCs are served as edge switches of a HOXC and perform wavelength multiplexing and grooming. However, such the introduction of a new architecture of optical networks will present challenges related to network optimization. With the evolution from SDM-based optical networks to SCNs, the network optimization problem will change from the RSSA/RSCA problem to the routing, spatial channel, and spectrum assignment (RSCSA) problem due to the additionally introduced characteristic of the spatial channel. Therefore, it is a challenging task that focuses on the evaluation of device cost and network performance by solving the RSCSA problem in SCN-based optical networks. On

the other hand, the sustained growth of capacity requirements leads to a remarkable expansion in the scale of datacenter networks (DCNs) including the number of servers and the coverage area. The introduction of SDM transmission technology can meet the high capacity demand in DCNs by scaling up the lane count per fiber. Due to the long-haul transmission in inter DCNs, low spectrally efficient modulation formats such as DP-BPSK and DP-QPSK are applicable. Therefore, there will be more possible that the entire C-band spectrum resource can only accommodate a single spectral superchannel in inter DCNs. Such a superchannel can be routed in an end-to-end manner based on spatial bypassing without wavelength switching. Therefore, how to solve the routing and spectrum assignment problem in SCN-based inter DCNs is a challenging task.

Bibliography

[1] Feit M. D., and J. A. Fleck, "Light propagation in graded-index optical fibers," *Applied optics*, vol. 17, no. 24, pp. 3990–3998, 1978.

[2] Simmons J. M., *Optical network design and planning*. Springer, 2014.

[3] Chen Y., Fatehi M. T., La Roche H. J., et al., "Metro optical networking," *Bell Labs Technical Journal*, vol. 4, no. 1, pp. 163–186, 1999.

[4] Arnon, Shlomi, et al., *Advanced optical wireless communication systems*. Cambridge university press, 2012.

[5] Yeh C. H., Lin M. C., Chi S., *ITU-T Standard G. 694.1*, 2002.

[6] Lee, Jie Hyun, et al., "First commercial deployment of a colorless gigabit WDM/TDM hybrid PON system using remote protocol terminator," *Journal of Lightwave Technology*, vol. 28, no. 4, pp. 344–351, 2010.

[7] Jinno M., "Spatial channel network (SCN): opportunities and challenges of introducing spatial bypass toward the massive SDM era," *Journal of Optical Communications and Networking*, vol. 11, no. 3, pp. 1–14, 2019.

[8] Jinno M., "Elastic optical networking: Roles and benefits in beyond 100-Gb/s era," *Journal of Lightwave Technology*, vol. 35, no. 5, pp. 1116–1124, 2016.

[9] Jinno M., et al., "Demonstration of novel spectrum-efficient elastic optical path network with per-channel variable capacity of 40 Gb/s to over 400 Gb/s," in *2008 34th European Conference on Optical Communication*, pp. 1–2, 2008.

[10] Jinno M., et al., "Spectrum-efficient and scalable elastic optical path network: architecture, benefits, and enabling technologies," *IEEE communications magazine*, vol. 47, no. 11, pp. 66–73, 2009.

[11] Jinno M., et al., "Distance-adaptive spectrum resource allocation in spectrum-sliced elastic optical path network [topics in optical communications]," *IEEE communications magazine*, vol. 48, no. 8, pp. 138–145, 2010.

[12] Kikuchi K., "Coherent optical communication technology," in *Optical Fiber Communication Conference*, pp. Th4F–4, 2015.

[13] Beppu, Shohei, et al., "2048 QAM (66 Gbit/s) single-carrier coherent optical transmission over 150 km with a potential SE of 15.3 bit/s/Hz," *Optics express*, vol. 23, no. 4, pp. 4960–4969, 2015.

[14] Zheng, Zhennan, et al., "Orthogonal-band-multiplexed offset-QAM optical superchannel generation and coherent detection," *Scientific Reports*, vol. 5, no. 1, pp. 1–10, 2015.

[15] Bonenfant, Paul A., and Mark Loyd Jones, "OFC 2003 workshop on wavelength selective switching based optical networks," *Journal of Lightwave Technology*, vol. 22, no. 1, pp. 305, 2004.

[16] Zong, Lei, et al, "Study on wavelength cross-connect realized with wavelength selective switches," in *National Fiber Optic Engineers Conferencee*, Optica Publishing Group, 2006.

[17] Pulikkaseril, Cibby, et al., "Spectral modeling of channel band shapes in wavelength selective switches," *Optics express*, vol. 19, no. 9, pp. 8458–8470, 2011.

[18] Baxter, Glenn, et al., "Highly programmable wavelength selective switch based on liquid crystal on silicon switching elements," in *2006 Optical Fiber Communication Conference and the National Fiber Optic Engineers Conference*, pp. 3, IEEE, 2006.

[19] López, Vıctor, and Luis Velasco, "Elastic optical networks," *Architectures, Technologies, and Control, Switzerland: Springer Int. Publishing*, 2016.

[20] Recalcati, Michael, et al., "Benefits of elastic spectrum allocation in optical networks with dynamic traffic," in *2014 IEEE Latin-America Conference on Communications (LATINCOM)*, IEEE, 2014.

[21] Christodoulopoulos, Konstantinos, Ioannis Tomkos, and Emmanuel A. Varvarigos, "Elastic bandwidth allocation in flexible OFDM-based optical networks," *Journal of Lightwave Technology*, vol. 29, no. 9, pp. 1354–1366, 2011.

[22] Recalcati, Michael, et al., "A study of the routing and spectrum allocation in spectrum-sliced elastic optical path networks," in *2011 Proceedings Ieee Infocom*, IEEE, 2011.

[23] Simmons, Jane M, "Flexible Optical Networks," *Optical Network Design and Planning*, Springer, Cham, pp. 401–440, 2014.

[24] Leuthold, Juerg, et al., "An all-optical grooming switch to interconnect access and metro ring networks," in *2008 10th Anniversary International Conference on Transparent Optical Networks*, IEEE, vol 3, pp. 207–210, 2008.

[25] Dey, Suman Kr, and Aneek Adhya, "Integrated grooming and regeneration capable OXC-based connection provision in WDM network," in *2011 Annual IEEE India Conference*, IEEE, 2011.

[26] Gerstel, Ori, et al., "Elastic optical networking: A new dawn for the optical layer?," *IEEE communications Magazine*, vol. 50, no. 2, pp. s12–s20, 2012.

[27] Shariati, Behnam, et al., "Investigation of mid-term network migration scenarios comparing multi-band and multi-fiber deployments," in *2016 Optical Fiber Communications Conference and Exhibition (OFC)*, IEEE, 2016.

[28] Farjady, F., et al., "Value of fiber overlays in WDM metro networks," *IEEE Photonics Technology Letters*, vol. 15, no. 2, pp. 329–331, 2003.

[29] Saitoh, Kunimasa, and Shoichiro Matsuo, "Multicore fiber technology," *Journal of Lightwave Technology*, vol. 34, no. 1, pp. 55–66, 2016.

[30] Kitayama, Ken-ichi, and Nikolaos-Panteleimon Diamantopoulos, "Few-mode optical fibers: Original motivation and recent progress," *IEEE Communications Magazine*, vol. 55, no. 8, pp. 163–169, 2017.

[31] Nakajima, Kazuhide, et al., "Transmission media for an SDM-based optical communication system," *IEEE Communications Magazine*, vol. 53, no. 2, pp. 44–51, 2015.

[32] Krummrich, Peter M, "Optical amplifiers for multi mode/multi core transmission," in *Optical Fiber Communication Conference*, pp. OW1D-1, Optical Society of America, 2012.

[33] Zimmerman, Donald R., and Leo H. Spiekman, "Amplifiers for the masses: EDFA, EDWA, and SOA amplets for metro and access applications," *Journal of lightwave technology*, vol. 22, no. 1, pp. 63, 2004.

[34] Ryf, R., et al., "Mode-multiplexed transmission over a 209-km DGD-compensated hybrid few-mode fiber span," *IEEE Photonics Technology Letters*, vol. 24, no. 21, pp. 1965–1968, 2012.

[35] Takara, Hidehiko, et al., "1000-km 7-core fiber transmission of 10 x 96-Gb/s PDM-16QAM using Raman amplification with 6.5 W per fiber," *Optics express*, vol. 20, no. 9, pp. 10100–10105, 2012.

[36] Yamada, Makoto, et al., "Optical fiber amplifier employing a bundle of reduced cladding erbium-doped fibers," *IEEE Photonics Technology Letters*, vol. 24, no. 21, pp. 1910–1913, 2012.

[37] Sasaki, Yusuke, et al., "Trench-assisted low-crosstalk few-mode multicore fiber," in *39th European Conference and Exhibition on Optical Communication (ECOC 2013)*, pp. 1–3, IET, 2013.

[38] Klaus, Werner, et al., "Free-space coupling optics for multicore fibers," *IEEE Photonics Technology Letters*, vol. 24, no. 21, pp. 1902–1905, 2012.

[39] Krummrich, Peter M, "Spatial multiplexing for high capacity transport," *Optical Fiber Technology*, vol. 17, no. 5, pp. 480–489, 2011.

[40] Thomson, Robert R., et al., "Ultrafast-laser inscription of a three dimensional fan-out device for multicore fiber coupling applications," *Optics express*, vol. 15, no. 18, pp. 11691–11697, 2007.

[41] Saridis, George M., et al., "Survey and evaluation of space division multiplexing: From technologies to optical networks," *IEEE Communications Surveys & Tutorials*, vol. 17, no. 4, pp. 2136–2156, 2015.

[42] "Optoscribe," [Online]. Available: http://optoscribe.com/.

[43] Khodashenas, Pouria Sayyad, et al., "Comparison of spectral and spatial super-channel allocation schemes for SDM networks," *Journal of Lightwave Technology*, vol. 34, no. 11, pp. 2710–2716, Apr.2016.

[44] Zheng, Weichang, et al., "Evaluation of Optical Transport Unit Line-Card Integration in Spatially and Spectrally Flexible Optical Networks in Terms of Device Cost and Network Performance," *Journal of lightwave technology*, vol. 40, no. 19, pp. 6319–6330, 2022.

[45] Klonidis, Dimitrios, et al., "Spectrally and spatially flexible optical network planning and operations," *IEEE Communications Magazine*, vol. 53, no. 2, pp. 69–78, 2015.

[46] Yang, Mingcong, et al., "Evaluation of device cost, power consumption, and network performance in spatially and spectrally flexible SDM optical networks," *Journal of lightwave technology*, vol. 37, no. 20, pp. 5259–5272, 2019.

[47] Tan, Yuanlong, et al., "Crosstalk-aware provisioning strategy with dedicated path protection for elastic multi-core fiber networks," in *2016 15th International Conference on Optical Communications and Networks (ICOCN)*, pp. 1–3, IEEE, 2016.

[48] Tode, Hideki, and Yusuke Hirota, "Routing, spectrum and core assignment on SDM optical networks," in *Optical Fiber Communication Conference*, pp. Tu2H-1, Optica Publishing Group, 2016.

[49] Winzer, Peter J., and David T. Neilson, "From scaling disparities to integrated parallelism: A decathlon for a decade," *Journal of Lightwave Technology*, vol. 35, no. 5, pp. 1099–1115, 2017.

[50] Jinno, Masahiko, "Spatial channel network (SCN): opportunities and challenges of introducing spatial bypass toward the massive SDM era," *Journal of Optical Communications and Networking*, vol. 11, no. 3, pp. 1–14, 2019.

[51] Jinno, Masahiko, "Spatial channel cross-connect architectures for spatial channel networks," *IEEE Journal of Selected Topics in Quantum Electronics*, vol. 26, no. 4, pp. 1–16, Feb. 2020.

[52] Yang, Mingcong, et al., "Hierarchical Routing and Resource Assignment in Spatial Channel Networks (SCNs): Oriented Toward the Massive SDM Era," *Journal of Lightwave Technology*, vol. 39, no. 5, pp. 1255–1270, Nov. 2020.

[53] Rivas-Moscoso, José Manuel, et al., "Cost and power consumption model for flexible superchannel transmission with all-optical sub-channel add/drop capability," in *2015 17th International Conference on Transparent Optical Networks (ICTON)*, pp. 1–4, IEEE, 2015.

[54] van Uden, Roy GH, et al., "Single DPLL joint carrier phase compensation for few-mode fiber transmission," *IEEE Photonics Technology Letters*, vol. 25, no. 14, pp. 1381–1384, 2013.

[55] Yaman, Fatih, et al., "Long distance transmission in few-mode fibers," *Optics Express*, vol. 18, no. 12, pp. 13250–13257, 2010.

[56] Vojnovic, Boris, "Notes on optical fibres and fibre bundles," *Gray Instutute, Department of Oncology, University of Oxford*, 2012.

[57] Matsui, Takashi, et al., "Design of 125 μm cladding multi-core fiber with full-band compatibility to conventional single-mode fiber," in *2015 European Conference on Optical Communication (ECOC)*, pp. 1–3, IEEE, 2015.

[58] Randel, Sebastian, "Space-division multiplexed transmission," in *2013 Optical Fiber Communication Conference and Exposition and the National Fiber Optic Engineers Conference (OFC/NFOEC*, pp. 1–60, IEEE, 2013.

[59] Shariati, Behnam, et al., "Evaluation of the impact of spatial and spectral granularities on the performance of spatial superchannel switching schemes," in *2016 18th International Conference on Transparent Optical Networks (ICTON)*, pp. 1–4, IEEE, 2016.

[60] Nelson, L. E., et al., "Spatial superchannel routing in a two-span ROADM system for space division multiplexing," *Journal of Lightwave Technology*, vol. 32, no. 4, pp. 783–789, 2014.

[61] Ahmad, Arsalan, et al., "Switching node architectures in flexible-grid networks: A performance comparison," in *2014 International Conference on Optical Network Design and Modeling*, pp. 49–54, IEEE, 2014.

[62] Filer, Mark, and Sorin Tibuleac, "N-degree ROADM architecture comparison: Broadcast-and-select versus route-and-select in 120 Gb/s DP-QPSK transmission systems," in *OFC*, pp. 1–3, IEEE, 2014.

[63] Marom, Dan M., et al., "Survey of photonic switching architectures and technologies in support of spatially and spectrally flexible optical networking," *Journal of Optical Communications and Networking*, vol. 9, no. 1, pp. 1–26, 2017.

[64] Rivas-Moscoso, José Manuel, et al., "Comparison of CD (C) ROADM architectures for space division multiplexed networks," in *Optical Fiber Communication Conference*, pp. Th2A-45, Optical Society of America, 2017.

[65] Garrich, Miquel, et al., "Architecture on demand design for high-capacity optical SDM/TDM/FDM switching," *Journal of Optical Communications and Networking*, vol. 7, no. 1, pp. 21–35, 2015.

[66] Huang, Haibin, et al., "Crosstalk-Aware Routing, Core, and Wavelength Assignment in MCF-based SDM-QKD Optical Networks," in *Asia Communications and Photonics Conference*, pp. M4A-188, Optica Publishing Group, 2020.

[67] Tang, Fengxian, et al., "Minimizing inter-core crosstalk jointly in spatial, frequency, and time domains for scheduled lightpath demands in multi-core fiber-based elastic optical network," *Journal of Lightwave Technology*, vol. 38, no. 20, pp. 5595–5607, 2020.

[68] Gan, Lin, et al., "Investigation of channel model for weakly coupled multicore fiber," *Optics Express*, vol. 26, no. 5, pp. 5182–5199, 2018.

[69] Puttnam, Benjamin J., et al., "Characteristics of homogeneous multi-core fibers for SDM transmission," *APL Photonics*, vol. 4, no. 2, pp. 022804, 2019.

[70] Flusberg, Benjamin A., et al., "Fiber-optic fluorescence imaging," *Nature methods*, vol. 2, no. 12, pp. 941–950, 2005.

[71] Klinkowski, Mirosław, Piotr Lechowicz, and Krzysztof Walkowiak, "A study on the impact of inter-core crosstalk on SDM network performance," in *2018 International Conference on Computing, Networking and Communications (ICNC)*, pp. 404–408, IEEE, 2018.

[72] Yang, Mingcong, et al., "Comparison of switching policies in terms of switching cost and network performance in static SDM-EONs," *Optical Switching and Networking*, vol. 38, pp. 100573, 2020.

[73] Mas C, Tomkos I, Tonguz O K, "Optical networks security: a failure management framework," in *Optical Transmission Systems and Equipment for WDM Networking II*, vol. 5247, pp. 230–241, SPIE, 2003.

[74] Kim S, Lumetta S, "Addressing node failures in all-optical networks," *Journal of Optical Networking*, vol. 1, no. 4, pp. 154–163, Apr.2002.

[75] Ahuja S S, Ramasubramanian S, Krunz M, "SRLG failure localization in optical networks," *IEEE/ACM Transactions on Networking*, vol. 19, no. 4, pp. 989–999, Aug.2011.

[76] V. Hou, "Update on Interim Results of Fiber Optic System Field Failure Analysis," in *NFOEC Proceedings*, vol. 1, pp. 539–545, 1991.

[77] Bouillet E, Ellinas G, Labourdette J F, et al, "Path routing in mesh optical networks," John Wiley & Sons, 2007.

[78] Nag A, Wang T, Mukherjee B, "Robust design of spectrum-efficient green optical backbone networks," *Journal of Lightwave Technology*, vol. 31, no. 7, pp. 1138–1144, Apr.2013.

[79] Yen J Y, "Finding the k shortest loopless paths in a network," *management Science*, vol. 17, no. 11, pp. 712–716, Jul.1971.

[80] Bertsimas D, Sim M, "Robust discrete optimization and network flows," *Mathematical programming*, vol. 98, no. 1, pp. 49–71, May.2003.

[81] Bertsimas D, Sim M, "The price of robustness," *Operations researchg*, vol. 52, no. 1, pp. 35–53, Feb.2004.

[82] ITU-T, "Extension of rec. g.694.1," Dec.2011.address